STRESS SIGNALING MEDIATED CHANGES TO CELL BEHAVIOR IN RESPONSE TO WOUNDING AND TUMOR GROWTH

Marco La Fortezza
Ludwig-Maximilians-Universität München

München 2016

STRESS SIGNALING MEDIATED CHANGES TO CELL BEHAVIOR IN RESPONSE TO WOUNDING AND TUMOR GROWTH

Dissertation
an der Fakultät für Biologie
der Ludwig-Maximilians-Universität München

vorgelegt von
Marco La Fortezza

München, den 12. July 2016

Erstgutacher: Dr. Anne-Kathrin Classen
Zweitgutachter: Prof. Dr. Barbara Conradt

Tag der Abgabe: 12. July 2016
Tag der mündlichen Prüfung: 6.12.2016

Declaration

Eidesstattliche Versicherung

Hiermit erkläre ich an Eides statt, dass ich die vorliegende Arbeit selbstständig und ohne unerlaubte Hilfe von Dritten angefertigt habe.

München, den 12.07.2016

……
Marco La Fortezza

Erklärung

Hiermit erkläre ich, dass die Dissertation weder als Ganzes, noch in Teilen an einem anderen Ort einer Prüfungskommission vorgelegt wurde. Ich habe weder an einem anderen Ort eine Promotion angestrebt, noch angemeldet oder versucht eine Doktorprüfung abzulegen.

München, den 12.07.2016

……
Marco La Fortezza

Publication

Parts of this work were used for a manuscript that was accepted for publication on 23.07.2016 by the journal Development (*DOI: 10.1242/dev.132340*).

JAK/STAT signaling mediates cell survival in response to tissue stress

Marco La Fortezza[1], Madlin Schenk[1], Andrea Cosolo[1], Addie Kolybaba[1], Isabelle Grass[1], Anne-Kathrin Classen[§1]

1 Faculty of Biology, Ludwig Maximilians University Munich, Germany
[§] *corresponding author*

Contributions

Madlin Schenk and Andrea Cosolo helped in collecting data on the study of compensatory proliferation using imaging approaches or FACS analysis, respectively. Addie Kolybaba ran preliminary experiments combining cell ablation with p35 over expression. Her observations were important for the further development of my research. Isabelle Grass helped in stock maintenance

Acknowledgments

At first it was just an empty lab, but I have found an enthusiastic scientist and a very friendly and happy person. Anne-Kathrin has been more than just a supervisor. She was a mentor during all my PhD. She guided me through science and through life. I will always bring with me what I found to be her biggest advice “Don’t be afraid to fail and learn to feel stupid. You can’t get smarter without knowing what it means to be wrong”. These words helped me a lot to deal with bad and good times. For all the work and time that she saved and dedicated to me, just saying thank you to Anne-Kathrin is reductive. I really hope that we will be able to do science together also in the future: as two scientists and friends.

Thanks to the all laboratory. Mondays have never been an issue and coming to work has been always pleasant. Christina, Andrea, Addie, Ramya, Vanessa, Isabelle and all the students. You helped me a lot, supported and encouraged me. Together I had the best beers I’ve ever drunk. I will bring all those moments with me, wherever I will be and whatever I will do.

Thanks to my TAC members, Dr. Jürg Müller and Prof. Heinrich Leonhardt that helped me through my research with theirs precious advises.

Thanks to Prof. Nicolas Gompel for his advises on science and on life. The discussions I had with him have been fundamental to me.

Thanks to Dr. Alexey Pindyurin and Prof. Bas van Steensel for the help they gave me on the project and for the nice scientific discussion.

Thanks to all my family. They have been always there since I was born, especially my mother, my father and my sisters. They supported me anytime and even if they were physically far we have always been close with our hearts.

There are many, many other people that should be thanked, women and men that helped me and made my living in Munich memorable.

To all of you, thanks.

Table of Contents

DECLARATION 5

ACKNOWLEDGMENTS 7

TABLE OF CONTENTS 9

LIST OF FIGURES 12

ABBREVIATIONS 15

SUMMARY 17

ZUSAMMENFASSUNG 19

1 INTRODUCTION 21

1.1 TISSUE HOMEOSTASIS AND STRESS RESPONSE 21

1.2 APOPTOSIS AND THE JNK SIGNALING 22

1.3 PROLIFERATION AND JAK/STAT SIGNALING 24

1.4 CHROMATIN DYNAMICS DURING TISSUE STRESS RESPONSE 26

1.5 DAMID-SEQ PROFILING TO STUDY CHROMATIN DYNAMICS 27

2 AIM OF THIS STUDY/ SCOPE OF THIS THESIS 30

3 RESULTS 32

3.1 ACTIVATION OF JNK-SIGNALLING BY *EIGER*-EXPRESSION ENABLES FUNCTIONAL STUDIES OF JNK-DEPENDENT TISSUE STRESS RESPONSES 32

3.2 JAK/STAT SIGNALLING IS ACTIVATED IN RESPONSE TO EIGER-INDUCED TISSUE DAMAGE 36

3.3 UNPAIRED-LIGANDS ARE TRANSCRIPTIONALLY UPREGULATED IN RESPONSE TO EIGER-INDUCED TISSUE DAMAGE 38

3.4 JAK/STAT ACTIVITY IS NOT REQUIRED FOR COMPENSATORY PROLIFERATION 39

3.5 JAK/STAT AND JNK SIGNALLING HAVE SPECIFIC ACTIVATION PATTERNS DURING TISSUE STRESS RESPONSE. 42

3.6 STRONG JNK ACTIVATION COINCIDES WITH JAK/STAT SIGNALLING INHIBITION 45

3.7 JAK/STAT ACTIVITY IS REQUIRED FOR SURVIVAL OF JNK-SIGNALLING CELLS 47

3.8 JAK/STAT ACTIVITY SUPPRESSES ACTIVATION OF JNK-SIGNALLING 49

3.9 A SURVIVAL-PROMOTING FUNCTION OF JAK/STAT IS MEDIATED BY ZFH2 51

3.10 JAK/STAT ACTIVITY PREVENTS EXCESSIVE TISSUE DAMAGE IN RESPONSE TO TISSUE STRESS 55

3.11 JAK/STAT ACTIVITY PROMOTES EFFICIENT INDUCTION OF COMPENSATORY RESPONSES 57

3.12 JAK/STAT REGULATES SURVIVAL IN A RAS^{V12}; SCRIB TUMOUR MODEL 59

3.13 TISSUE STRESS RESPONSES ARE MEDIATED BY DYNAMIC REGULATION OF CHROMATIN. 62

3.14 ESTABLISHMENT OF AN INDUCIBLE DAMID-SEQ TECHNIQUE TO ANALYSE DNA-PROTEIN INTERACTION IN *DROSOPHILA* WING IMAGINAL DISCS. 63

3.15 ANALYSIS OF THE DAMID-SEQ DATA 65

3.16 DIFFERENCES IN PC BINDING AFFECT NEIGHBOURING DOMAINS. 67

3.17 CHANGES IN PC BINDING HAPPEN AT SPECIFIC *LOCI* DURING TUMOUR FORMATION. 69

3.18 ANALYSIS OF PC BINDING AROUND TSS OF DIFFERENTIALLY EXPRESSED GENES REVEALED COMPLEX CHROMATIN DYNAMICS IN TUMOUR. 70

3.19 CHANGES IN PC BINDING CORRELATE WITH ENRICHMENT OF SPECIFIC TRANSCRIPTIONAL FACTORS BINDING SITES (TFBS). 73

3.20 INFLUENCE OF GATC FRAGMENT SIZE ON DAM-ID DATA ANALYSIS RESULTS. 75

4 MATERIAL AND METHODS 78

4.1 MATERIALS 78

4.1.1 TECHNICAL DEVICES 78

4.1.2 BUFFER, CHEMICALS AND CONSUMABLES 78

4.1.3 ENZYMES AND KITS 79

4.1.4 ANTIBODIES 79

4.1.5 KITS 80

4.1.6 OLIGONUCLEOTIDES 80

4.1.7 MICROSCOPES 81

4.1.8 SOFTWARE 82

4.1.9 FLY STOCKS 83

4.2 FLY HUSBANDRY AND GENERAL EXPERIMENTAL PROCEDURES 84

4.3 CELL BIOLOGICAL METHOD 85

4.3.1 FLOW CYTOMETRY 85

4.3.2 IMMUNOHISTOCHEMISTRY 85

4.3.3 IMAGE QUANTIFICATION 86

4.4 MOLECULAR BIOLOGICAL METHODS 87

4.5 ADULT WINGS SIZE ANALYSIS 88

4.6 BIOINFORMATICS 88

5 DISCUSSION 90

5.1 JAK/STAT ACTS AS PRO-SURVIVAL SIGNALING DURING TISSUE STRESS RESPONSE. 90

5.2 THE JAK/STAT AND JNK SIGNALING CROSS TALK. 92

5.3 POLYCOMB PROTEIN REGULATES SPECIFIC GENES DURING TUMOR GROWTH. 94

5.4 POLYCOMB ACTIVITY MAY INTERACT WITH SPECIFIC SIGNALING PATHWAYS 95

5.5 DAMID-SEQ TECHNIQUE CAN BE USED TO STUDY CHROMATIN ACCESSIBILITY. 97

6 CONCLUSIONS 98

REFERENCES 99

APPENDIX 108

6.1 APPENDIX I – EXPERIMENTAL PROCEDURE FOR CELL ABLATION INDUCTION IN WING IMAGINAL DISCS 108

6.2 APPENDIX II – WING SIZE ANALYSIS 112

6.3 APPENDIX III – DAMID-SEQ ANALYSIS 114

6.4 APPENDIX IV – RAW DATA. 116

7 CURRICULUM VITAE 138

List of figures

Figure 1. JNK signaling in *Drosophila* stress responses. 23

Figure 2. The JAK/STAT signaling in wing imaginal discs. 25

Figure 3 Schematic representation of the DamID-seq protocol. 29

Figure 4. Eiger-expression enables functional studies of JNK-dependent tissue stress responses. 33

Figure 5. Eiger-expression induces activation of compensatory proliferation. 35

Figure 6. Cell ablation by expression of pro-apoptotic gene reaper doesn't induce broad activation of JNK signaling. 36

Figure 7. JAK/STAT is activated in response to Eiger-induced tissue damage. 37

Figure 8. JAK/STAT activation declines during recovery time after cell ablation. 38

Figure 9. The extent of the JAK/STAT activation correlates with the ability of the tissue to respond to stress induction. 39

Figure 10. JAK/STAT activation is not required for compensatory proliferation. 41

Figure 11. Nuclei counts confirm automated Fiji quantification of volumes and cell proliferation. 42

Figure 12. JNK and JAK/STAT have specific activation patterns around the wound site upon cell ablation. 43

Figure 13. Cell death inhibition defines JNK and JAK/STAT activations in three distinct regions in *rn>egr* discs. 44

Figure 14. Cell death is non-autonomously induced in wild type cells surrounding the Eiger-p35 undead-cells. 45

Figure 15. Eiger-p35 cells do not have translocation of STAT92E into the nucleus. 46

Figure 16. Reduction in JAK/STAT activity increases apoptosis in Eiger-induced discs. 48

Figure 17. Transient down regulation of the JAK/STAT pathway does not cause cell death in wild type discs during normal development. 49

Figure 18. Down regulation of JAK/STAT, in ablated discs, results in broader activation of JNK signaling. 50

Figure 19. Transcriptional analysis of the pro-apoptotic genes *hid, grim, rpr* and the AP-1 component *kay.* 52

Figure 20. Bioinformatic prediction of Zfh2 and AP-1 binding sites on *hid* and *kay loci.* 53

Figure 21. Zfh2 is activated in response to tissue damage. 54

Figure 22. Ectopic induction of *zfh1* promotes survival in *eiger*-expressing discs. ...55

Figure 23. Down regulation of the JAK/STAT pathway during cell ablation, affects proper wound healing. 56

Figure 24. JAK/STAT also prevents excessive tissue damage upon mechanical tissue damage. 57

Figure 25. Reduction of the JAK/STAT activity reduces injured induced development delay. 58

Figure 26. Development delay mediated by *dIlp-8* depends on the JAK/STAT activation. 59

Figure 27. JAK/STAT doesn't promote compensatory proliferation in a Ras^{V12}*;scrib* tumour model. 60

Figure 28. JAK/STAT regulates survival in a Ras^{V12}*;scrib* tumour model. 61

Figure 29. Zfh2 is activated during tumor formation and it depends on JAK/STAT signaling. 62

Figure 30. Down regulation chromatin factor activity during cell ablation, affects proper wound healing. 63

Figure 31. DamID inducible constructs. 64

Figure 32. Preliminary controls on the DamID-seq protocol. 65

Figure 33. Preliminary analysis of Pc-DamID data suggests specific reorganization of Pc binding in tumor. 66

Figure 34. Transition-State analysis. 67

Figure 35. Analysis of Pc domains. 68

Figure 36. Study of the transcriptional-associated GATC fragments linked to differentially expressed genes. 70

Figure 37. Dynamics of Pc binding affect specific genes expression during tumor formation. 72

Figure 38. Pc binding is rearranged around the TSS of genes differentially expressed in tumor. 73

Figure 39. Pc binding is not indepented on GATC fragment size. 76

Figure 40. Large GATC fragments tend to be localized in highly repressed chromatin regions. 77

Figure 41. JAK/STAT promotes cell survival. 90

Figure 42. Model for repression of injured-induced apoptosis through the activation of Zfh2. 91

Figure 43. The three states model of JNK-JAK/STAT cross-talk during tissue stress response. 93

Abbreviations

General abbreviations

AED	After Egg Deposition
CA	Cell Ablation
dGFP	degradable-GFP
G-Trace	GFP-Trace
GATCf	GATC fragment
GFP	Green Flourescent Protein
HS	Heat-Shock
HSp	Heat-Shock promoter
I	Intermediate
MNase	Micrococcal Nuclease
NT	Non-Target
PC	Pouch Centre
PRC	Polycomb Repressive Complex
PWM	Position Wieghted Matrix
R0, R24, R48	Recovery time poin: 0, 24, 48 h
RFP	Red Flourescent Protein
T	Target
T-S	Transition-State
taGATCf	transcription-associated GATC fragment
TFBs	Transcription Factor Binding site
TRE	TPA Response Element

Gene abbreviations

ash	absent, small, or homeotic discs
Atf3	Activating transcription factor 3
bsk	basket
chinmo	Chronologically inappropriate morphogenesis
CTCF	CCCTC-binding Factor
Dcp-1	Death caspase-1
Diap	Death-associated inhibitor of apoptosis

dIlp-8	drosophila Insulin-like peptide 8
dom	domino
Drice	Death related ICE-like caspase
Dronc	Death regulator Nedd2-like caspase
E(z)	enhancer of zeste
egr	eiger
Ets21C	Ets at 21C
hid	head involution defective
hop	hopscotch
HP1	Heterochromatin protein 1
hpo	hippo
Ino80	INO80 compex subunit
JHDM	Jumonji Domain-containing Histone Demethylase
Jil-1	JIL-1 kinase
Jra	Jun-related antigen
Kay	Kayak
kis	kismet
lid	little imaginal discs
Lsd-1	Lipid storage droplet-1
Nej	Nejire
Nf-YA	Nuclear factor Y-box A
Pc	Polycomb
Ph	polyhomeotic
Psc	posterior sex comb
Ptip	PAX transcription activation domain interacting protein
puc	puckered
pvf	PDGF- and VEGF-realated factor
Rpd3	Histone deacetylase 1
rpr	reaper
sce	sex comb extra
scrib	scribble
Socs36E	Suppressor of cytokine signaling at 36E
Stat92E	Signal-transducer and activator of transcription protein at 92E
Su(var)2-40	Suppressor of variegation 2-40
Su(Z)2	Suppressor of zeste 2
trx	trithorax
upd	unpaired
Utx	Utx histone demethylase
vg	vestigial
wg	wingless
wds	will die slowly
yki	yorkie
Zfh	Zn finger homeodomain
ZW5	Zeste-White 5

Summary

Cells within a tissue are able to respond to external insults, such as UV irradiation or wounding in order to maintain tissue homeostasis. This ability is of vital importance at all stages of an organism's life. In the last decade, the high degree of complexity that orchestrated responses to tissue stress have became more and more evident have. Dissecting the intricate network of cell signalling underlying these responses has become a fundamental step to understand how tissues reestablish homeostasis under stress conditions.

My doctoral studies have focused on dissecting the role of JAK/STAT signalling in tissue stress responses using *Drosophila melanogaster* as model organism. In the literature, the JAK/STAT pathway has been largely described as activator and promoter of compensatory proliferation during tissue stress. However, by using a genetic tool to induce tissue regeneration, my research brought me to elucidate and describe a novel role of the JAK/STAT signalling in wounding responses. Rather than being a direct activator of proliferative responses, this pathway works as mediator of cell survival through its repressive effect on the JNK signalling, which is known to be the main activator of the apoptotic pathway in flies. In the transcriptional repressor Zfh2, I identified the best candidate to be the mediator of the buffering effect that JAK/STAT signalling has on JNK-induced apoptosis. As expected, regenerating tissues with impaired JAK/STAT activity showed spatial spreading of the pro-apoptotic wave activated by non-autonomous activation of the JNK signalling. Such abnormal induction of injury-induced apoptosis resulted in the lack of the proper compensatory responses, which are necessary to re-establish tissue integrity.

Interestingly, my results also apply to a chronic stress contexts, such as tumor formation. In fact, tumorous tissues are characterised by the activation of the same cellular signalling pathways that are also activated in the acute wounding and regeneration model. However, the activation of these pathways in tumours lacks the fine-tuning that helps wild type tissue to respond and reconstitute the proper tissue homeostasis.

My research extended to investigate the changes that occur at the level of chromatin during cellular stress responses. I centred my studies on analyzing the differential binding of the Polycomb Repressive Complex 1 (PRC1) during tumour formation by using DamID-seq profiling technology. Specifically, I mapped genome-wide binding sites of Polycomb protein (Pc), component of the PRC1, in wild type and tumorous tissues. My results confirmed that DamID-based approaches are suitable to profiling of DNA binding sites in Drosophila imaginal discs in vivo and gave me the opportunity to identify a list of potentially novel Pc target genes regulated differentially during neoplasiae formation. Moreover, analysis of enriched regulatory element in differentially bound regions brought me to link dynamic Pc activity to specific signalling pathways impinging on gene activity in tumours.

My work redirects the definition of the JAK/STAT signalling from being a direct inducer of cell proliferation to be the key mediator of the survival-apoptosis dichotomy during tissue stress responses. Moreover, I brought clear evidences that the JNK signalling is strongly linked to the JAK/STAT pathway. My data support the conclusion that the cross talk between these two pathways is the key mediator of the changes in cellular behaviour upon stress induction. My study indicates that these changes also occur at a chromatin level. I demonstrated that dynamic rearrangements of chromatin are fundamental during tissue stress responses. Furthermore, my analysis of Pc binding in tumor suggests that modification in the chromatin interactions happen on specific *loci* and that redistribution of Pc binding is linked to specific signalling.

Zusammenfassung

Zellen eines Gewebes sind in der Lage auf äußere Einflüsse, wie zum Beispiel UV-Strahlung oder Verletztungen, zu reagieren. Dies ermöglicht ihnen die Gewebehomöostase aufrecht zu erhalten, was von lebensnotwendiger Bedeutung während allen Lebensabschnittes eines jeden Organismus ist. Im letzten Jahrzehnt wurde immer deutlicher, wie hochkomplex diese fein regulierten Stressantworten sind. Um besser zu verstehen, wie Gewebe auf Stressbedingungen reagieren, ist es deshalb unabdingbar die komplexen, zu Grunde liegenden Signalwege zu analysieren.

Meine Doktorarbeit konzentrierte sich auf die Rolle der JAK/STAT Signalkette während der Antwort eines Gewebes auf externen Stress, wozu *Drosophila melanogaster* als Modelorganismus verwendet wurde. In der Literatur ist der JAK/STAT Signalweg bisher hauptsächlich als Aktivator von kompensativer Proliferation aufgrund von Stress beschrieben. Mit Hilfe einer genetischen Methode, welche Geweberegeneration auslöst, konnte ich jedoch eine neue Rolle für die JAK/STAT Signalkette während verletztungsbedingten Stressantworten aufzeigen. Anstatt direkt kompensative Proliferation zu aktivieren, fördert der JAK/STAT Signalweg ein verstärktes Überleben von Zellen in der Wunde, was durch seine repressive Wirkung auf den JNK Signalweg, der Hauptaktivator von Apoptose in Fliegen, erklärt werden kann. Des Weiteren konnte ich den transkriptionellen Repressor Zfh2 als möglichen Kandidat für den hemmenden Effekt von JAK/STAT auf den JNK-vermittelten Zelltod identifizieren. Erwartungsgemäß kam es in regenerierenden Geweben mit eingeschränkter JAK/STAT Aktivität zu einer räumlichen Ausbreitung der pro-apoptotischen Welle, welche von der nicht-autonomen Aktivierung der JNK Signalkette herrührte. Das dadurch erhöhte Auftreten von verletztungsbedingtem Zelltod führt zu einem Mangel an kompensativen Antworten, welche notwendig sind, um die Gewebeintegrität erneut aufzubauen.

Interessanterweise können diese Ergebnisse auch auf chronische Stresssituationen angewandt werden, wie zum Beispiel im Fall von Tumorbildung. In der Tat werden in tumorösen Geweben Signalwege aktiviert, welche auch im akuten Stressmodel nachgewiesen werden konnten. Andererseits fehlt in Tumoren jedoch die feingesteuerte Regulierung dieser Signalwege, welche in wildtypischen Geweben helfen, die Gewebehomöostase wieder herzustellen.

Ich erweiterte meine Forschung auf stressbedingte Veränderungen, die auf der Ebene von Chromatin statt finden. Dabei konzentrierte ich mich spezifisch darauf, das differentielle Binden des Polycomb Repressive Complex 1 (PRC1) während der Tumorbildung zu analysieren, was ich mit Hilfe der DamID-seq Technik durchführte. Genauer gesagt identifizierte ich die Bindungsstellen der PRC1-Komponente Polycomb (Pc) über das gesamte Genom in wildtypischen und tumorösen Geweben. Meine Ergebnisse bestätigten, dass Dam-ID eine geeignete Methode zur Analyse von DNA-Bindestelle in Imaginalscheiben von *Drosophila* ist. Die Ergebnisse ermöglichten mir das Erstellen einer Liste von potentiell neuen Pc-Zielgenen, welche während Neoplasie differentiell reguliert werden. Darüber hinaus konnte ich auf Grund der Analyse von angereicherten regulatorischen Elementen in differentiell gebundenen Regionen, die Aktivität von Pc mit spezifischen Signalwegen, welche Einfluss auf die Genaktivität in Tumorgeweben nehmen, verknüpfen.

Meine Arbeit verändert die Definition des JAK/STAT Signalwegs von einem direkten Aktivator der Zellproliferation zu dem Schlüsselregulator des Gleichgewichts zwischen Überleben und Zelltod während Stressantworten. Darüber hinaus konnte ich darlegen, dass die Regulierung des JNK Signalwegs stark mit der JAK/STAT Signalkette verknüpft ist. Meine Daten unterstützen die Schlussfolgerung, dass die Interaktion dieser zwei Signalwege ausschlaggebend für Veränderungen von zellulären Antworten auf Stresssituationen ist. Meine Arbeit zeigt auf, dass diese Veränderungen auch auf Chromatinebene vermittelt werden. Ich konnte darlegen, dass dynamische Umstrukturierungen von Chromatin wichtig für Gewebe sind, um auf Stress zu antworten. Darüber hinaus legt meine Analyse der Pc Bindestellen in tumorösen Geweben nahe, dass Veränderungen der Chromatininteraktionen an spezifischen *loci* stattfinden und dass die Umverteilung von Pc-Bindungen mit spezifischen Signalwegen verknüpft ist.

1 Introduction

1.1 Tissue homeostasis and stress response

Every biological system, from a single cell up to an entire ecosystem, needs to be able to deal with changes in the environment in which it is developing and living. The property to maintain internal conditions relatively stable, despite external insults, is defined as homeostasis. Tissue homeostasis relies on the ability of tissues to respond to stress caused by damaging insults from the environment. Physical wounding, toxins, reactive oxygen species or UV irradiation can irremediably disrupt tissue integrity. Therefore, mounting an appropriate response is essential to repair the tissue and prevent chronic cellular stress that could lead to diseases [1]. Tumour formation and tumour growth induce cellular and tissue stress and affect cellular homeostasis. In case the tumour prevails over the wild type cells, the loss of homeostasis can turn to be systemic and fatal, spreading to the entire organism [2]. Although missregulated, the cellular signals that are activated in tumorous cells are similar to the ones that are initiated in wild type cells in acute stress conditions.

During the last years, much progress has been made to uncover the signalling pathways that seal wounds, remove damaged cells, promote regenerative proliferation or mediate patterning of regenerated tissue [3-5]. However, how cross talks between different pathways coordinates repair processes to successfully restore homeostasis is not fully understood.

Drosophila progenitor organs called imaginal discs have provided deep insights into cellular adaptations to tissue stress. Easy to dissect and analyse, these tissues are characterised by fast proliferation rates and well-studied specification patterns. These features and the low genetic redundancy make *Drosophila* imaginal discs a perfect platform to study alteration of cell signalling during tissue stress responses. For example, surgical

excision [6-8] and cell ablation induced by transient expression of pro-apoptotic transgenes [9-11] have elucidated cellular responses that promote wound healing [3, 12, 13]. Restoration of tissue size is mediated by accelerated proliferation of cells proximal [14, 15] and distal [10] to the wound site. Lacking tissue-resident stem cells, cell fate plasticity displayed by parenchymal disc cells facilitates re-patterning of the replaced tissue [10, 16-18]. In contrast to imaginal discs, tissue regeneration of the *Drosophila* adult midgut is driven by tissue-resident stem cells [19-22]. Strikingly, while the midgut and imaginal discs utilize stem cell-dependent and stem cell-independent repair processes, both tissues activate similar signal pathways that underlie potentially highly conserved stress responses.

1.2 Apoptosis and the JNK signaling

Apoptosis is a tightly controlled physiological process that leads to cell death. Unlike necrosis, apoptosis can be defined as *programmed cell death*. During development, apoptosis plays very important roles in controlling organ size and in shaping them. Therefore, the apoptotic process is not only important for the removal of unfit cells but also for the removal of cells that are not needed after a certain stage of the development [23-27]. Classical examples of the important developmental role of the apoptotic signalling are the digits and joints formation in vertebrates as well as the shaping of appendages and the head in insects [26, 28-30]. In *Drosophila,* apoptosis has also been shown to be fundamental in driving the left/right asymmetry during organogenesis, such as in the genitalia [31]. All these processes are tightly controlled in time and space.

Programmed cell death should be seen as a complex biological communication system that spread its message from the dying cells to the neighbouring ones. Apoptotic cells are known to be able to non-autonomously induce additional cell death in the surrounding tissue [32]. However, the same highly controlled event can also lead to the activation of proliferative signalling in the surrounding tissue by mitogens produced by dying cells [25, 33]. The induction of compensatory proliferation and the non-autonomous activation of additional cell death are both fundamental processes during tissue stress response [12, 34, 35]. The c-Jun N-terminal kinase (JNK) signalling is the main regulator of apoptosis in *Drosophila* stress responses. Despite the important role they play from nematodes to chordates in regulating the programmed cell death, mitochondria are rarely involved in initiating the apoptotic process in flies. Yet, mitochondria are associated with the function of the pro-apoptotic genes *head involution defective (hid)* and *reaper (rpr)*, both targets of the JNK signalling [36, 37].

The JNK-branch of the MAPK-cascade is among the earliest pathways activated in damaged tissues, for example, by loss of epithelial polarity [27, 38-41], by apoptosis of cells [33, 42] or by physical wounding [43-45]. JNK regulates stress responses via activation of the transcription factor AP-1 [46], formed by Jun (Jun-related antigen) and Fos (Kayak) homo- and heterodimers (Fig. 1). JNK activation is required for rearrangement of the cytoskeleton during wound closure [43, 47] and promotes elimination of damaged cells by injury-induced apoptosis [36, 37, 42, 48, 49]. Importantly, JNK drives compensatory proliferation to replace damaged tissues, potentially through cell-autonomous [9, 15, 50] and non-autonomous [33, 51, 52] mechanisms.

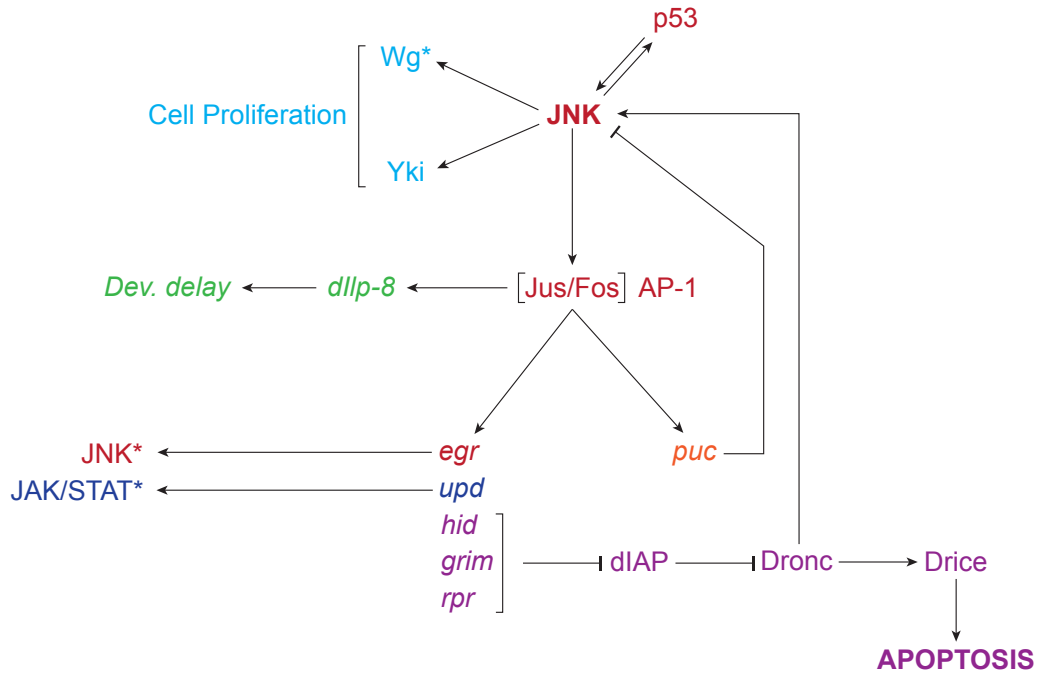

Figure 1. JNK signaling in *Drosophila* stress responses.

Schematic representation of the JNK signaling in *Drosophila melanogaster.* Stars represent non-autonomous activation.

JNK targets, which mediate injury-induced apoptosis, have been identified. Activation of the dIAP-inhibitors *rpr* and *hid* or activation of *p53* [36, 37, 42] by JNK facilitates clearing of damaged cells. Strikingly, activation of *rpr*, *hid* and *p53* drives further activation of JNK via the initiator caspase Dronc [42]. JNK also activates the TNFα homologue Eiger [32], leading to non-autonomous activation of JNK in nearby cells [32, 40, 51]. This positive feedback could drive excessive JNK-mediated cell elimination and therefore, needs to be restrained to prevent unlimited spatial propagation of pro-apoptotic JNK activity. How spatial constraints on JNK-signal propagation are established, is poorly understood.

Importantly, apoptosis of damaged cells stimulates compensatory proliferation in nearby cells by JNK-dependent activation of tissue growth pathways including Wnt/β-catenin, TFGβ/SMAD, JAK/STAT, Hippo/Yorkie and EGF signalling [3, 50, 53-57] (Fig. 1). By controlling the transcriptional levels of the gene *dilp-8,* JNK signalling has been shown to be involved in promoting development delay in response to stress induction. While the requirements of these pathways differ depending on contexts [10, 11, 34], many have been implicated in metazoan responses to stress [3, 49, 58]. Strikingly, preventing execution of apoptosis in damaged cells causes sustained proliferative signalling and eventual tumour formation in *Drosophila* [25, 33, 54, 55, 59, 60], emphasizing how strongly apoptotic, survival and proliferative signals need to be balanced to re-establish normal tissue size, shape and function.

In my doctoral studies, I addressed a central question that remained unanswered on how these very different responses – proliferation, apoptosis and survival - are brought into an intricate equilibrium downstream of the activation of a single pathway, JNK, to successfully restore tissue homeostasis.

1.3 Proliferation and JAK/STAT signaling

Highly conserved through out evolution, the JAK/STAT signalling pathway is known to be of crucial importance during many developmental processes as well as to a large variety of different physiological responses [61-66]. Current models propose that JAK/STAT (Janus kinase/Signal transducer and activator of transcription) signalling is a major mediator of compensatory, cancerous and developmental proliferation.

JAK/STAT cytokine-like ligands in *Drosophila* are encoded by *upd (unpaired), upd2*, and *upd3* and signal through conserved pathway components encoded by single genes, specifically the receptor Domeless (Dome), the Janus kinase Hopscotch (Hop) and the transcription factor STAT92E [65]. During normal development, at early stages, the signalling covers the entire wing imaginal discs. Subsequently, at late stage, the activation of the pathway is visible only at the hinge region of the disc (Fig. 2B).

A proliferative function for JAK/ STAT was suggested by early studies of tissue growth during imaginal disc development [67-69]. Subsequently, JAK/STAT has been

widely implicated in promoting proliferation of neoplastic cells [40, 66, 70-72] and in promoting aberrant non-autonomous proliferation of wild type cells in fly models of tumorigenesis [73-75]. Tissue damage has been linked to activation of *upd* transcription and compensatory proliferation in imaginal discs and adult guts [8, 20, 40, 72, 76, 77]. Other studies suggest that JAK/STAT signalling is involved in cell competition, where the signalling either promotes compensatory proliferation in response to elimination of looser cells [78] or promotes winner cell state in developing or tumorous discs [79, 80].

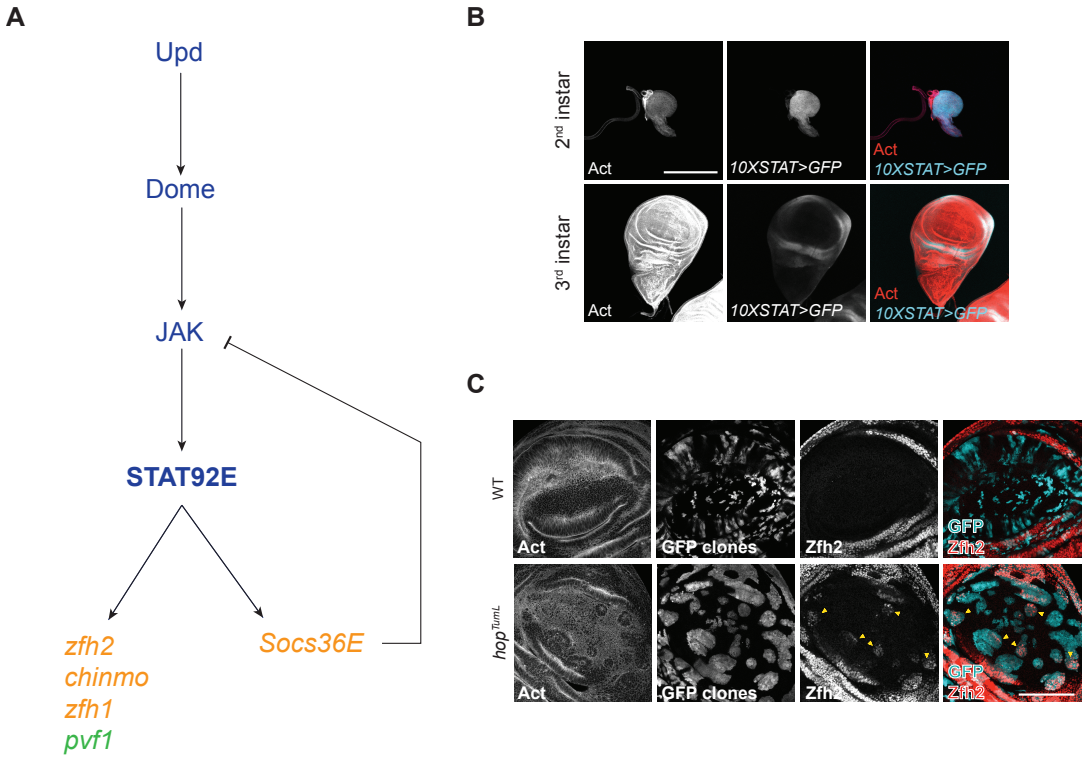

Figure 2. The JAK/STAT signaling in wing imaginal discs.

(A) Schematic representation of the JAK/STAT pathway in *Drosophila*. (B) *10XSTAT>GFP* reporter in wing imaginal discs of 2nd and 3rd instar larvae (cyan in overlay) co-stained with Act (red in overlay). Scale bar = 300 µm. (C) Mosaic tissue of cells (GFP positive cells, cyan in overlay) over expressing the dominant mutant Hop^{TumL} show ectopic activation of Zfh2 (red in overlay) in the GFP positive clones (yellow arrowheads). Scale bar = 100 µm.

Despite this wealth of work, little is known about target genes mediating proliferative JAK/STAT function. In a fly tumour model, STAT92E-responsive enhancers have been mapped [71], but only a few potential target genes regulating tissue size have been described [68, 81, 82]. However, multiple studies have shown that developmental functions of JAK/STAT signalling are mediated by the transcriptional repressors Chinmo [83], Zfh1 [84, 85] and Zfh2 [64, 86, 87] (Fig. 2C).

In my thesis, I link the activation of JAK/STAT signalling to a pro-survival function rather than a direct mediator of compensatory proliferation upon stress induction.

1.4 Chromatin dynamics during tissue stress response

Tissue stress response is a complex mechanism that works at many different levels. Intuitively, cells need to change their transcriptome in order to overcome alteration to their physiological state and re-establish homeostasis. In the last decade, the importance of chromatin regulation during such response has been extensively demonstrated [88, 89]. Alterations in the function of chromatin regulators can lead to the loss of the ability of tissues to properly respond to stress. Among many chromatin regulators, the Polycomb Repressive Complexes 1 and 2 (PRC1 and PRC2) are known to be essential in such responses [90]. By driving the lysine 27 (K27) tri-methylation on the histone H3 (H3K27me3), PRC2 complex creates an epigenetic mark to recruit the PRC1 complex through the activity of the chromodomain in the Polycomb (Pc) protein, which binds the methyl group on histone lysine residues. Pc protein is a stoichiometric component of the PRC1 complex together with Polyhomeotic (Ph), Posterior Sex Comb (PSC) and dRING. Once bound, PRC1 is thought to maintain chromatin in a highly condensed state and thereby limiting DNA accessibility to other factors [91-95]. Highly condensed chromatin is usually associated with a repressed state of gene transcription. Thus, PRCs function has been related to gene silencing [94]. Interestingly, signalling activated during stress response can modulate the activity of the PRCs inducing changes in gene expression and on the organisation of the genome [45, 70, 96-98]. Stress-dependent changes to the activity of the PRC1 in response to wounding have been shown to lead to trans-determination of cells, indicating the important role that this protein complex plays in establishing and maintaining cell identity [45].

The importance in regulating chromatin during tissue stress response doesn't concern only chromatin repressors. Trithorax Group Complexes (TrxC) counteract the activity mediated by PRCs. TrxC mediate methylation of the lysine 4 of histone H3 (H3K4me3), methylation of lysine 36 of the histone H3 (H3K36me3) and histone acetylation, thereby creating the proper conditions for transcriptional activation through chromatin de-condensation [91]. Recent studies have shown that during wound healing, impaired activity of the Trithorax protein (Trx) strongly affect the proper activation of JNK signalling interfering with tissue stress responses [99]. TrxCs are not only characterised by the presence of methyltransferases. but also by Histone Acetyl Transferases (HATs) essential for the

process of chromatin de-condensation. The HAT protein Nejire (Nej, CBP in mammals), is known to associate with the two proteins Absent Small or Homeotic discs 1 (ASH1) and the cleaved N-terminal domain of the Trx [91]. The formation of this complex is essential to allow gene transcription.

To date, our state of knowledge refers to a complex cross talk between chromatin and cell signalling during tissue stress responses. However, which specific signalling can affect the chromatin landscape and to what extent chromatin regulation facilitates tissue stress response, needs to be further investigated.

1.5 DamID-seq profiling to study chromatin dynamics

DamID-seq profiling is a method relying on genetic tools that allows the analysis of DNA-protein interactions at a genome-wide scale. A *protein of interest* (POI) is used to create a *protein of fusion* (POF) made of the POI and the bacterial protein Dam cloned from *E. coli.* The Dam protein drives DNA methylation on adenine (m6A) solely in GATC sequences. In prokaryotes, the function of the Dam protein is of crucial importance in many cellular processes [100]. Absent or at almost undetectable levels in eukaryotes, the GA^{m}TC modification can be ectopically add to the genome by expression of the DamID POF construct. In this way, GATC sequences, which flank regions bound by the POI, will be preferentially methylated and converted in GA^{m}TC. Considering that too high of m6A levels are toxic to cells, low expression levels of the DamID POF construct are crucial to properly identify protein-DNA interaction. Therefore, a careful choice about the genetic conditions to induce DamID POF expression is needed, which should be in a low range but still high enough to acquire reliable information about the protein-DNA interactions. Once methylated, the GA^{m}TC sequences of an extracted genome can be recognised and restricted by the Dpn-I restriction enzyme. This protocol step creates fragments that are defined by two terminal GA^{m}TCs. The length of such fragments primarily depends on the nature of the POI as well as the actual localisation of the GATC along the genome (at every 600 bp on average in the fly genome). The digested GATC fragments are subsequently ligated to specific adaptors, which facilitate PCR-mediated amplification of methylated DNA fragments before NGS sequencing. Notably, not all GATCs of a genome are methylated after induction of the DamID construct. These unmethylated GATC sequences are not recognised by Dpn-I enzyme and therefore do not create free DNA ends for adaptor ligation. After adaptor ligation, digestion of un-methylated GATC sites by an Dpn-II restriction enzyme increases the detection of POI binding sites [101].

Compared to chromatin immunoprecipitation (ChIP), DamID doesn't require sample fixation or immunoprecipitation. These two steps are crucial in ChIP protocols and they can drastically affect the read out of the technique. Fixation and antibody usage always needs to be optimized for the protein that is studied. Thus, DamID has the potential to facilitate assembly of more standardise profiles obtained from different protein-DNA interactions. However, DamID cannot be used to study protein-DNA interaction linked to different post-translational modifications (PTMs) on chromatin (e.g. PTMs on histone or transcription factors).

Importantly, because genetically encoded, any DamID POF construct can be spatially induced in a subset of cells during a specific time period [102]. I personally supervised and tutored the project that led our lab to demonstrate that DamID can also be used to study protein-DNA interactions in a specific cell lineage [103]. Thus, in contrast to ChIP, DamID overcomes problems of signals coming from cells outside the region of interest and avoids cell-sorting necessary for ChIP protocols. Despite these differences, ChIP and DamID protocols have been shown to give results that are in agreement between each other and have comparable resolution of binding profiles [104-109].

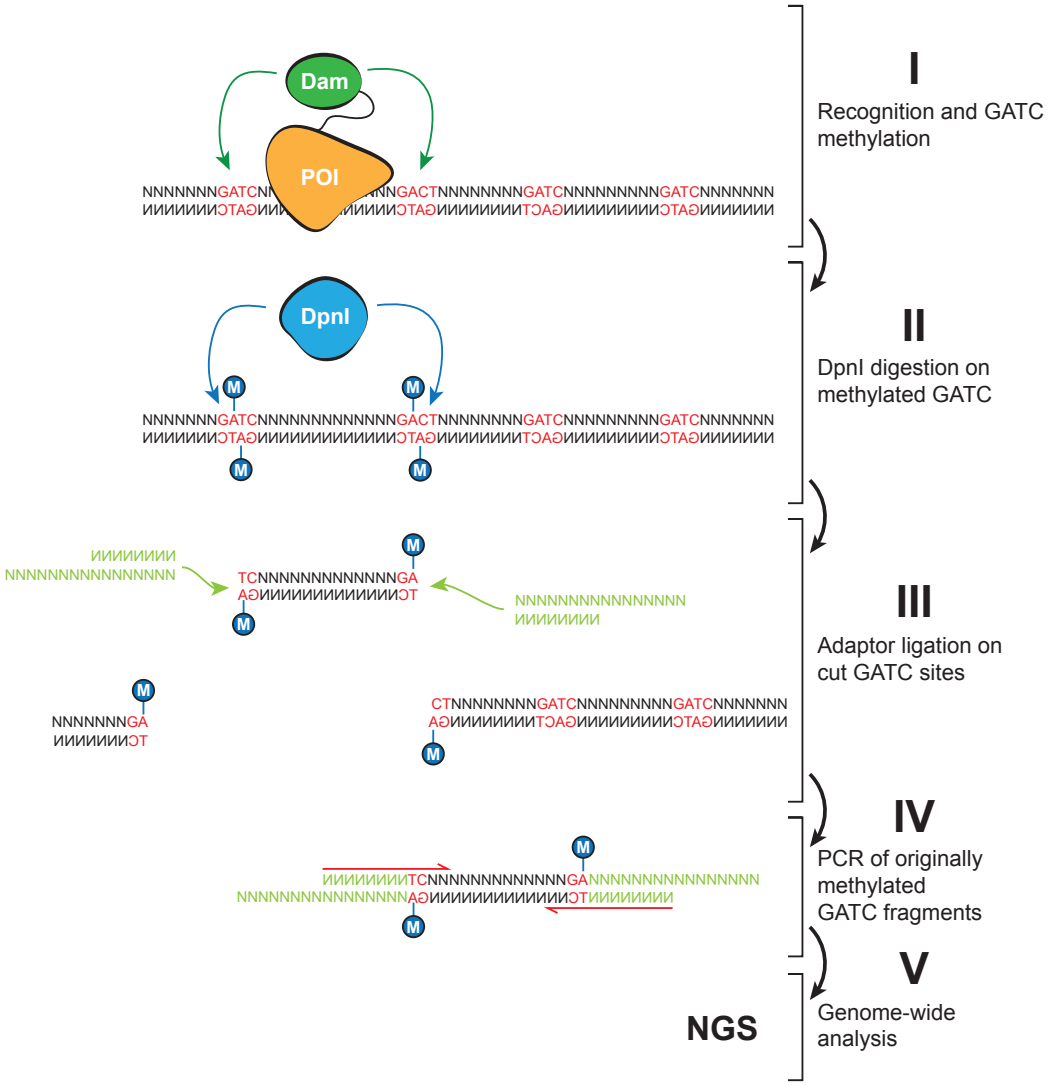

Figure 3 Schematic representation of the DamID-seq protocol.

Here, I made use of the DamID-seq technique to study the binding profile of PRC1 during tumour formation and development. To do so, I chose to analyse the binding of the Pc protein in tumorous wing imaginal discs of *Drosophila*. To date, DamID has never been applied to imaginal discs; thus, my approach led me to establish a DamID-seq protocol for the purpose of obtaining profiles from these widely studied progenitor tissues (Appendix III).

In my thesis, I also provide evidence that, although being a suitable approach to compare specific protein-DNA interactions between different samples, the DamID technique needs to be critically evaluated to look at differences in protein-DNA interactions at different *loci* within the same sample. In addition, I provide preliminarily results that tested hypothesis that DamID is a useful tool to study the localisation of open chromatin domains.

2 Aim of this study/ Scope of this thesis

The overall aim of this work was to elucidate the role of a JAK/STAT signalling as well as the analysis of signalling-mediated chromatin dynamics during JNK-dependent tissue stress responses.

During tissue stress responses, cells in a tissue need to balance pro-survival and apoptotic signalling, both of which are essential to restore overall tissue homeostasis. The JNK pathway is the key regulator of compensatory responses as well as elimination of unfit cells through apoptosis. To address this aim of my thesis, I made use of an inducible genetic system under spatial and temporal control that drove cell death by the activation of JNK signalling in vivo. This method allowed me to analyse diverse cellular behaviours in response to stress induction. This objective was extended to the analysis of conditions representing chronic stress, such as tumour formation. Specifically, I wanted to study how crosstalk between JAK/STAT and JNK cooperates in neoplasiae driven by a mutation in the cell polarity organiser gene *scribble (scrib)*. I furthermore aimed to enhance these signalling studies by providing an analysis on dynamic chromatin behaviour during stress. Given its previously suggested relevance during tissue stress responses, I wanted to generate binding profiles of Polycomb protein (Pc), component of the Polycomb Repressive Complex 1 (PRC1), in tumour and wild type tissues using DamID-seq technology. I aimed to link changes in Pc binding at specifically deregulated genes to specific activated signalling pathways during tumor formation and stress induction. This analysis would led me to define how specific these cross talks are and whether they could be specifically descriptive of stress conditions during tumor growth.

3 Results

3.1 Activation of JNK-signalling by *eiger*-expression enables functional studies of JNK-dependent tissue stress responses

In order to induce cell death, I expressed *eiger* under the control of *rotund (rn)-GAL4* [11]. *rn* is known to be expressed in the pouch of the wing imaginal disc (Fig. 4A) [110], which is fated to give rise to the future adult wing blade. I start inducing *eiger*-expression at day 7 of development after egg deposition. The *UAS-eiger* expression was temporally limited to 40 hours by using a temperature-sensitive version of the GAL80-repressor (Appendix I). After the induction of Eiger expression, I could observe the expected extensive cell ablation in imaginal discs, which resulted in about 50% reduction in adult wing size (Appendix I). FACS analysis revealed that about 85% of the *rnGAL4*-expressing cells where eliminated after 40 h of Eiger-expression. This analysis was possible by using the G-trace lineage labelling method [111], which I used to mark the *rnGAL4*-lineage cells (Fig. 4A-B'').

In agreement with previous studies [112], I found that induction of *eiger* resulted in a broad activation of the JNK-responsive *TRE*-reporter (Fig. 4D) [113]. Completely absent in the wild type discs, the *TRE*-reporter was significantly high at the wound site in the pouch (Fig. 4C-D). Its activation was not limited to the actual wound site. *TRE* activation extended beyond the *eiger*-expressing cells (G-trace labelled) in agreement with the cell non-autonomous activation of JNK by Eiger [32] and by tissue damage (Fig. 4D). Quantification by FACS analysis proved that 29% of cells in the disc activated *TRE-GFP* compared to 5% of cells in unablated wild type discs, while only the 4.5% of cells in the disc belonged to the surviving *rnGAL4*-lineage (Fig. 4E-E').

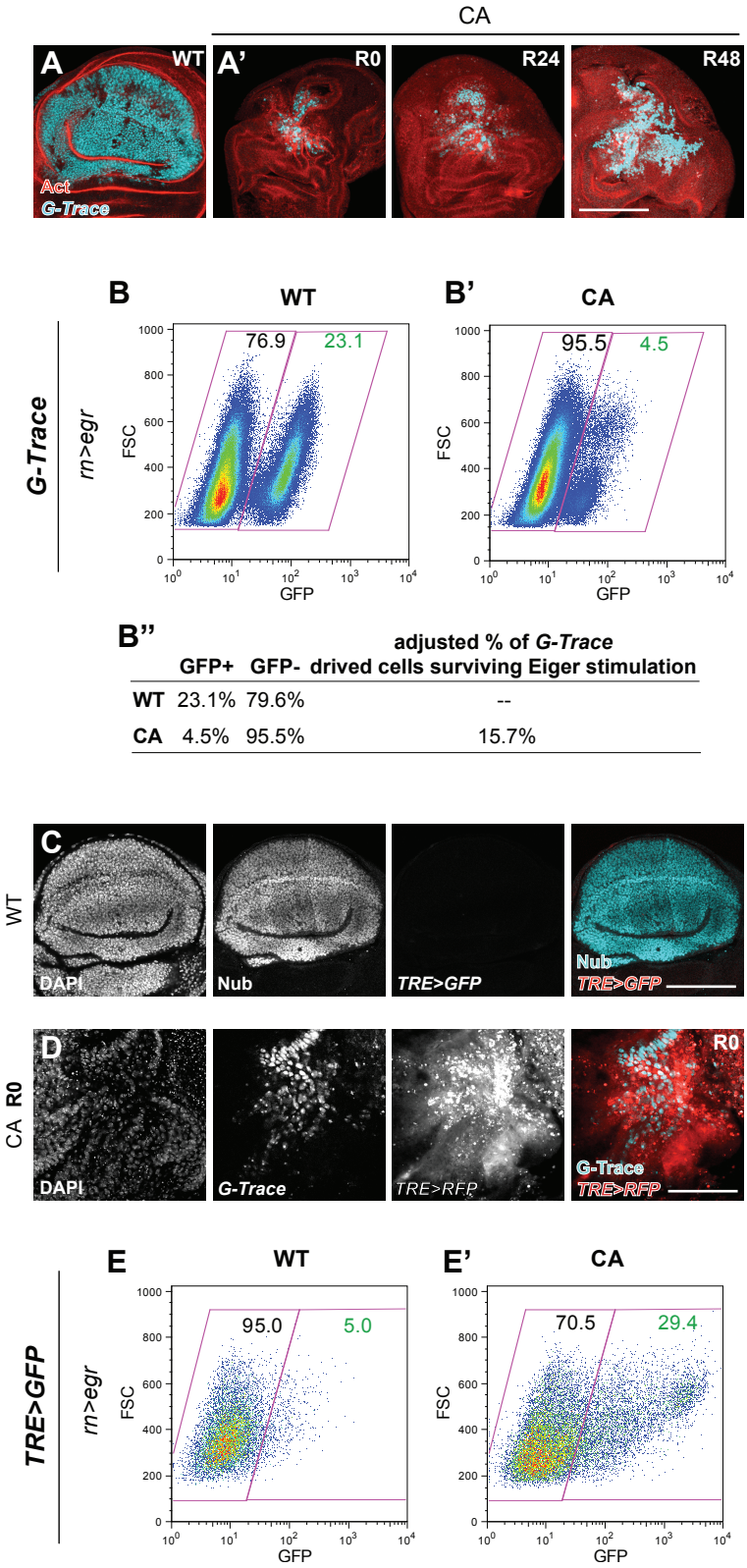

Figure 4. Eiger-expression enables functional studies of JNK-dependent tissue stress responses.

(A) G-trace lineage labelling (cyan) visualizes cells belonging to a rotund(rn)GAL4-derived lineage in the wing pouch of third instar wing imaginal discs. (A') Progeny of *rnGAL4*, *G-trace* labeled cells (cyan) after 40 h of Eiger-mediated cell ablation (CA) at recovery time points R0, R24, R48 hours. Discs were stained for Actin (red). (B) FACS analysis of *rnGAL4*, *G-trace*-labeled cells expressing GFP in wild type

(B) and in wing disc after Eiger-mediated cell ablation (B'). Data is plotted as a function of GFP-levels and forward scatter (FSC). To quantify the relative number of *rnGAL4*, *G-trace*-labeled cells that survive (B''), we made use of the following equation $X = (CA_{GFP+} * WT_{GFP-}) / (CA_{GFP-} * WT_{GFP+})$. (C) Wing pouch of a wild type wing disc expressing the JNK-reporter *TRE-GFP* (red in overlay), stained for DAPI, and for Nubbin (cyan in overlay) to visualize a cell lineage similar to *rnGAL4*-derived cells. (D) Wing pouch after Eiger-mediated cell ablation (CA) expressing the JNK-reporter *TRE-RFP* (red in overlay) and containing *rnGAL4*, *G-trace* labeled cells (cyan in overlay) stained for DAPI. All scale bars: 100 µm.

To additionally prove the efficacy of the *eiger*-expressing method to study compensatory mechanism triggered by stress induction, I wanted to monitor cell proliferation in Eiger-stimulated discs during the recovery time after cell ablation induction. The quantification was run around the wound site only as well as in the whole disc at different recovery time points: at 0 h (R0), at 24 h (R24) and at 48 h (R48) (Appendix.1). Combining different algorithm in Fiji, I developed an automated image-quantification method to specifically measure total wing disc volume, the size of the surviving *rnGAL4*-lineage (G-Trace labelled), the number of cells in mitosis marked by phospho-histone 3 (pH3) or in S-phase marked by BrdU incorporation (Fig. 5A-B, 5D-F, Appendix I). G-trace labelled cells in the pouch at R0 accounted for about 3% of the total disc volume (Fig. 5A), which was in agreement with the previous FACS analysis. It is important to notice that FACS measurements also detected an additional subset of G-trace labelled cells in the disc notum. Thus, this specific FACS quantification was affected by an overestimation.

The automated image analysis unveiled a significant increase in cell proliferation between R0 and R24, at wound site (Fig. 5C) as well as in the entire disc (Fig. 5D-E). pH3 counts do not show any difference between R24 and R48 (Fig. 5C-D). Quantification of the G-trace labelled cell population compared to the total disc volume demonstrated an increased size by 36% and 126% respectively from R0 to R48 (Fig. 5A-B).

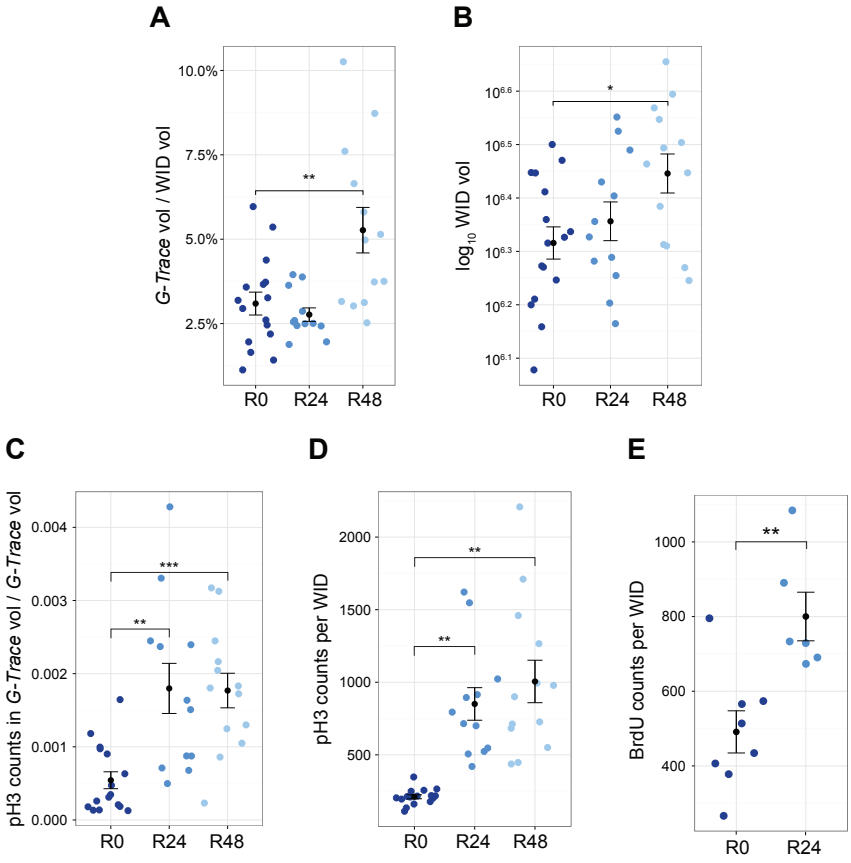

Figure 5. Eiger-expression induces activation of compensatory proliferation.

(A) Quantification of volume space occupied by *rnGAL4*, *G-trace* labeled cells at recovery time points R0, R24 and R48. (B) Quantification of total wing disc volumes at recovery time points R0, R24 and R48. (C) Quantification of pH3-positive, mitotic events within *rnGAL4*, *G-trace* labeled volume space at R0, R24, R48. Mitotic counts were normalized to total *rnGAL4*, *G-trace* labeled volume per disc. (D) Quantification of pH3-positive, mitotic events within total disc volumes at R0, R24, R48. (E) Quantification of BrdU-positive events within Eiger-stimulated discs at R0 (n= 8 discs) and R24 (n= 6 discs). Graphs display mean ± S.E.M for R0 n=16, R24 n=12, R48 = 13 discs. U-tests were performed to test for statistical significance (* p<0.05, ** p<0.01, *** p<0.001).

Cell ablation can be also induced by transient expression of other pro-apoptotic transgenes. Using the same protocol for *eiger*-expression, I induced *reaper*-expression [10]. Although Reaper is more efficient in inducing cell death than Eiger, I did not observe a broad and persistent activation of JNK in this additional experimental condition compared to *eiger* ablated discs (Fig. 5A-B).

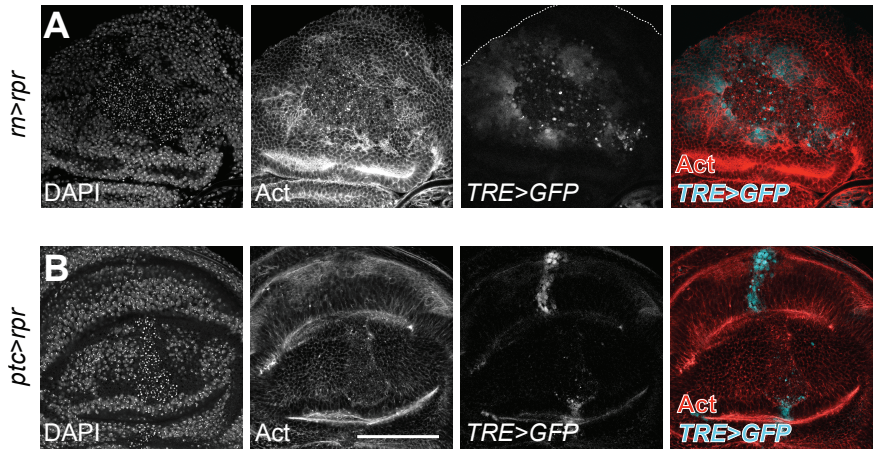

Figure 6. Cell ablation by expression of pro-apoptotic gene reaper doesn't induce broad activation of JNK signaling.

Wing pouch of discs expressing the JNK-reporter *TRE-GFP* (cyan in overlay), co-stained for DAPI or Actin (red in overlay). Discs were subjected to transient cell ablation driven by *rnGAL4*, *UAS-reaper (rn>rpr)* (A) or by *patched(ptc)*-GAL4, UAS-*reaper (ptc>rpr)* (B). Compare to Fig. 1C, D.

Given the broad JNK-activation and the genetic access to JNK-signalling cells, I chose to perform my experiments using the pro-apoptotic gene *eiger* to investigate the role of JAK/STAT in JNK-mediated responses upon tissue stress induction.

3.2 JAK/STAT signalling is activated in response to Eiger-induced tissue damage

In order to understand whether JAK/STAT plays a part in tissue stress response upon cell ablation, I studied JAK/STAT activity in response to *eiger*-expression. To study JAK/STAT activation I made use of the *10xSTAT-dGFP* reporter [114]. Mostly undetectable in the wild type imaginal disc, *dGFP* (*degradable-GFP*) signal allowed me to detect JAK/STAT activation at a real time scale by diminishing background noise (Fig. 7A). Induction of cell ablation at day 5 (D5) or day 7 (D7) of development showed activation of the JAK/STAT signalling (Fig. 7B,C). JAK/STAT activation was also induced upon *UAS-reaper* mediated cell ablation, suggesting that tissue stress caused by ectopic cell death is sufficient to lead to JAK/STAT activation (Fig. 7E). It is important to mention that in Eiger-stimulated discs JAK/STAT activation was not restricted at the wound site only. Its activation spread away from the pouch periphery and thus extended beyond domains with active JNK signalling marked by the *TRE*-reporter (Fig. 12A-B).

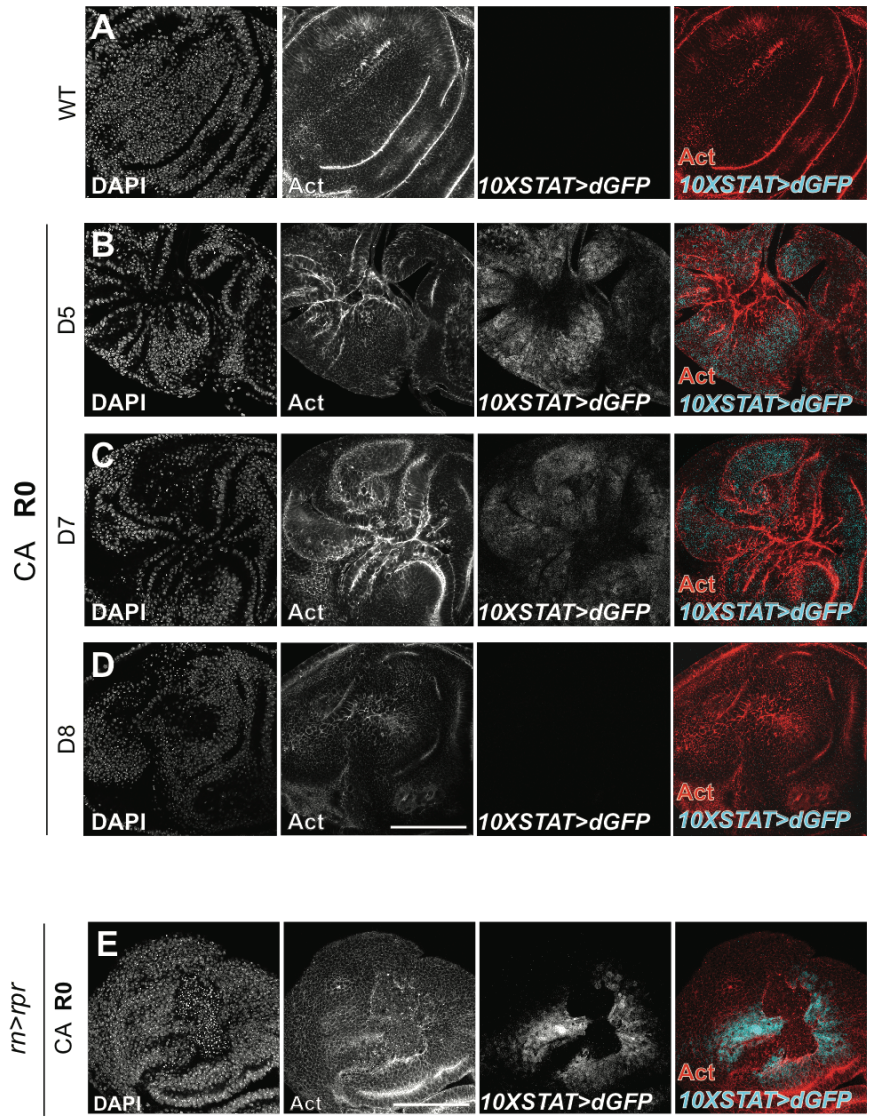

Figure 7. JAK/STAT is activated in response to Eiger-induced tissue damage.

(A) Wild type wing disc expressing the JAK/STAT-reporter *10XSTAT-dGFP* (cyan in overlay) stained for DAPI and Actin (red in overlay). (B-D) Wing pouch after Eiger-mediated cell ablation (CA) induced at developmental day 5 (B), day 7 (C) or day 8 (D). Discs express the *10XSTAT-dGFP* reporter (cyan in overlay) and were stained for DAPI and Actin (red in overlay). (E) Wing pouch after transient cell ablation (CA) was induced by *rnGAL4*, *UAS-reaper* (*rn>rpr*). Disc expresses the *JAK/STAT-reporter 10XSTAT-dGFP* (cyan in overlay), and was stained for DAPI and Actin (red in overlay). Compare to Fig. 4B. All scale bars: 100 µm.

Within the following 24 h, JAK/STAT signalling declined suggesting that its activity is successively down regulated after *eiger*-expression terminated (Fig. 8A-B compare to Fig. 8A'-B'). Analysis of JAK/STAT activation patterns, when *eiger* was expressed at later stages of larval development, revealed that JAK/STAT activity resulted to be almost undetectable when cell ablation was driven at day 8 (D8) (Fig. 7D, Fig. 8C-C').

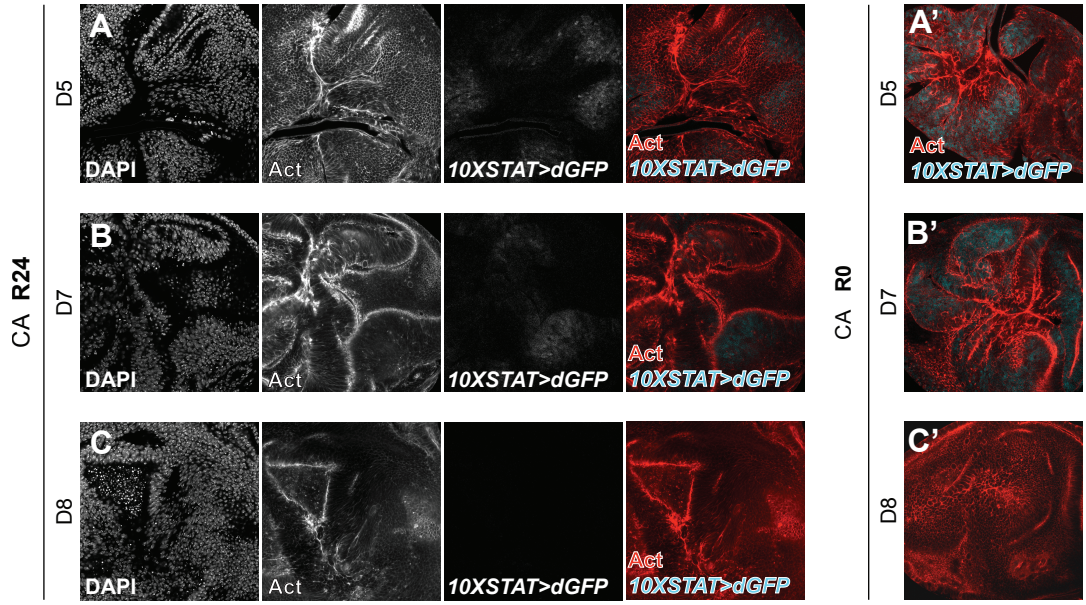

Figure 8. JAK/STAT activation declines during recovery time after cell ablation.

(A-C) Wing pouch after eiger-expression was induced at developmental day 5 (A), day 7 (B) or day 8 (C) and imaged at R24. Discs express the JAK/STAT-reporter *10XSTAT-dGFP* (cyan in overlay) and were stained for DAPI or Actin (red in overlay). Overlay images obtained at R0 are shown for comparison (A'-C').

3.3 Unpaired-ligands are transcriptionally upregulated in response to Eiger-induced tissue damage

Previous reports and my work demonstrated that the JAK/STAT ligands *upd1, upd2* and *upd3* are transcriptionally upregulated in response to stress from physical injury [8, 76] or tumorous growth [40, 72], suggesting that pathway upregulation may be driven by JNK-dependent *upd* ligand transcription.

Using qPCR, I confirmed that transcription of *upd* genes were high in their transcriptional levels in Eiger-stimulated discs, whereas the other major component of the pathway *dome*, *hop* and *Stat92E* were not (Fig. 9A). Recapitulating the decline of *10xSTAT-dGFP* reporter activities, *upd1, upd2* and *upd3* transcription was strongest at day 5 and day 7 but dropped by more than half when *eiger* was induced at day 8 (Fig. 9A). Decrease of JAK/STAT activation at day 8 was not due to a decline in Eiger-mediated JNK-activation.

Notably, *TRE*-reporter activation did not show any recognizable difference between day 8 and day 7 (Fig. 9B-C). Although JNK has been proposed to be a JAK/STAT activator [8, 76], my data indicates that JNK alone is not sufficient to induce JAK/STAT pathway during tissue stress response. Interestingly, drop in the JAK/STAT activity at late

developmental stages positively correlated with a failure in the ability of larvae to mediate a developmental delay at the larval-pupal transition (Fig. 9D) and with a significant reduction in recovered adult wing size (Fig. 9E). These correlations indicate the JAK/STAT pathway as a crucial mediator of JNK-induced compensatory responses during stress response in imaginal disc.

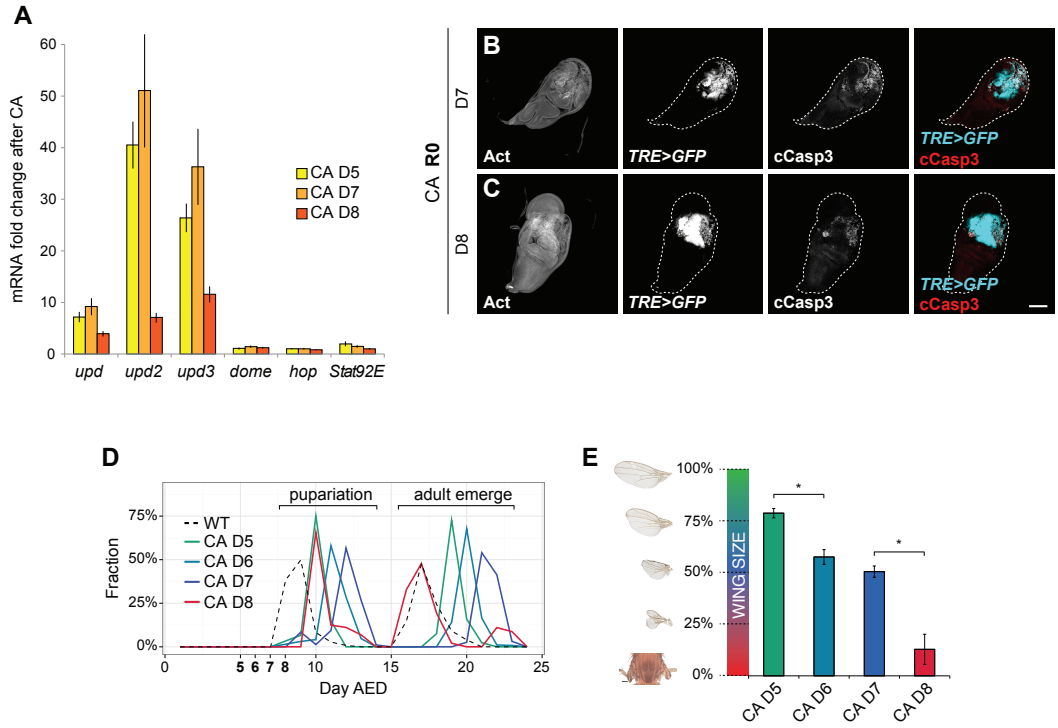

Figure 9. The extent of the JAK/STAT activation correlates with the ability of the tissue to respond to stress induction.

(A) qRT-PCR analysis of mRNA expression levels of the JAK/STAT components *upd1*, *upd2*, *upd3*, *dome*, *hop* and *Stat92E* after Eiger-mediated cell ablation (CA) was induced at developmental day 5 (D5), day 7 (D7) or day 8 (D8). Fold-induction relative to unablated control discs at R0 is reported. Graphs display mean ± S.E.M for n≥3 biological replicates. (B-C) Wing discs after Eiger-stimulated cell ablation (CA) induced on D7 (B) or D8 (C). Discs expressing the JNK reporter *TRE-GFP* (cyan in overlay) were stained for Actin and for cleaved Caspase-3 (cCasp3, red in overlay) to visualize apoptotic cells. (D) Incident analysis of larva-to-pupae transition timing as well as adult eclosion timing in wild type animals and in animals where eiger-mediated CA was induced at D5, D6, D7 or D8. (E) Quantification of average adult wing sizes developing from disc after eiger-mediated cell ablation was induced at D5, D6, D7 or D8. All scale bars: 100 μm.

3.4 JAK/STAT activity is not required for compensatory proliferation

JAK/STAT signalling has been largely reported to promote cell proliferation in wild type [67-69] or tumorous imaginal discs [40, 66, 70-72]. More recently JAK/STAT has been suggested to do so also in surgically injured imaginal discs [8], linking its activity directly to

one of the major compensatory mechanism during tissue stress response. To test whether JAK/STAT is generally required to drive compensatory proliferation, I analysed mitotic event in the Eiger-induced system with impaired JAK/STAT signalling. I reduced JAK/STAT activity by using two different genetic approaches: (1) by lowering gene dosage of JAK/STAT components in the entire animal during development, Eiger-stimulation and recovery period by heterozygosity for $dome^{G0441}$, hop^{34} and $Stat92E^{85C9}$ alleles (Appendix I) or (2) by interfering with JAK/STAT signalling exclusively in *eiger*-expressing cells by expressing RNAi constructs targeting JAK/STAT components (Appendix I), as well as a dominant-negative version of *dome* ($dome^{\Delta cyt}$) or the pathway inhibitor *Socs36E*, all under the control of $rnGAL4\text{-}tubGAL80^{ts}$. Even though about 50% of the ablated discs activated JAK/STAT signalling (Fig. 7B-C), discs heterozygous for $dome^{G0441}$, hop^{34} and $Stat92E^{85C9}$ alleles did not have any reduction in cell proliferation or total disc size (Fig. 10A-F). Instead, I could observe a significant, although mild, increase in cell divisions in Eiger-stimulated hop^{34} discs. Opposite to what has been previously suggested, this result uncoupled the JAK/STAT function to directly promote compensatory proliferation. Given its relevance, I wanted to additionally confirm this result by reducing JAK/STAT activity specifically in Eiger-stimulated cells. *rnGAL4*-driven co-expression of *dome* RNAi, $dome^{\Delta cyt}$ or *Socs36E* did not result in reduced number of mitotic events within surviving *eiger*-expressing cells (Fig. 10G-K). Manual count of the number of nuclei and pH3 positive cells confirmed the data obtained by the automated quantifications (Fig. 11A-B). Once more, mitotic rates slightly increased in the survived tissue, while remaining stable in the rest of the disc (Fig. 10K, Fig. 11B, 11D).

It is important to notice that the effect of GAL4-activity declines with time from R0 on during the recovery time. Thus, effects on cell division rates in *eiger*-expressing cells co-expressing transgenic constructs are stronger at R0 than later (Fig. 10K). Taken together, these results argue against the role of JAK/STAT signalling in directly stimulating compensatory proliferation in response to tissue stress.

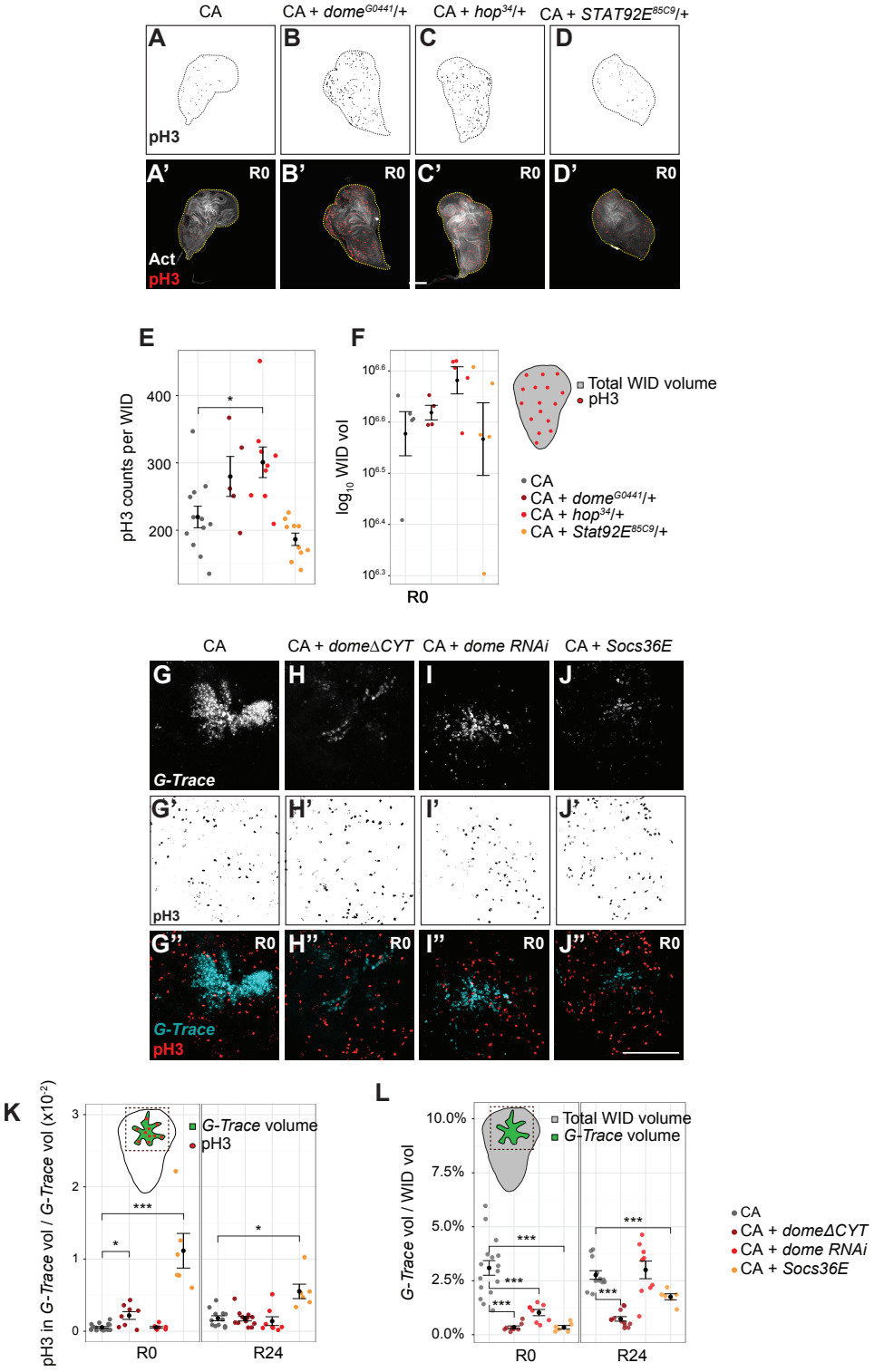

Figure 10. JAK/STAT activation is not required for compensatory proliferation.

(A) Wing disc after Eiger-mediated cell ablation (CA) stained for pH3 to visualize mitotic events (A, red in A', Actin in grey in A'). (B-D) Wing disc heterozygous for *dome*^{G0441} (B,B'), *hop*^{34} (C,C') or *Stat92E*^{85C9} (D, D') after Eiger-mediated cell ablation (CA) stained for pH3 to visualize mitotic events (B-D, red in B'-D'; Actin in grey in B'-D'). (E) Quantification of pH3-positive, mitotic events per disc and (F) quantification of total wing disc volume in wild type (n=12 discs) and in discs heterozygous for domeG0441 (n=5 discs), hop34 (n=9 discs), or Stat92E85C9 (n=10 discs) after Eiger-mediated cell

ablation (CA). (G-J) Wing pouch containing *rnGAL4*, *G-trace* labelled cells that survived Eiger-stimulation (grey in G-J, cyan in G''-J''), stained for pH3 to visualize mitotic events (G'-J', red in G''-J''). A wild type disc (G) and discs with *rnGAL4*-mediated co-expression of *domeΔcyt* (H), *dome* RNAi (I) or *Socs36E* (J) in eiger-expressing cells is shown. (K) Quantification of pH3-positive, mitotic events within *rnGAL4*, *G-trace* labelled volume space and (L) quantification of relative proportions of disc volume occupied by *rnGAL4*, *G-trace* labelled volume at R0 and R24. Wild type discs (CA) (R0 n=16, R24 n=12 discs) and discs with rnGAL4-mediated co-expression of *domeΔcyt* (R0 n= 8, R24 n=12 discs), *dome* RNAi (R0 n=8, R24 n= 9 discs) or *Socs36E* (R0 n= 6, R24 n= 6 discs) in eiger-expressing cells were quantified. Mitotic counts in (K) were normalized to total volume labelled by *G-trace*. Graphs display mean ± S.E.M. U-tests were performed to test for statistical significance (* p<0.05, ** p<0.01, *** p<0.001). All scale bars: 100 µm.

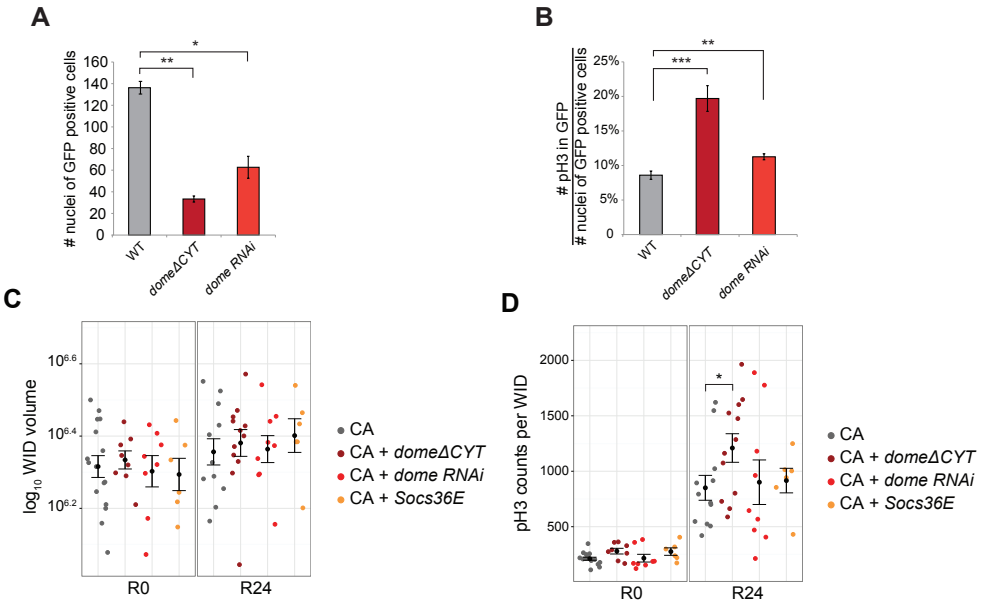

Figure 11. Nuclei counts confirm automated Fiji quantification of volumes and cell proliferation.

(A) Absolute number of nuclei within the *G-Trace* GFP positive area were counted manually (compare to Fig. 7L). (B) Ratio of pH3 counts over the total number of nuclei in the GFP positive region. Counts for both pH3 positive nuclei and total nuclei were done manually (compare to Fig. 7K). Graphs display mean ± S.E.M, n=3 for all genotypes. U-tests were performed to test for statistical significance (* p<0.05, ** p<0.01, *** p<0.001). (C, D) Quantification of pH3-positive, mitotic events per disc (D) and of total wing disc (WID) volume (C) at R0 and R24 after Eiger-stimulation. Wild type discs (CA) (R0 n=16, R24 n=12 discs) and discs with *rnGAL4*-mediated co-expression of *domeΔCYT* (R0 n= 8, R24 n=12 discs), *dome RNAi* (R0 n=8, R24 n= 9 discs) or *Socs36E* (R0 n= 6, R24 n= 6 discs) in eiger-expressing cells were quantified.

3.5 JAK/STAT and JNK signalling have specific activation patterns during tissue stress response.

In order to better understand the spatial activation of JNK and JAK/STAT signalling, I combined the two reporters *TRE* and *10xSTAT-dGFP* respectively, in *eiger*-expressing discs. Cell ablated discs where quantified for both reporter's intensities along segments traced from the centre of the wing disc pouch (PC) toward the hinge (Fig. 12A). *TRE-*

reporter intensity decreased with the increase of distance from the PC. As previously shown (Fig. 7B-C), STAT activation levels are lower at the PC proximity. Interestingly, JAK/STAT activation increased in concomitance to the JNK reduction (Fig. 12A-B).

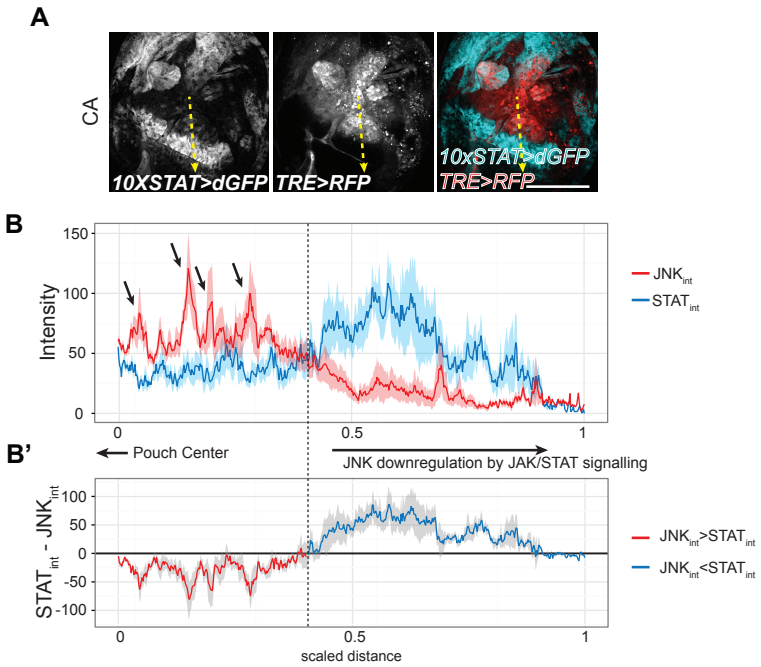

Figure 12. JNK and JAK/STAT have specific activation patterns around the wound site upon cell ablation.

(A) Cell ablated disc carrying both JAK/STAT and JNK reporters were imaged to study the spatial relationship between the two signalling activations. Quantifications of reporters' intensities were obtained on drawn lines of arbitral lengths (yellow dashed arrow) running from the pouch centre towards the hinge region of the imaginal disc. (B) Fluorescence intensity of *rnGAL4*, *G-trace* (n=5 discs), *TRE-RFP* (n=6 discs) and *10XSTAT-dGFP* (n=12 discs) reporter signals were measured at R0. Intensity trace plots were scaled to maximum measured intensity values; averages were interpolated and reported as function of their relative positions between the pouch centre and the disc edge. (B') Difference of averaged scaled reporters' intensities (*10XSTAT-dGFP$_{int}$* - *TRE-RFP$_{int}$*) were calculated and plotted as function of the scaled distance from the pouch centre. All graphs display interpolated mean ± S.E.M. All scale bars: 100 µm.

The *TRE-reporter* profile appeared to be noisier in the region close to the PC with relatively broad and high peaks. These peaks were due to the presence of apoptotic bodies that tend to cluster closer to the wound site or PC in this case. Outside these apoptotic peaks, JAK/STAT and JNK reporter activity resulted to be similar when compared to each other (Fig. 12B). I wanted to better analyse the cross talk between these two signalling pathways in a spatial manner. To do so, I expressed *eiger* in cells together with the inhibitor of apoptosis *p35* using the *rotundGAL4* driver. This approach created a population of undead cells in the *rn*-expressing region. These cells were characterised by high levels of *TRE-reporter* (Fig. 13A). Contrary to the previous experiment, the same cells lacked STAT activation (Fig. 13A). It is important to note that the *TRE-reporter* gradually declined only outside the Eiger-

p35 positive cells, indicating a non-autonomous activation of the JNK pathway in the surrounding tissue (Fig. 13B).

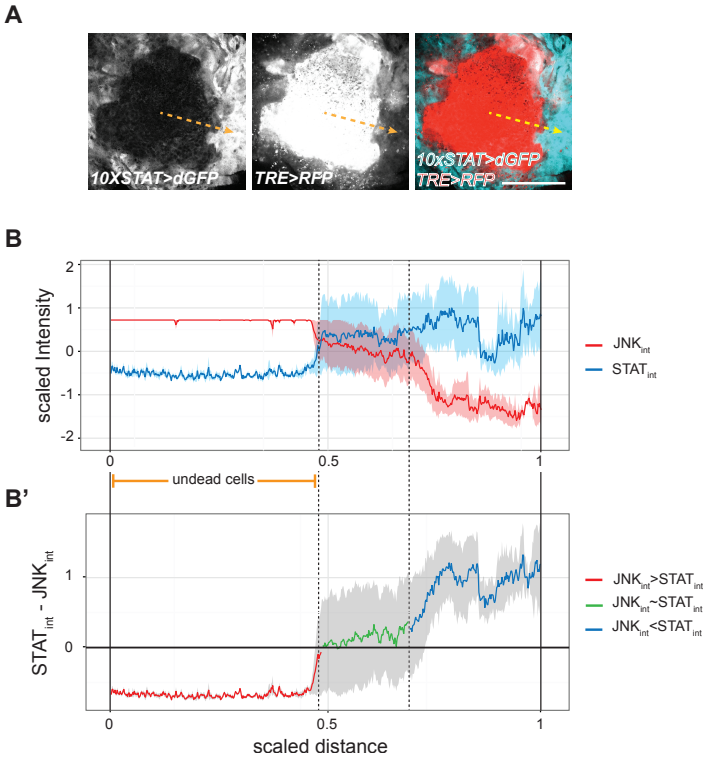

Figure 13. Cell death inhibition defines JNK and JAK/STAT activations in three distinct regions in *rn>egr* discs.

(A) Cell ablated disc carrying both JAK/STAT and JNK reporters were crossed to *UAS-p35* in order to block cell death. Quantifications of reporters' intensities were obtained on drawn lines of arbitral lengths (yellow dashed arrow) running from the centre of the undead cells mass towards the disc hinge. (B) Fluorescence intensity of *rnGAL4*, *G-trace* (n=3 discs), *TRE-RFP* (n=3 discs) reporter signals were measured at R0. Intensity trace plots were scaled to maximum measured intensity values; averages were interpolated and reported as function of their relative positions between the pouch centre and the disc edge. (B') Difference of averaged scaled reporters' intensities (*10XSTAT-dGFP$_{int}$ - TRE-RFP$_{int}$*) were calculated and plotted as function of the scaled distance from the pouch centre. All graphs display interpolated mean ± S.E.M. All scale bars: 100 µm.

In some of the cells outside of the p35-Eiger expressing domain, JNK activation led to induction of apoptosis (Fig. 14A-A'''). Marked by *G-Trace*, p35-Eiger expressing cells did not overlap with strong Dcp-1 staining, which was high in the region outside of the undead-cells (Fig. 14A''). This data confirm published reports that the apoptotic cell-death program is also activated in the wild type cells neighbouring the source of stress [25].

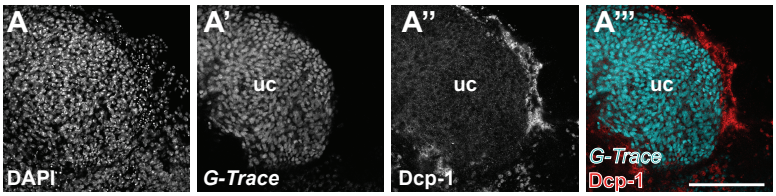

Figure 14. Cell death is non-autonomously induced in wild type cells surrounding the Eiger-p35 undead-cells.

(A-A''') (A) DAPI staining to visualize nuclei in p35-Eiger discs (cyan in overlay). Undead-cells (uc) are marked by *G-Trace* in *rn>egr; UAS-p35* expressing discs (A'). (A'') Apoptotic cells are stained with Dcp-1. (A''') Merge of Dcp-1 and *G-Trace* signal.

Notably, JNK activation seemed to follow a specific pattern that I summarised as a three-state-model: 1- strong activation in p35-Eiger positive (Fig. 13B' red line), 2- constant signaling at lower levels in cells adjacent to the p35-Egier region (Fig. 13B' green line), 3- drastically decreased or no JNK signaling in cells far from the p35-Eiger (Fig. 13B' blue line). JAK/STAT signaling, on the other hand, behaved almost opposite to the JNK pattern described above. Absent in the Eiger-p35 expressing cells, STAT activity increased drastically in cells that were directly apposing undead cells and, JAK/STAT activation was maintained also in those cells far from the PC (Fig. 13B'). These data suggested the two pathways may counteract eachother in regulating tissue stress response.

3.6 Strong JNK activation coincides with JAK/STAT signalling inhibition

Given the lack of STAT activation in the Eiger-p35 cells, I wanted to assess whether the JAK/STAT pathway wasn't activated or even inhibited. I started by looking at the induction of the *upd* gene (Fig. 12A-B'').

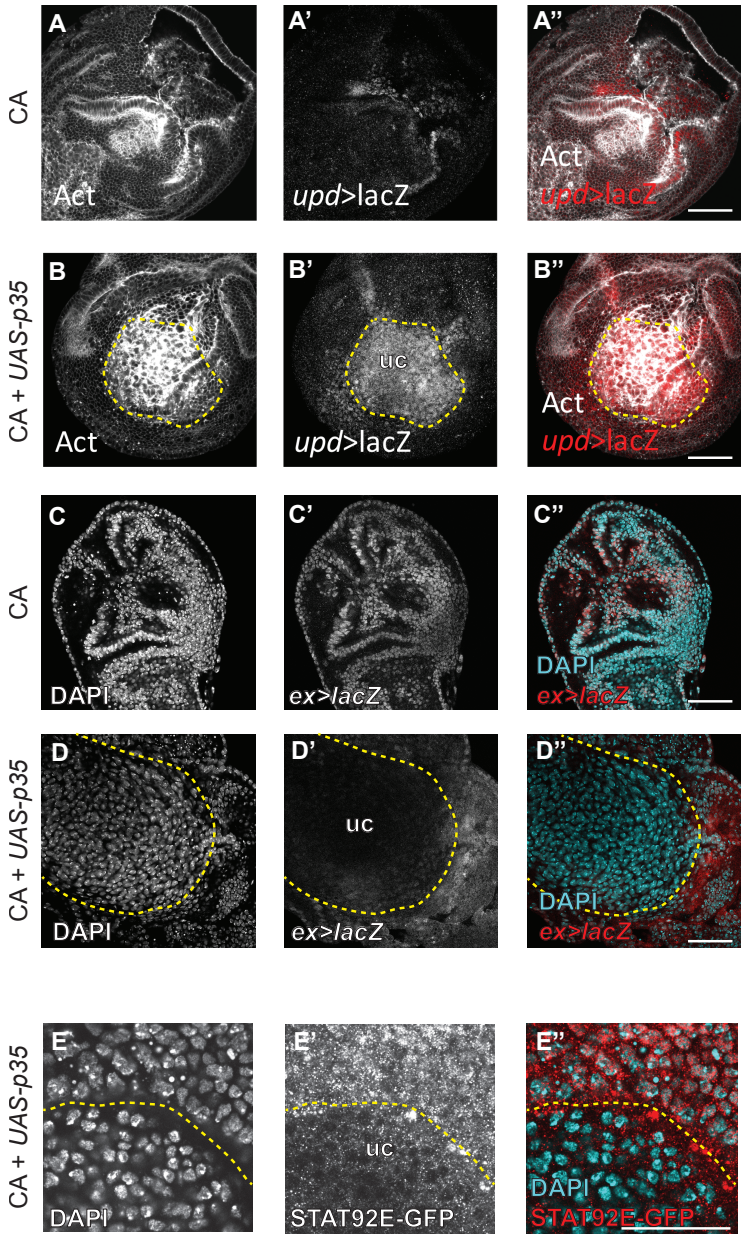

Figure 15. Eiger-p35 cells do not have translocation of STAT92E into the nucleus.

(A-A'') Cell ablated discs (CA) carrying the *upd>lacZ* reporter gene (A'). (B) *upd>lacZ* reporter in disc expressing Eiger-p35. Yellow dashed line highlights the undead-cells (uc). (C-C'') *ex>lacZ* line shows activation of the Hpo/Yki pathway in cell ablated discs. (D-D'') Eiger-p35 discs carrying *ex>lacZ* reporter. Yellow dashed line highlights undead-cells (uc) region. (E-E'') STAT-GFP fusion protein is visualized in Eiger-p35 discs. Yellow dashed line highlights the margin between undead-cells (uc) and wild type tissue. All scale bars= 50 µm.

By using an *upd>lacZ* line, I could show that the expression of the ligand was higher in undead cells and decreased with increasing distance from the PC (Fig. 12A', 12B'). Interestingly, a similar analysis of *expanded* gene expression, which is commonly used as a read-out for Hpo/Yki pathway activity, demonstrated low expression levels of *ex* in undead cells and high expression in the surrounding tissue (Fig. 12C', 12D'). This data confirms

previous reports suggesting that *upd* activation depends on JNK signalling rather than Hpo pathway activity during tissue stress responses [22]. Using a line carrying a STAT92E-GFP fusion protein, I analysed the behaviour of the STAT92E transcription factor in discs co-expressing Eiger-p35. Surprisingly, the STAT92E-GFP tagged protein didn't show translocation into the nucleus in undead cells (Fig. 12E'). On the other hand, STAT92E-GFP translocation happened in the surrounding mwild type tisue. This data was in agreement with *10xSTAT-dGFP* intensities profiles suggesting that the lack of reporter activity was due to the lack of STAT92E translocation into the nucleus (Fig. 10B'', 12E').

3.7 JAK/STAT activity is required for survival of JNK-signalling cells

Quantification of total volumes of Eiger-stimulated discs compared to disc with genetically impaired JAK/STAT activity did not result in any significant difference (Fig. 10F, Fig. 11C). On the other hand, the number of G-trace labelled cells that survived *eiger*-expression was dramatically reduced when JAK/STAT signalling was inhibited. I could demonstrate that induction of cell ablation with co-expression of *dome RNAi*, $dome^{\Delta cyt}$ or *SOCS36E* caused a 3 to 10-fold reduction in the size of G-trace labelled cell populations at R0 (Fig. 10L, Fig. 11A).

These evidences pointed out to a higher dying rate in cell expressing *eiger* when JAK/STAT signalling was impaired. To test such hypothesis, I quantified ablated discs stained for activated cleaved Caspase-3 (cCasp-3). This analysis resulted in a 2-fold increase in the cCasp-3 volumes when JAK/STAT activity was exclusively reduced in *eiger*-expressing cells (Fig. 16A-E). In Eiger-stimulated discs heterozygous for $dome^{G0441}$, hop^{34} and $Stat92E^{85C9}$ the increase in cCasp-3 volume went up to 10-fold (Fig. 16F-I). Notably, the stronger effect observed for heterozygous mutant genotypes could be explained by the global tissue reduction of JAK/STAT activity in these mutants. Indeed, in the heterozygous mutant genotype, this reduction could be also achieved in domains that displayed JAK/STAT and JNK activation but were located outside of the *rnGAL4*-lineage (Fig. 4C).

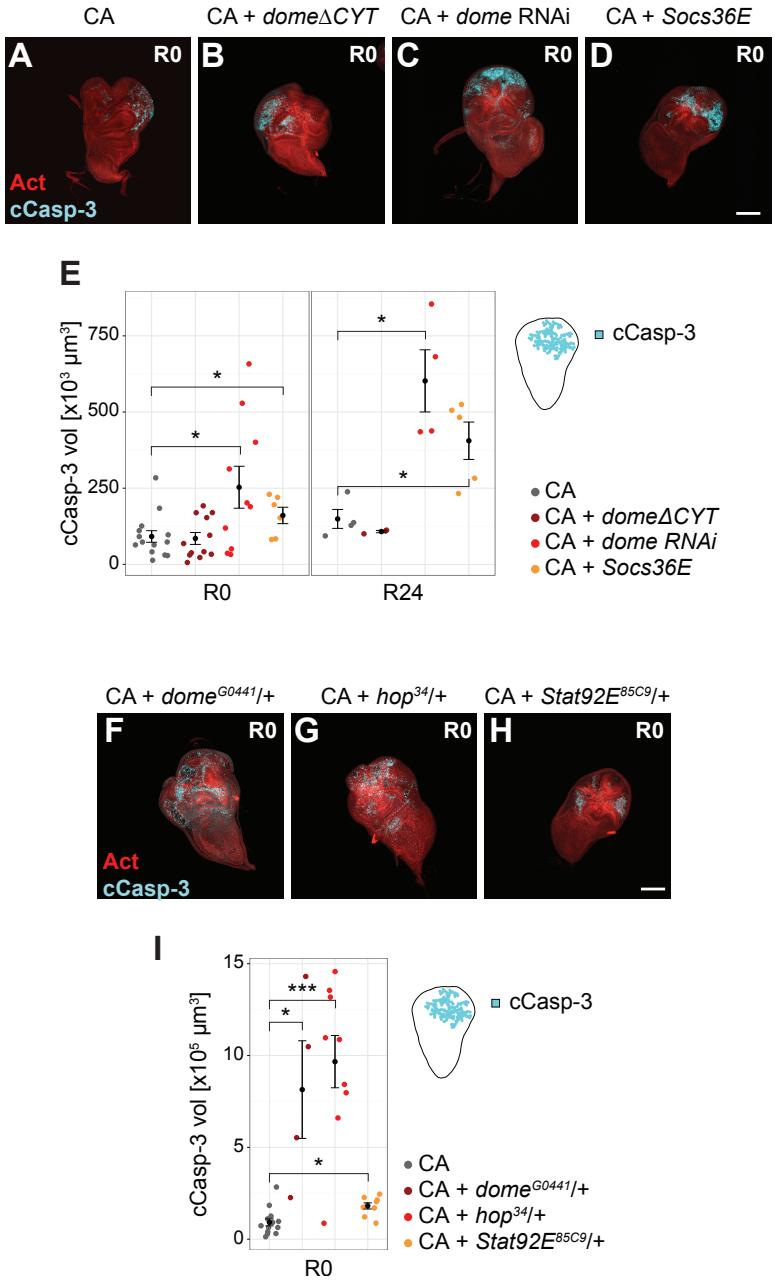
CA
CA + domeΔCYT
CA + dome RNAi
CA + Socs36E
A
B
C
D
R0
Act
cCasp-3
E
cCasp-3 vol [x10³ µm³]
750
500
250
0
R0
R24
cCasp-3
CA
CA + domeΔCYT
CA + dome RNAi
CA + Socs36E
CA + dome^G0441/+
CA + hop^34/+
CA + Stat92E^85C9/+
F
G
H
I
cCasp-3 vol [x10⁵ µm³]
15
10
5
0
CA + dome^Δcyt (B), dome RNAi (C), or Socs36E (D) in eiger-expressing cells stained for Cleaved Caspase-3 to visualize apoptotic cells (cyan) and Actin (red). (E) Cleaved Caspase-3 volume in ablated discs (CA, R0 n=15, R24 n= 4 discs) or with rnGAL4-mediated co-expression of dome^Δcyt (R0 n= 12, R24 n= 3 discs), dome RNAi (R0 n= 10, R24 n= 4 discs), or Socs36E (R0 n= 6, R24 n= 6 discs) in eiger-expressing cells at R0 and R24. (F-H) Ablated discs heterozygous for dome^G0441 (F), hop^34 (G) or Stat92E^85C9 (H) stained for Cleaved Caspase-3 (cyan) and Actin (red) at R0. (I) Cleaved Caspase-3-positive volumes per disc after cell ablation (CA) (n= 12 discs) or in discs heterozygous for dome^G0441 (n= 4 discs), hop^34 (n= 9 discs), or Stat92E^85C9 (n= 8 discs) at R0. Graphs display mean ± S.E.M. U-tests were performed to test for statistical significance (* p<0.05, ** p<0.01, *** p<0.001). All scale bars: 100 µm.

Confirming the specificity of JAK/STAT role in tissue stress response, genetic reduction of JAK/STAT signalling in developing wild type discs under the same conditions does not cause any elevation of apoptotic cell counts (Fig. 17A-D).

The data points out to a specific role for JAK/STAT as an important mediator of cell survival specifically in JNK signalling cells, which initiate compensatory responses to tissue damage.

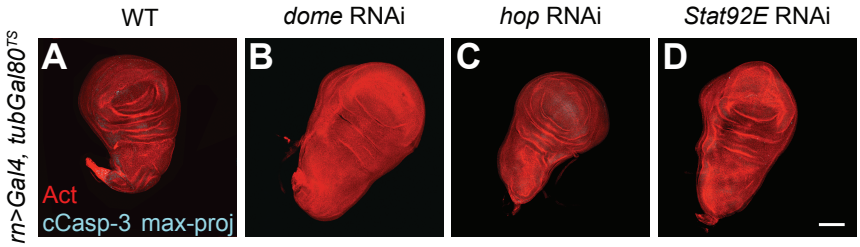

Figure 17. Transient down regulation of the JAK/STAT pathway does not cause cell death in wild type discs during normal development.

(A-D) Wild type wing disc (A) and wing discs with *rnGAL*4-driven expression of *dome* RNAi (B), *hop* RNAi (C) or *Stat92E* RNAi (D) induced at D7 for 40 hours were stained for Actin (red) and for Cleaved Caspase-3 (cyan) to visualize apoptotic cells. Maximum projections of entire image stacks are shown. Graphs display mean ± S.E.M. U-tests were performed to test for statistical significance (* *p<0.05,* ** *p<0.01,* *** *p<0.001*). All scale bars: 100 µm.

3.8 JAK/STAT activity suppresses activation of JNK-signalling

To understand how JAK/STAT signalling may promote cell survival, I tested if genetic reduction of JAK/STAT activity resulted in further elevation of JNK, which could alter JNK-dependent compensatory responses and lead to apoptosis. I controlled JNK-activity using the *TRE*-reporter in *eiger*-expressing discs heterozygous for $dome^{G0441}$, hop^{34} and *Stat92E* ^{85C9} alleles. Quantifications for the *TRE* positive area suggested that upon Eiger-mediated cell ablation, 14% of the wing disc area activated the *TRE*-reporter in wild type discs (Fig. 18A, E).

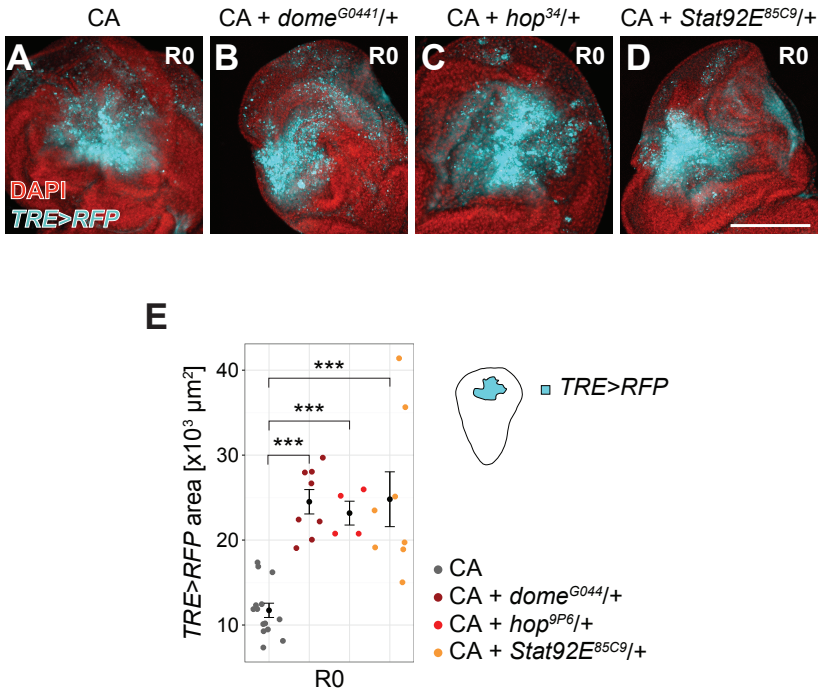

Figure 18. Down regulation of JAK/STAT, in ablated discs, results in broader activation of JNK signaling.

(A-D) Disc expressing the JNK reporter *TRE*-RFP (cyan) after cell ablation (CA) (A) or if heterozygous for *dome*^{G0441}(B), *hop*^{34} (C), or *Stat92E*^{85C9} (D) at R0. (E) Quantification of *TRE*-RFP positive area per disc after cell ablation (CA) (n= 14 discs) and in discs heterozygous for *dome*^{G0441} (n= 8 discs), *hop*^{34} (n= 4 discs), or *Stat92E*^{85C9} (n= 8 discs). Graphs display mean ± S.E.M. U-tests were performed to test for statistical significance (* *p<0.05,* ** *p<0.01,* *** *p<0.001*). All scale bars: 100 µm.

In heterozygous disc for *dome*^{G0441}, *hop*^{34} and *Stat92E*^{85C9} we observed a 2 to 3-fold increase in the area positive for *TRE*-reporter activation after Eiger induction (Fig. 18B-E). These results indicate that broad reduction of JAK/STAT signalling induces non-autonomous expansion of JNK activation far beyond *eiger*-expressing cells and that this may underlie the observed increase in apoptotic index in JAK/STAT-impaired, Eiger-stimulated discs (Fig. 16A-I).

These observations led to two hypotheses. First, the broad activation of JNK in JAK/STAT impaired discs suggested that JAK/STAT acts as a suppressor of JNK signalling. Repression of JNK by JAK/STAT could either be mediated by direct transcriptional effects on JNK core components, or indirectly, by suppression of apoptosis through prevention of Dronc-driven positive feedback activation of JNK. This mechanism would restrain non-cell autonomous activation of JNK, excessive apoptosis and tissue damage. A second prediction implies that interfering with JAK/STAT increases the extent of tissue damage due to elevation of cell death. Thereby, the ability of discs to mount an appropriate regenerative

response is reduced as cells required to drive regenerative responses are eliminated by excessive cell death.

3.9 A survival-promoting function of JAK/STAT is mediated by Zfh2

I did not find any evidence that STAT92E transcriptionally activates negative JNK regulators. Thus, I wanted to investigate if JAK/STAT signalling could regulate cell survival by impinging on the pro-apoptotic JNK target genes *rpr, hid* and *grim* that fuction as inhibitors of dIAP (*Drosophila* Inhibitor of Apoptosis) proteins. To this end, I first performed bioinformatics analysis by using Clover [115] at the promoter regions of *rpr*, *hid* and *grim* to analyse their genomic region for transcription factor binding sites (TFBs). Indeed, as suggested by previous studies [36, 37, 42], the results identified multiple AP-1 binding motifs associated with *rpr*, *hid* and *grim loci* (Fig. 19D-E, Fig. 20A). As previously indicated in studies on JNK-induced apoptosis [36, 37, 42], I could prove that Eiger-stimulated disc specifically induce *hid* expression (Fig. 19A). The mild increase in *hid* transcript levels likely represents a strong underestimate because *eiger*-expressing cells make up only 4.5% of the entire imaginal disc used for qRT-PCR analysis (Fig. 4B-B'). *Eiger*-expressing discs heterozygous for *Df(3L)H99*, a deficiency which lacks the *rpr*, *hid* and *grim loci*, resulted in a pronounced 'undead-cell' phenotype (Fig. 19B-C) [25, 54, 60], suggesting that upregulation of *hid* functionally contributes to Eiger-mediated cell death. Combined, previous reports and our results support the notion that induction of cell death in *eiger*-expressing discs is mediated by AP-1/JNK-dependent activation of *hid*.

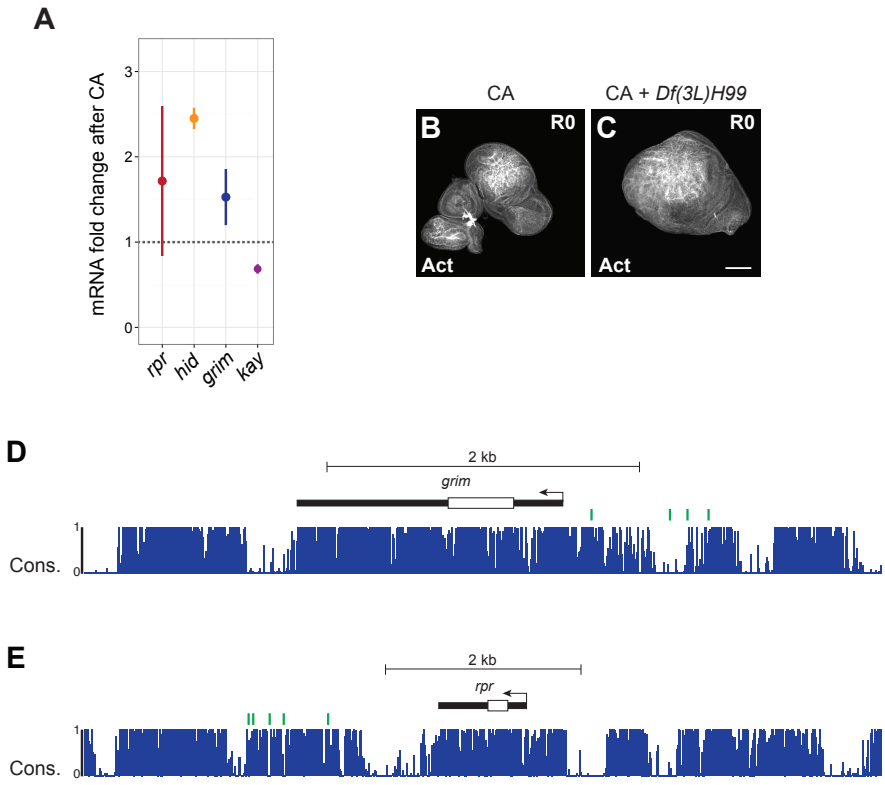

Figure 19. Transcriptional analysis of the pro-apoptotic genes *hid, grim, rpr* and the AP-1 component *kay.*

(A) qRT-PCR analysis of rpr, hid, grim and fos (kay) transcripts at R0. Fold-induction relative to unablated discs is reported. Each graph shows mean ± S.E.M for n≥3 biological replicates. (B-C) Wild type wing disc (B) and wing disc heterozygous for Df(3L)H99 (C) after Eiger-stimulated cell ablation were stained for Actin. Image in (B) also displays haltere and leg discs associated with the larger wing disc on the right. (D-E) Presence of AP-1 binding sites and lack of ZEB/Zfh binding sites in regulatory regions of the pro-apoptotic genes grim (D) and rpr (E) predicted by bioinformatic analysis using Clover.

Clover analysis also revealed multiple, highly clustered mammalian ZEB1-binding motifs in conserved sequences of the *hid* promoter (Fig. 20A) as well as in the promoter of the *kay* gene coding for the AP-1 component dFos (Fig. 20B). Transcriptional repressors, ZEB-proteins are homologous to *Drosophila* Zfh1 and Zfh2 (Zinc-finger homeobox) proteins [116, 117]. Both Zfh1 and Zfh2 were previously identified to be downstream effectors of JAK/STAT signalling [64, 85]. This is also reflected by Zfh2-expression closely mirroring JAK/STAT-activation patterns in developing wing imaginal discs (Fig. 21C-D) [64].

In this case, in order to implement the TFBs analysis on *kay* and *hid loci,* I run two additional analyses. First, I looked at conservation levels of the two genes *kay* and *hid* across the *genus Drosophila*. To do so, I used the mVISTA algorithm [118, 119] to create conservation plots between species. Second, I aligned the conservation plots to previously published ATAC-seq profiles obtained in wild type *Drosophila melanogaster* (GEO access number: GSE59078) [71]. ATAC-seq is a technique used to describe open chromatin and it is widely used to characterise regulatory regions at a genome-wide scale [120]. Combining the

two approaches, predicted TFBs that were found in highly conserved regions with open chromatin having a higher likelihood to represent true regulatory elements than TFBs found in poorly conserved sequences with inaccessible chromatin (Fig. 20 A-B).

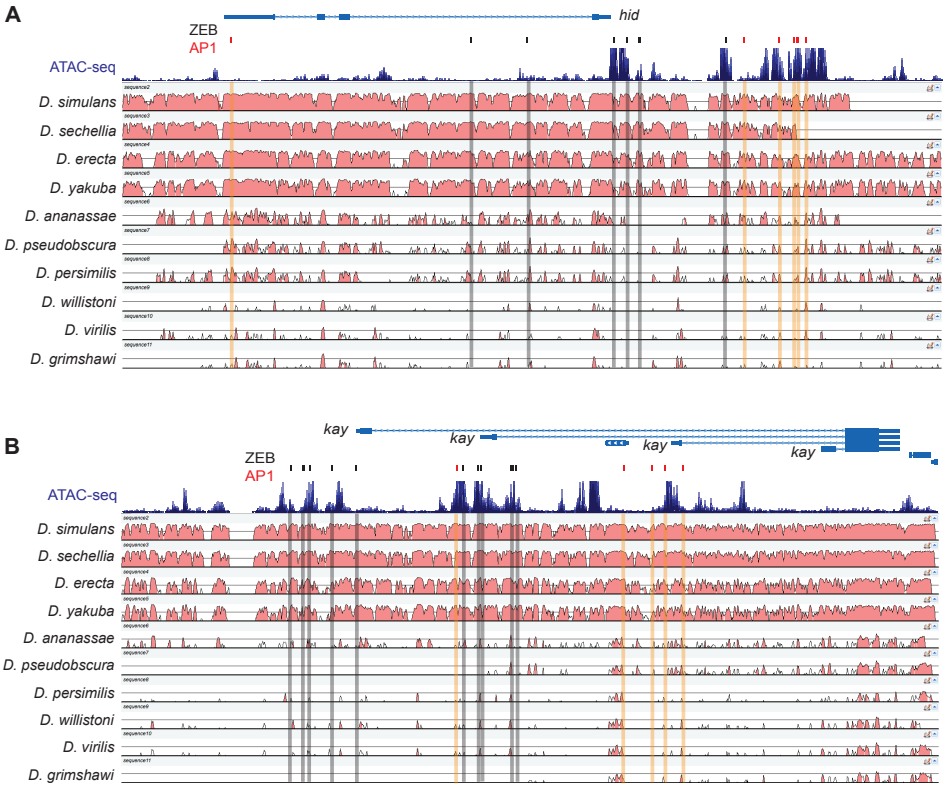

Figure 20. Bioinformatic prediction of Zfh2 and AP-1 binding sites on *hid* and *kay loci*.

(A, B) Visualization of AP-1 and ZEB/Zfh binding sites in regulatory regions of hid (A) and fos(kay) (B) predicted by bioinformatic analysis using Clover. ATAC-seq data (blue profile) from *D. mel.* wild type tissue, indicates open chromatin (Davie et al., 2015). mVISTA plots (red profiles) visualize conservation among *D. mel.* and species listed in the figure. Positions of predicted ZEB binding sites are shown in black/grey, predicted AP-1 binding sites in red/orange.

From this data, I drew the hypothesis that *Drosophila* ZEB-proteins could directly repress *kay* in Eiger-stimulated discs, so restraining JNK-activation to promote cell survival. At the same time, Zfh-proteins could compete with AP-1 in controlling *hid* transcriptional levels, thereby limiting AP-1/Hid-induced apoptosis to promote cell survival. It is important to report that the link between Zfh2-mediated repression and Hid-induced apoptosis has been previously suggested during leg disc development [87].

Immunofluorescence analysis on Eiger-stimulated discs indicated that protein levels of Zfh2, but not of Zfh1, are elevated in response to *eiger*-expression (Fig. 21A-D). Zfh2 protein increased specifically in regions where I had observed high levels of JAK/STAT activation (compare Fig. 7B, C with Fig. 21D). In addition, I found transcript levels of *zfh2* but not of *zfh1* to be mildly elevated (Fig. 21E). The observed mild increase in *zfh2*

transcription likely represents a strong underestimate, as cell expressing *zfh-2 de novo* in the pouch make up only a small portion of entire imaginal discs used for qRT-PCR analysis.

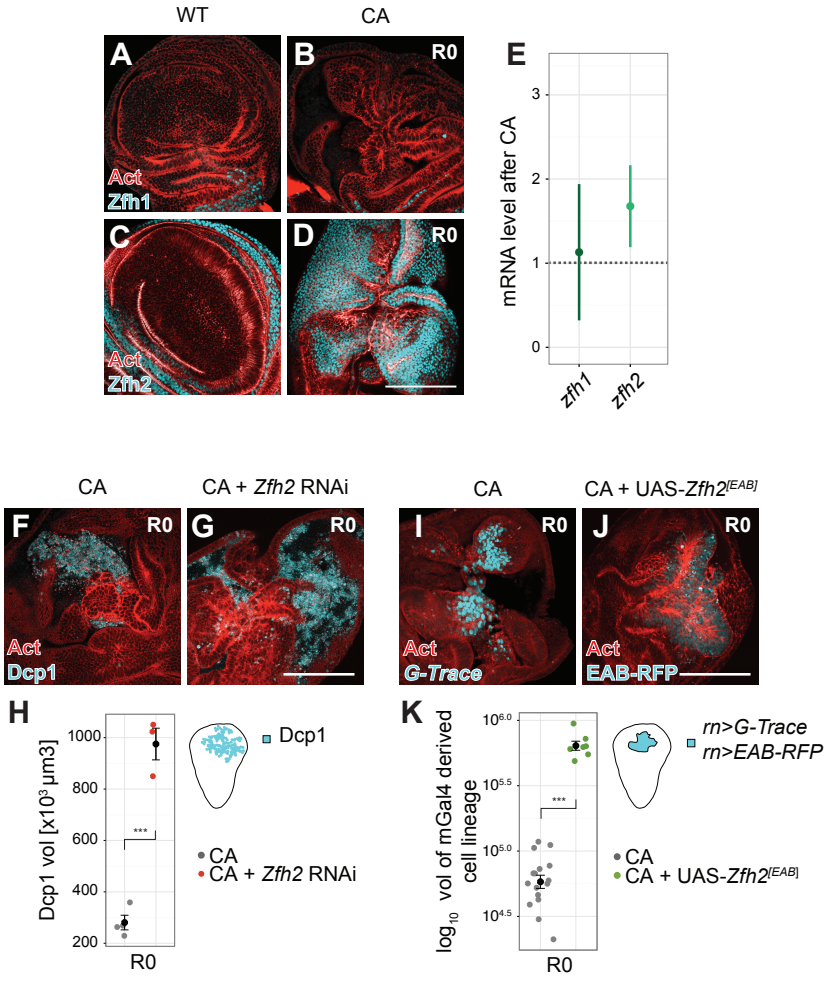

Figure 21. Zfh2 is activated in response to tissue damage.

(A-D) Unablated discs (A, C) and ablated discs (B, D) stained for Zfh1 (A, B) or Zfh2 (C,D) at R0. (E) qRT-PCR analysis of *zfh1* and *zfh2* transcripts at R0. Fold-induction relative to unablated discs is reported. Each graph shows mean ± S.E.M for n=3 biological replicates. (F, G) Disc after cell ablation (F) or with *rnGAL4*-mediated co-expression of *zfh2* RNAi (G) in *eiger*-expressing cells stained for Dcp-1 to visualize apoptotic cells (cyan) and Actin (red) at R0. (H) Dcp1-positive volume per disc after cell ablation (CA) (n=4 discs) or in discs with *rnGAL4*-mediated co-expression *zfh2* RNAi (n= 3 discs) in *eiger*-expressing cells at R0. (I, J) Disc after cell ablation (I) or discs with *rnGAL4*-mediated co-expression of *UAS-zfh2* (J) in *eiger*-expressing cells stained for Dcp-1 (cyan) and Actin (red) at R0. (K) *rnGAL4,* G-trace-labelled volume in ablated discs (n= 16 discs) and RFP-labelled volume in discs with *rnGAL4*-mediated co-expression *UAS-Zfh2*$^{[EAB]}$ (n= 7 discs) in *eiger*-expressing cells at R0. Graphs display mean ± S.E.M. U-tests were performed to test for statistical significance (** p<0.05, ** p<0.01, *** p<0.001*). All scale bars: 100 µm.

To test if Zfh2 in Eiger-stimulated discs may be required to promote JAK/STAT-dependent survival by repressing *hid* and *kay* transcription, I reduced or increased Zfh2 function genetically. Expression of an RNAi construct targeting *zfh2* (Appendix I) increased the extent of apoptosis in *eiger*-expressing wing discs by almost 4-fold (Fig. 21F-H). On the

other hand, over-expression of *UAS-zfh2* strongly promoted survival of *eiger*-expressing cells and resulted in a 10-fold increase in the size of the surviving *rnGAL4*-derived cell population (Fig. 21I-K). While I had found that Zfh1 levels were not up regulated in response to Eiger-stimulation, over-expression of *zfh1* strongly promoted survival of *eiger*-expressing cells as well, even phenocopying the over-expression of the strong apoptosis inhibitor p35 (Fig. 22A-D). The survival-promoting function of either Zfh1 or Zfh2 suggests that both proteins are capable to induce potent survival signals in stressed tissues, but may only do so depending on tissue context ([84] and Fig. 21A-E).

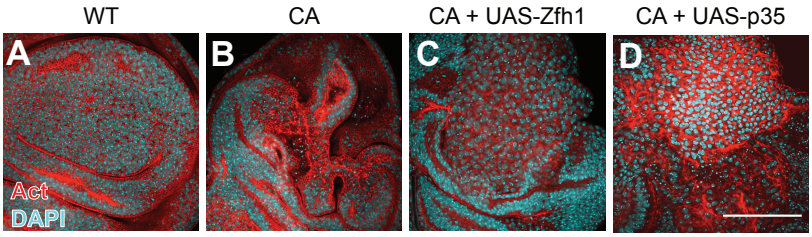

Figure 22. Ectopic induction of *zfh1* promotes survival in *eiger*-expressing discs.

(A-D) Wild type wing disc (A), wing disc after Eiger-stimulation (B) and wing disc after Eiger-stimulation with *rnGAL4*-mediated co-expression of *Zfh1* (C) and *p35* (D) stained for DAPI (cyan) and Actin (red). All scale bars: 100 µm.

3.10 JAK/STAT activity prevents excessive tissue damage in response to tissue stress

My thesis affirms that interfering with JAK/STAT signalling, and therefore also with Zfh2 function, must cause an increase in the extent of tissue damage incurred by *eiger*-expression in wing discs due to elevation of cell death. Consistent with what I observed at larval stages, Eiger-stimulated wing discs with genetically reduced JAK/STAT activity developed into significantly smaller adult wings (Fig. 23A, Appendix II). Expression of $dome^{\Delta cyt}$, *Socs36E* or RNAi constructs targeting multiple pathway components, including *zfh2*, as well as heterozygosity for $dome^{G0441}$, hop^{34} and $Stat92E^{85C9}$, caused a significant drop in the adult wing size index by 30-90% (Fig. 23A). It is important to notice that genetic down regulation of JAK/STAT activity in wild type discs under the control of *rnGAL4* for 40 h at day 7 does not cause a comparable reduction in wing sizes (Appendix II), emphasizing the pro-survival function of JAK/STAT that is specifically required during tissue stress responses.

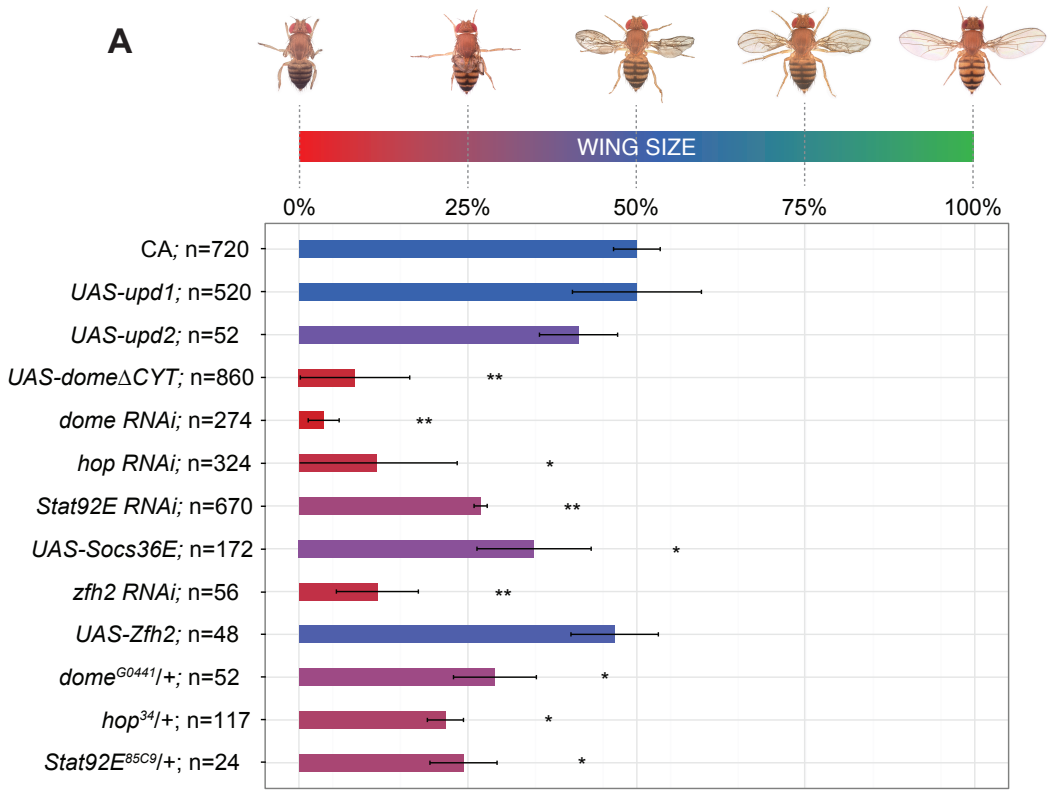

Figure 23. Down regulation of the JAK/STAT pathway during cell ablation, affects proper wound healing.

(A) Average wing sizes developing from Eiger-stimulated disc (CA) or combined with *rnGAL4*-mediated co-expression of UAS-transgenes or in genetic backgrounds heterozygous for $dome^{G0441}$, hop^{34}, or $Stat92E^{85C9}$. Graphs display mean ± S.D. of average scores derived from ≥3 experiments. T-tests were performed to test for statistical significance (* $p<0.05$). n= number of wings scored.

My data confirmed previous results obtained in the lab by analysis of adult wings that developed from discs of surgically pinched larvae [12, 76]. Reducing JAK/STAT function in the posterior compartment by expressing an RNAi construct targeting *hop* caused a pronounced reduction in adult wing sizes developing from imaginal discs, in which pinching was targeted to the posterior compartment visualized by co-expression of GFP (Fig. 24A). In contrast, no reduction in size of the posterior compartment was observed for adult wings derived from undamaged control wing disc raised under the same conditions (data not shown).

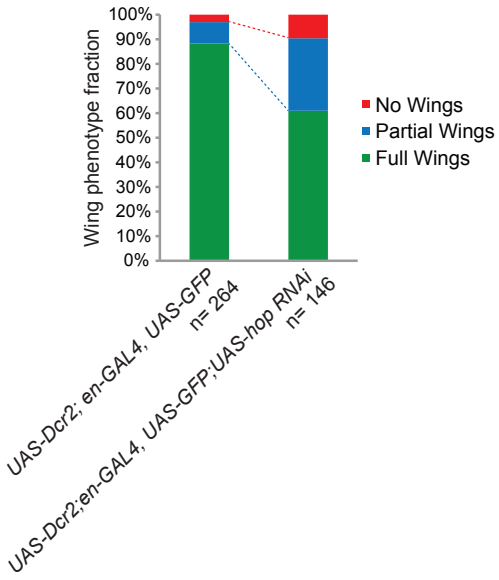

Figure 24. JAK/STAT also prevents excessive tissue damage upon mechanical tissue damage.

(Quantification of 3 adult wing size classes developing from wing discs expressing GFP or GFP together with an RNAi-construct targeting *hop* in the posterior compartment. All wing discs were injured during larval development by targeted pinching using forceps.

Notably, *rnGAL4*-driven overexpression of *upd1*, *upd2* or *zfh2* in *eiger*-expressing cells did not reduce and rescued the extent of tissue damage compared to wild type Eiger-stimulated wings (Fig. 23A). Extra Upd ligands may not translate into JAK/STAT hyper activation, due to intrinsic pathway saturation in *eiger*-expressing cells. While *zfh2* overexpression promoted cell survival, it did not rescue other Eiger-induced defects such as loss of epithelial polarity, which interferes with wing morphogenesis during pupal stages (Fig. 21J).

These data suggest that cellular responses to genetically or surgically induced tissue damage critically rely on JAK/STAT activation to facilitate restoration of normal tissue homeostasis. Taken together, my results demonstrate that a reduction in final tissue size upon JAK/STAT inhibition reflects an excessive loss of tissue due to cell death rather than a failure of the tissue to undergo compensatory proliferation.

3.11 JAK/STAT activity promotes efficient induction of compensatory responses

I wanted to further investigate whether the observed reduction in adult wing sizes upon JAK/STAT inhibition is exclusively caused by a loss of tissue due to cell death or if

other regenerative processes during the recovery phase may be disturbed. An important process that tissue repair possible is the induction of a dILP8-dependent developmental delay at the larval-pupal transition, which extends the time available for the tissue to heal before metamorphosis [121, 122]. Interfering with JAK/STAT activity in *eiger*-expressing cells also caused a profound reduction in the developmental delay induced by Eiger-stimulation (Fig. 25A).

To understand if altered *dILP8*-expression in Eiger-stimulated discs underlies this observation, I quantified expression of a *GFP*-reporter driven from the endogenous *dILP8* locus [122]. The *GFP*-reporter was strongly expressed in the pouch region of Eiger-stimulated discs (Fig. S7C). In contrast, interfering with JAK/STAT activation by expression of *dome* RNAi or *dome*$^{\Delta cyt}$ in *eiger*-expressing cells reduced the area of *GFP*-expression (Fig. 26B-D). This suggests that loss of *dILP8*-expression, caused by impaired JAK/STAT in JNK-signalling cells, underlies the observed failure to efficiently induce a developmental delay.

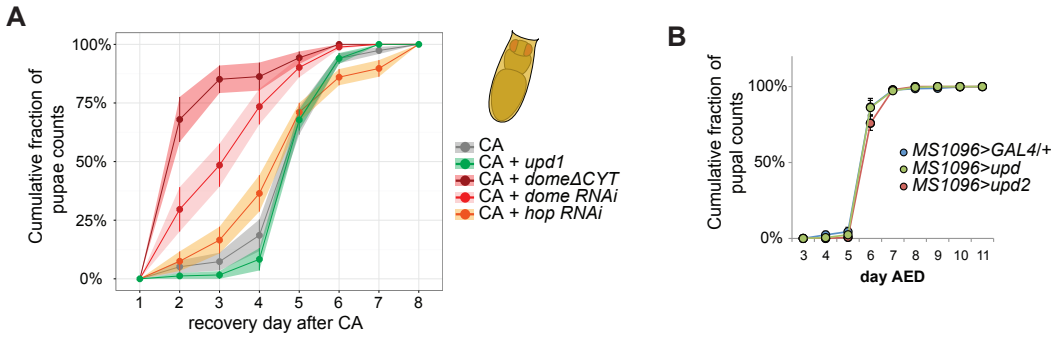

Figure 25. Reduction of the JAK/STAT activity reduces injured induced development delay.

(A) Cumulative fraction of larvae undergoing larval-pupal transitions, which carry Eiger-stimulated discs (CA) (n= 210) or were combined with rnGAL4-mediated co-expression of upd1 (n= 213), *domeΔcyt* (n=201), *dome RNAi* (n= 196), or *hop RNAi* (n=230). Graphs display mean ± S.E.M. of average scores from ≥3 experiments. (B) Cumulative fraction of larvae undergoing larval-pupal transitions, which carry control discs (MS1096GAL4/+) and discs expressing *upd* or *upd2* under the control of *MS1096*GAL4. Graph shows mean ± S.D. for average scores from at least 3 independent experiments.

To test whether JAK/STAT signalling is sufficient to induce developmental delays, I expressed the JAK/STAT-ligands Upd1 or Upd2 in wild type discs using *MS1096-GAL4*. However, no difference in pupariation timing between *upd*-expressing and stage-matched wild type larvae was observed (Fig. 25B). While a recent study links *dILP8*-expression to JAK/STAT signalling [8], these data implies that *dILP8* is not a direct target gene of STAT92E. Instead I suggest that cells, which normally express *dILP8* in response to JNK activation tend to die more likely when JAK/STAT signalling is reduced, thereby preventing efficient expression of *dILP8* and induction of a developmental delay. The failure to induce this important systemic response reduces the time available for tissue repair and likely

contributes to the decrease in recovered adult wing sizes I observed upon genetic reduction of JAK/STAT signalling (Fig. 26B).

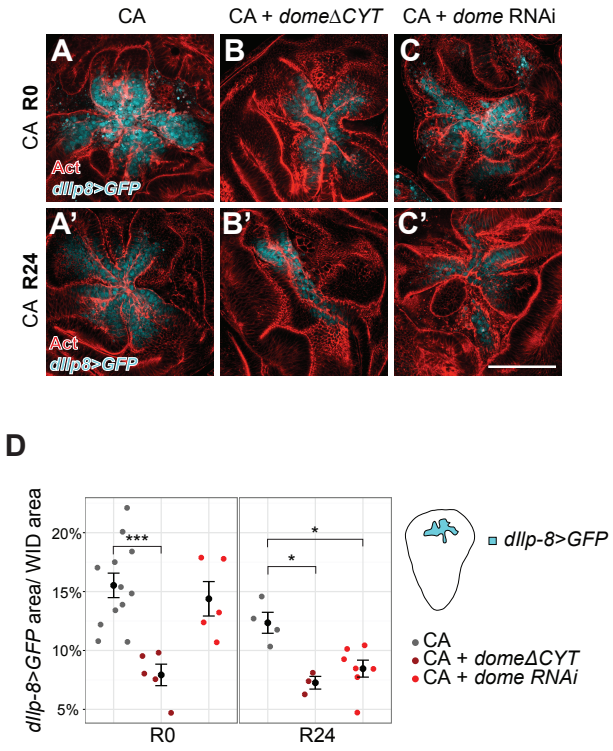

Figure 26. Development delay mediated by *dllp-8* depends on the JAK/STAT activation.

(A-C) Wing disc after after Eiger-mediated cell ablation (CA) (A) and discs combined with rnGAL4-mediated co-expression of *domeΔcyt* (B) or *dome RNAi* (C) in eiger-expressing cells, imaged at R0 (A-C) and R24 (A'-C') expressing the dILP8-GFP reporter (cyan) and stained for Actin (red). (D) Relative disc area expressing *dILP8*-GFP after cell ablation (CA) (R0 n=12, R24 = 4 discs) and in discs combined with *rnGAL4*-mediated co-expression of *domeΔcyt* (R0 n= 5, R24 n= 3 discs) or *dome* RNAi (R0 n= 5, R24 n= 7 discs) in *eiger*-expressing cells. Graphs display mean ± S.E.M. U-tests were performed to test for statistical significance (* *p<0.05*, ** *p<0.01*, *** *p<0.001*).

3.12 JAK/STAT regulates survival in a Ras^{V12}; scrib tumour model

To understand if the pro-survival role of JAK/STAT is more general and acts so in different context of tissue stress, I revisited the role of JAK/STAT signalling in established fly tumour models. Previous studies suggest that activation of JAK/STAT drives tumorous overgrowth in discs mutant for tumour suppressor genes, such as *scribbled (scrib)* or *Psc-Su(z)2* [40, 70]. $scrib^{1}$ mutant cells, similar to *eiger*-expressing cells, exhibit strong JNK-activation that correlates with elevated transcription of *upd* cytokines [38, 40, 72, 123]. While

scrib mutant cells have a growth disadvantage if surrounded by wild type cells, they efficiently cooperate with oncogenic Ras^{V12} to create invasive tumours in clonal assays [38, 40]. Larvae carrying Ras^{V12}; $scrib^{2}$ clones completely fail to pupariate (Fig. 27F), a known response linked to *dILP8*-activation that correlates with tumour load [122]. We found that MARCM-induced Ras^{V12}; $scrib^{2}$ clones covered about 47% of eye-antennal discs, compared to 19% for wild type clones (Fig. 27A, B, D). When I probed Ras^{V12}; $scrib^{2}$ clones for activated Dcp-1, I did not observe any difference in apoptotic patterns compared to wild type tissue (Fig. 28A, B).

When I completely removed JAK/STAT function in Ras^{V12}; $scrib^{2}$ clones by homozygosity for a $Stat92E^{85C9}$ allele, Ras^{V12}; $scrib^{2}$ clone size was reduced from 47% to 28% of the eye disc area (Fig. 27B-D). Comparison of cell division rates within Ras^{V12}; $scrib^{2}$ and Ras^{V12}; $scrib^{2}$, $Stat92E^{85C9}$ clones did not show any significant changes upon loss of JAK/STAT function (Fig. 27B', C', E).

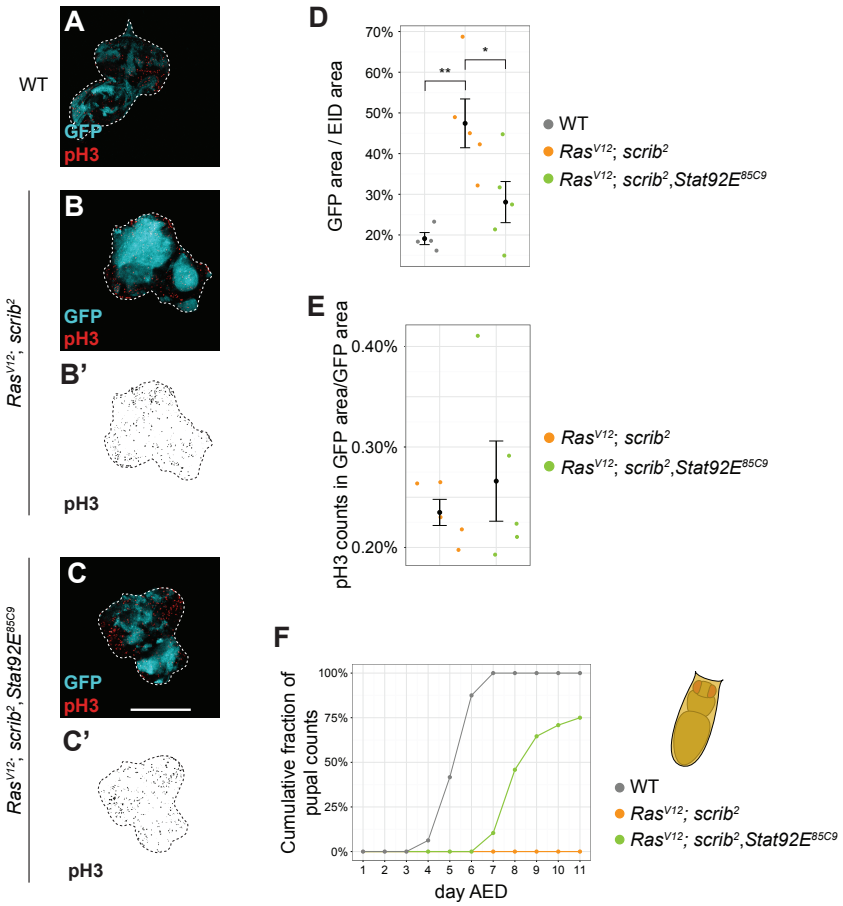

Figure 27. JAK/STAT doesn't promote compensatory proliferation in a Ras^{V12};*scrib* tumour model.

(A-C) Eye imaginal discs carrying neutral (A), Ras^{V12};$scrib^{2}$ (B, B') or Ras^{V12};$scrib^{2}$,$Stat92E^{85C9}$ (C, C') GFP-marked MARCM clones (cyan in A-C) stained for pH3 (B', C', red in A-C). (D) Area occupied by neutral (n= 4), Ras^{V12};$scrib^{2}$ (n= 5) or Ras^{V12};$scrib^{2}$,$Stat92E^{85C9}$ (n= 5) clones, normalized to total eye imaginal disc (EID) area. (E) pH3-events in Ras^{V12};$scrib^{2}$ (n= 5) or Ras^{V12};$scrib^{2}$,$Stat92E^{85C9}$ (n= 5)

clones per eye disc normalized to total clone area per disc. (F) Cumulative fraction of larvae undergoing larval-pupal transitions carrying RasV12;scrib2 or Ras^{V12};$scrib^{2}$,$Stat92E^{85C9}$ clones. Graphs display mean ± S.E.M. U-tests were performed to test for statistical significance (* *p<0.05, ** p<0.01, *** p<0.001*). All scale bars: 100 µm.

However, in contrast to Ras^{V12}; $scrib^{2}$ clones, Ras^{V12}; $scrib^{2}$, $Stat92E^{85C9}$ clones displayed a 4.3-fold increase in areas of Dcp-1 activation (Fig. 28A-D), strongly indicating that increased cell death of *Stat92E* mutant cells underlies the smaller clone sizes of Ras^{V12}; $scrib^{2}$, $Stat92E^{85C9}$ clones (Fig. 28D). Notably, the reduction in Ras^{V12}; $scrib^{2}$, $Stat92E^{85C9}$ clone size reduced total tumour load and allowed a significant proportion of host larvae to progress to pupal stages (Fig. 27F).

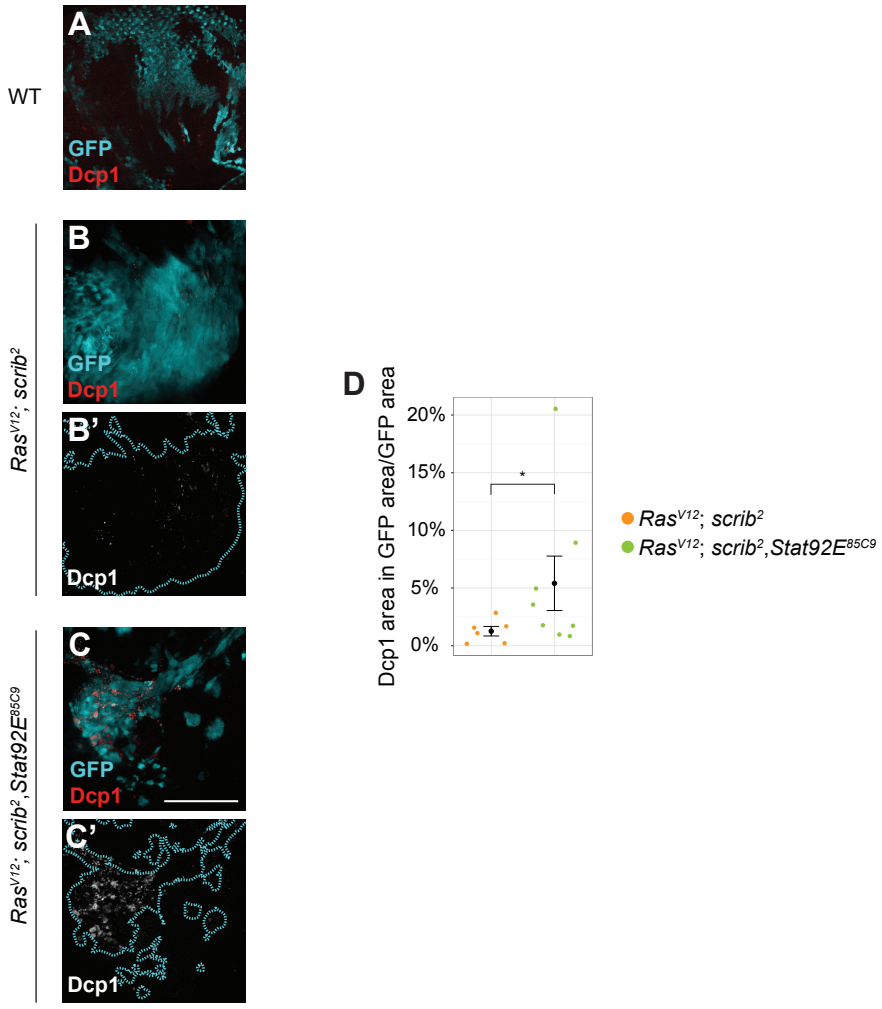

Figure 28. JAK/STAT regulates survival in a Ras^{V12};*scrib* tumour model.

(A-C) Eye discs carrying neutral (A), Ras^{V12};$scrib^{2}$ (B, B') or Ras^{V12};$scrib^{2}$,$Stat92E^{85C9}$ (C, C') clones (cyan in A-C) stained for Dcp-1 (A'- C', red in B-C). Clone borders indicated by outline in B', C'. (D) Dcp-1-positive area within Ras^{V12};$scrib^{2}$ (n= 6) or Ras^{V12};$scrib^{2}$,$Stat92E^{85C9}$ (n= 8) clones normalized to total clone area per disc. Graphs display mean ± S.E.M. U-tests were performed to test for statistical significance (* *p<0.05, ** p<0.01, *** p<0.001*). All scale bars: 100 µm.

Following the results found in the Eiger-induced system, *Ras^{V12}; scrib^{2}* clones displayed ectopic activation of Zfh2 but not of Zfh1 (data not shown), indicating potential activation of a JNK-JAK/STAT-Zfh2 stress module by neoplastic transformation. Ectopic expression of Zfh2 was completely abolished within *Ras^{V12}; scrib^{2}, Stat92E ^{85C9}* clones (Fig. 29A-C). These results support the notion that Zfh2 expression is regulated by JAK/STAT signalling in multiple contexts of cellular stress and that stress-dependent Zfh2 activation in imaginal discs directly correlates with cell survival.

These results support a model in which cellular stress caused by genetic cell ablation, physical wounding or tumorous growth drives activation of JAK/STAT to promote survival of JNK-signalling cells. Activation of JAK/STAT signalling thereby facilitates the induction and execution of local and systemic compensatory responses, rather than directly promoting compensatory cell proliferation.

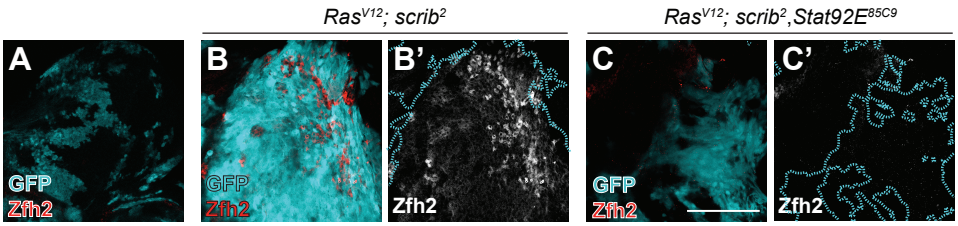

Figure 29. Zfh2 is activated during tumor formation and it depends on JAK/STAT signaling.

(A-C) Eye discs carrying neutral (A), *Ras^{V12};scrib^{2}* (B, B') or *Ras^{V12};scrib^{2},Stat92E^{85C9}* (C, C') clones (cyan in B-C) stained for Zfh2 (B', C', red in B-C).

3.13 Tissue stress responses are mediated by dynamic regulation of chromatin.

To understand how genes, such as those belonging to the Upd or ZEB gene families, are activated in response to tissue wounding and how they are subsequently downregulated, I wanted to test the importance that dynamic regulation of chromatin plays during tissue stress responses. To this end I expressed 26 different RNAi targeting different chromatin factors in wing discs in combination with the *eiger*-induced cell ablation system. To this list of 26 RNAi lines, I added one transgene allowing for the overexpression of the demethylase UTX, previously shown to be involved in regenerative processes [90, 124]. For adults habing expressed these constructs in wing imaginal discs, I quantified and compared their wing sizes

to those of cell-ablated control wings (Fig. 30). The data was analysed by clustering the screened lines in three distinctive groups: chromatin activators, chromatin repressors and chromatin remodelers. None of these three groups displayed a distinctive phenotypic behaviour. Instead all lines tested resulted in either not having any effect on final wing size or in causing a decrease in wing size (Fig. 30). This data indicates that all three chromatin regulatory functions that have been analysed are necessary to build up a proper cellular response to wounding stress.

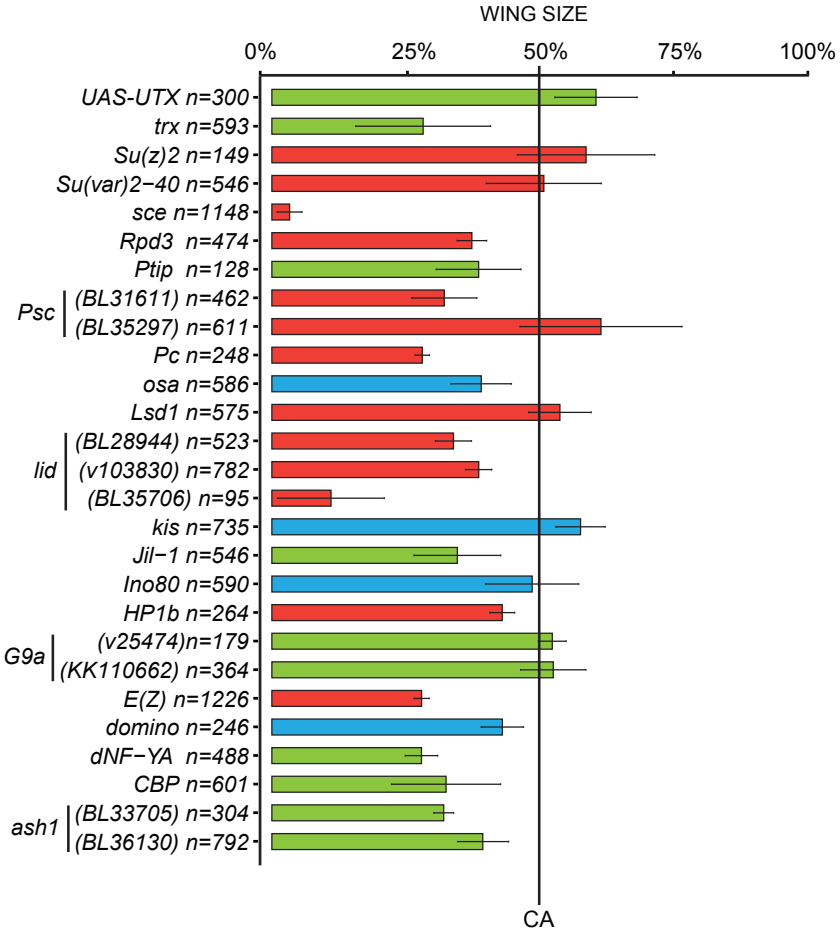

Figure 30. Down regulation chromatin factor activity during cell ablation, affects proper wound healing.

Average wing sizes developing from Eiger-stimulated disc (CA) or combined with *rnGAL4*-mediated co-expression of UAS-transgenes. Graphs display mean ± S.D. of average scores derived from ≥3 experiments. T-tests were performed to test for statistical significance (* $p<0.05$). n= number of wings scored.

3.14 Establishment of an inducible DamID-seq technique to analyse DNA-protein interaction in *Drosophila* wing imaginal discs.

To further investigate how chromatin associated factors may contribute to dynamic regulation of cellular stress responses, I wanted to be able to map their DNA-binding sites during stress responses in vivo. DamID-seq technique has been previously shown to be a suitable approach to study specific DNA-protein interaction [104, 125]. So far, DamID-seq has not been performed in wing imaginal discs of *Drosophila*. Thus, in collaboration with the van Steensel laboratory, I established a novel protocol to apply DamID techniques to these specific tissues to study chromatin dynamics (Appendix III). The chromatin factor I focused on was Polycomb (Pc), a component of the Polycomb Repressive Complex 1 (PRC1). For these experiments, I employed Dam and Dam-Pc constructs created in the van Steensel group by Dr. Alexey Pindyurin (Fig. 31A-B).

Making use of a full-length heat-shock promoter (HSp) controlling expression of the DamID constructs, I was able to establish an inducible DamID-seq protocol in imaginal discs (Appendix III). I decided to provide a proof of principle by analysing Pc binding dynamics in *scrib*^{1} mutant larvae, which are characterised by loss of cell polarity and tumour formation in imaginal discs.

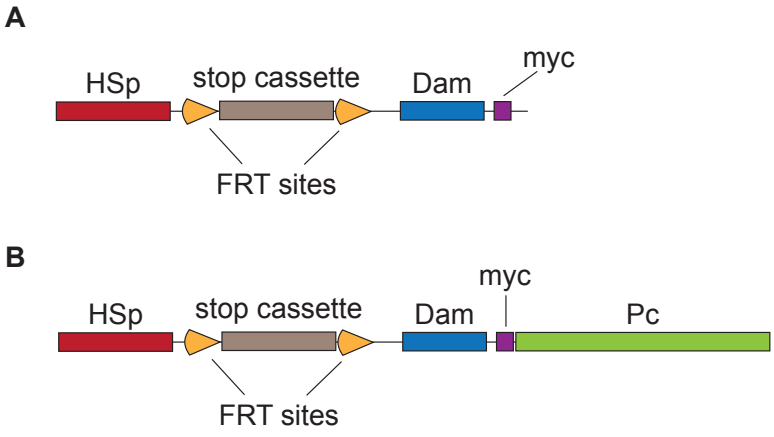

Figure 31. DamID inducible constructs.

(A-B) DamID constructs carrying the STOP cassette flanked by two FRT sites. (A) DamID construct encoding for the control Dam protein only. (B) DamID construct carrying Polycomb (Pc) fused to the protein Dam.

Several considerations guided optimization of DamID protocols: Expression levels of the DamID construct are known to be crucial for the outcome of the technique. High expression levels can result in cell death due to excessive DNA methylation driven by the Dam methyltransferase [102]. On the other hand, low expression levels can obviously result in low specific signals, which will affect the quality of the sequencing profiles and analysis. A PCR step (mePCR) included in the sample preparation for sequencing that is necessary to

achieve the right DNA yield for the library preparation, allowed me to control for both these aspects before sequencing.

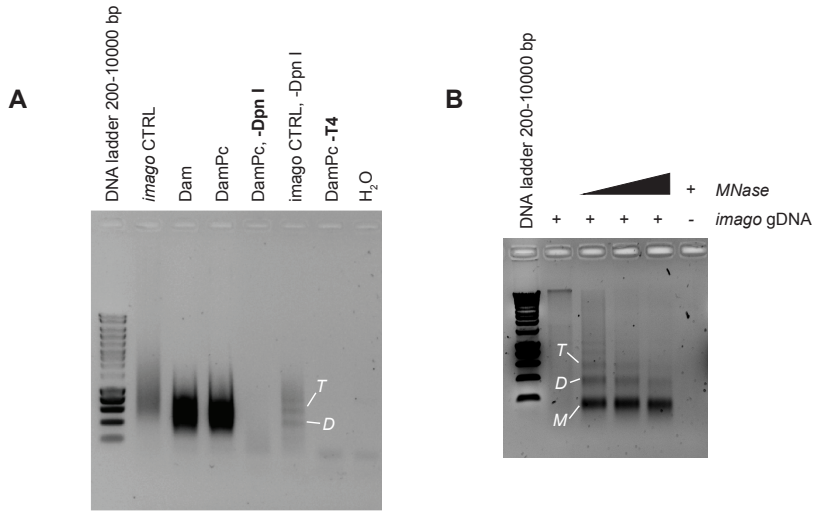

Figure 32. Preliminary controls on the DamID-seq protocol.

(A) PCR of the methylated fragments (mePCR) after restriction (DpnI reaction) and adaptor ligation (T4 reaction) give rise to specific smears on gel of agar. Negative control (-DpnI) on *imago* extraction results in typical nucleosomes ladder from unspecific DNA digestion due to physiological apoptotic levels (T, trimer-nucleosomes; D, dimer-nucleosomes). (B) Genomic DNA digested by MNase with increasing incubation times (compare A to B) (M, mono-nucleosome; D, dimer-nucleosomes; T, trimer-nucleosomes).

During programmed cell death, CADs (Caspase-Activated DNase) enzymes are known to be responsible to DNA degradation [126]. This process results in DNA fragments, which are independent from the DNA methylation (Fig. 32, DpnI negative control). Although the actual cut is unspecific, it is biased by nucleosomes accessibility. Thus, apoptosis-induced DNA fragmentation results in a characteristic band pattern on gel, which is similar to the typical nucleosome ladder obtained after MNase (Micrococcal Nuclease) treatment (Fig. 32B). Apoptosis is a fundamental process in many different physiological contexts during development; therefore, mePCR amplification performed on total larvae (*imago)* showed apoptotic DNA degradation (Fig. 32A-B).

3.15 Analysis of the DamID-seq data

Replicates of samples prepared from wild type discs expressing Dam alone and a DamPc fusion construct were firstly compared and then the Pc-Dam profiles were normalised for unspecific Dam activity against the Dam alone expressing samples (Appendix III). The

two independent replicates were averaged and an analysis of their correlation provided values of around 50% for both Spearman's and Person's analysis (Fig. 33A). These values suggested that my profiles were of good quality also compared to previously published data [104, 125].

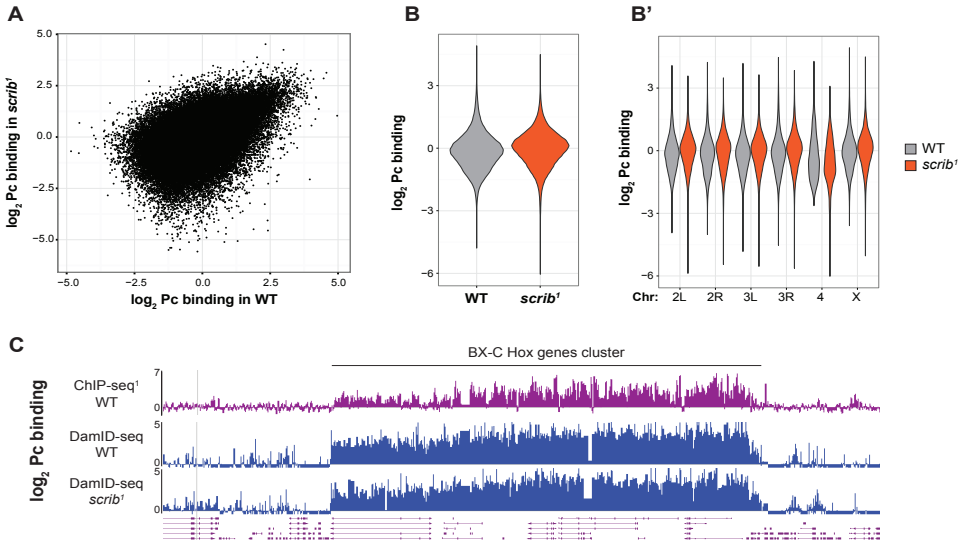

Figure 33. Preliminary analysis of Pc-DamID data suggests specific reorganization of Pc binding in tumor.

(A) Scatter plot of Pc binding between wild type (WT) and *scrib*^{1} tumor. (B) Violin plot of Pc binding distribution of wild type (WT, grey) and *scrib*^{1} tumor (orange). (B') Violin plots of Pc binding across different chromosomes in both wild type (WT, grey) and *scrib*^{1} tumor (orange). (C) Comparison of DamID-seq profiles and ChIP-seq profiles of Pc over the BX-C *locus*.

Subsequently, I wanted to investigate how methylated GATC (GA^{m}TC) fragments distribute as a function of Pc binding (Appendix III). The distributions peaked around 0 indicating a higher amount of GA^{m}TC that are actually unbound by Pc in either condition. Comparing the densities between wild type and *scrib*^{1} tumour, the data indicated the lack of a global rearrangement of the Pc binding between the two samples (Fig. 33B). This result held true when I compared Pc binding values for each single chromosome (Fig. 33B'). The sequencing data also showed good auto-correlation (ACF) profiles indicating the specificity of Pc binding and right levels of the DamID construct induction (Appendix III). Finally, my inducible DamID-seq protocol resulted in similar Pc binding profiles compared to already published Polycomb ChIP-seq data obtained from wing imaginal discs (Fig. 33C). Taken together, these observations suggest that DamID analysis of chromatin dynamics in imaginal discs in vivo is feasible and represents a true alternative to standard ChIP approaches.

Pc binding on GA^{m}TC fragments can also be described by the probability of certain GA^{m}TC fragment to be or not to be a Pc target. The method I used was based on a three states Hidden Markov Model (HMM) previously developed in the van Steensel lab [104]. The HMM generated by this model had three possible outcomes, namely: Non-Target (NT), Target (T) or Intermediate Target (I) (FIG). I implemented this analysis to define Transition-States (TS) for each GA^{m}TC fragment. The TS was simply defined as the difference or change of Pc binding states (NT, T or I) from the HMM analysis for each GA^{m}TC fragment between wild type control and *scrib*^{1} tumourous discs (Fig. 34).

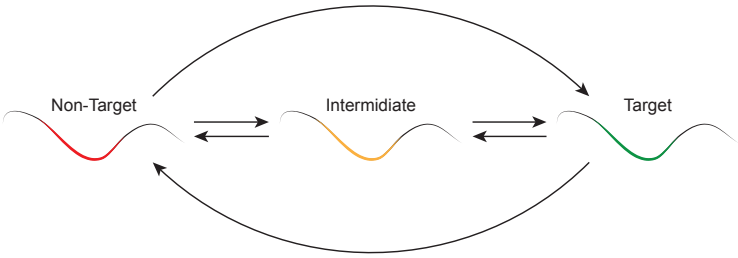

Figure 34. Transition-State analysis.

Protein-DNA interaction on a specific GATC fragment (colored in the scheme) is described by three different binding states: Non-Target (red), Intermediate (yellow) or Target (green). Between samples, differential binding on a specific GATC fragment is describe as transition from one binding state to another.

3.16 Differences in Pc binding affect neighbouring domains.

Pc is known to bind chromatin in large domains if compared to transcription factors, which have more defined and unique binding sites across the genome [104, 109]. Comparison of ACF plots (Appendix III) of the positive transcriptional factor Will Die Slowly (WDS) and Pc confirmed the expected difference. ACF scores for WDS decreased faster than Pc data sets, implying that Pc profiles displayed higher correlation between methylated GATC far from each other.

The definition of Pc bindings sites as binding domains allowed me to also describe them by their TS. Most of the transitions between wild type and *scrib* mutant imaginal discs resulted in stable states at Intermediate (I>I) or Non-Target (NT>NT) sites. In contrast, transitions from (NT>T and T>NT) were observed less frequently (Fig. 35C). From these results, I wanted to perform a more in depth explorative analysis of the behaviour of Pc binding domains between wild type and tumorous samples.

First, I asked whether Pc binding domains described by their TS covered genomic regions with similar lengths. Interestingly, most of the TS that gain Pc binding tended to cover shorter genomic regions if compared to the ones where Pc binding was lost (Fig. 35A).

Secondly, I analysed the frequency of specific TS events in neighbouring domains (Fig. 35 B-C). As expected, highly represented TS tended to flank each other (e.g. I>I and NT>I) (Fig. 35C). Interestingly, when a genomic region was gaining or loosing Pc binding, the neighbouring regions tended to have a similar trend (Fig. 35C). Therefore, specific transitions were more likely to be flanked by similar ones. However, the distribution of the different TS events between wild type and tumorous discs did not look to follow any specific pattern when visualised across the entire genome (Fig. 35D).

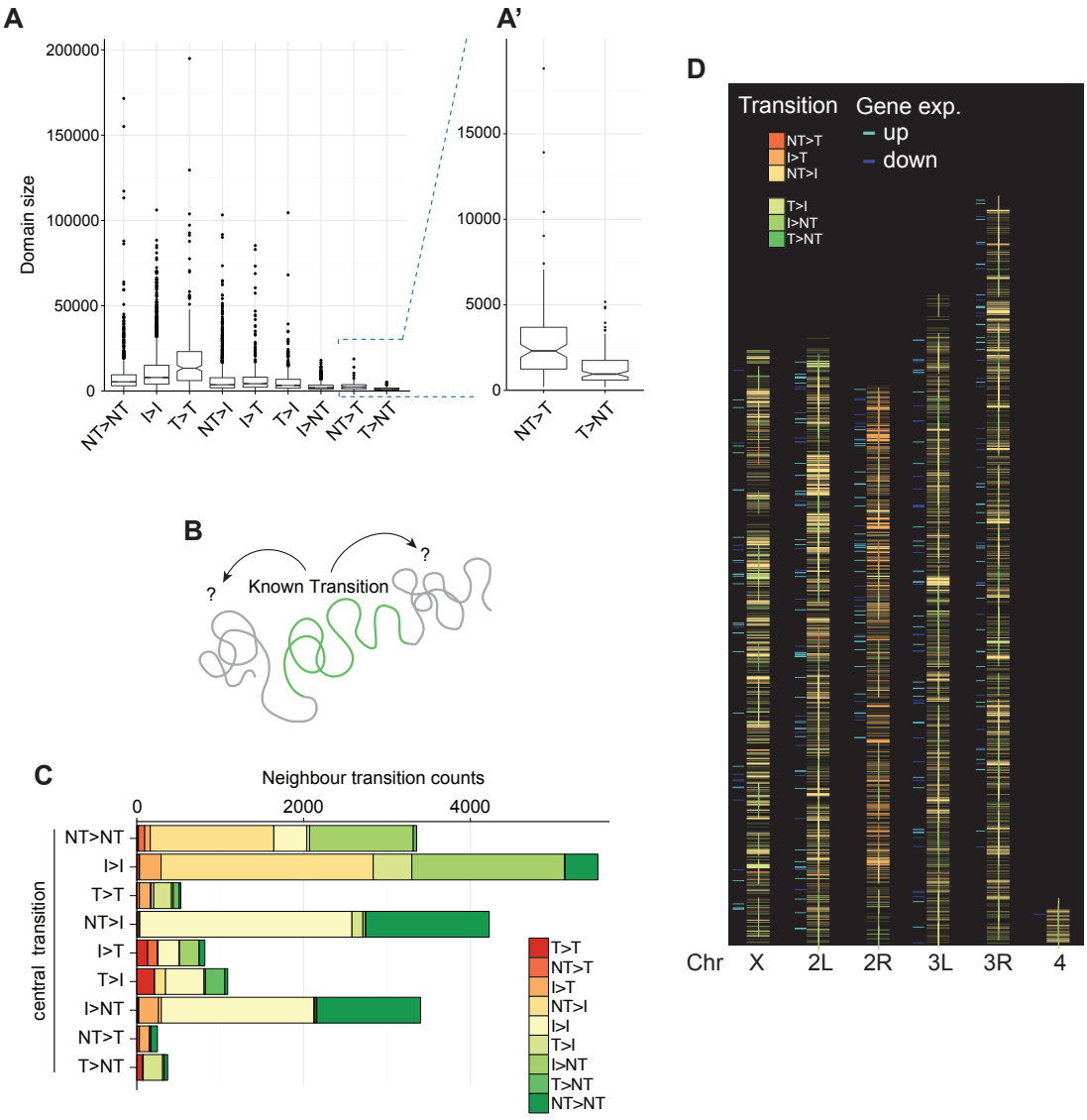

Figure 35. Analysis of Pc domains.

(A) Notched box plots representing distribution of domain sizes (bp) defined by their T-S. Notched box plots show median and CI. (A') Zoom-in of domain size (bp) distribution of Non-Target to Target (NT>T) and Target to Non-Target (T>NT). Notched box plots show median and CI. (B) Scheme representing the analysis of neighboring domain T-S. (C) Counts of all neighboring T-S domains for each specific T-S (increasing in Pc binding tends to red, decreasing to green). (C) Chromosomes map of all T-S domains that show differential Pc binding between WT and *scrib*^{1} tumor (increasing in Pc binding tends to red, decreasing to green).

3.17 Changes in Pc binding happen at specific *loci* during tumour formation.

The DamID-seq profiles pointed to specific local changes in Pc binding rather than a global redistribution of Pc binding. Thus, I wanted to analyse the differential binding of Pc in *scrib*^{1} tumours in a more *locus*-specific manner. The question I asked was whether any specific change in Pc binding could be linked to differences in transcriptional levels between normal and tumour tissue. To perform such comparison, I made used of already published RNA-seq data obtained form wild type wing imaginal discs and *scrib*^{1} tumours [72]. First, I extrapolated differentially expressed genes from the published transcriptome analysis. Second, I combined the Pc DamID-seq profiles with these genes. To do so, I selected a presumptive regulatory region around the transcriptional start site (TSS) for each gene. More precisely, each presumptive regulatory region spanned from 2,5 kb upstream to 1 kb downstream of the TSS (refering to the transcription directionality associated to the TSS). Once these regions were defined, I identified the GA^{m}TC fragments covering those specific regions. Hereafter, I will refer to this GA^{m}TC fragment subset as taGA^{m}TCf, *transcription-associated-GA^{m}TCf* (Fig. 36 A-B).

Thus, each taGA^{m}TCf could be linked with a specific transcriptional level (taGA^{m}TCf$_{RNA\ level}$) and to a specific Pc binding value (taGA^{m}TCf$_{Pc\ binding}$) that represent the change between wild type and *scrib* mutant discs. Surprisingly, these two variables didn't show any correlation when compared to eachother (Fig. 36C). This conclusion suggests that the specific differences in Pc binding during tumour formation couldn't be described as simple function of the overall changes in transcriptional levels.

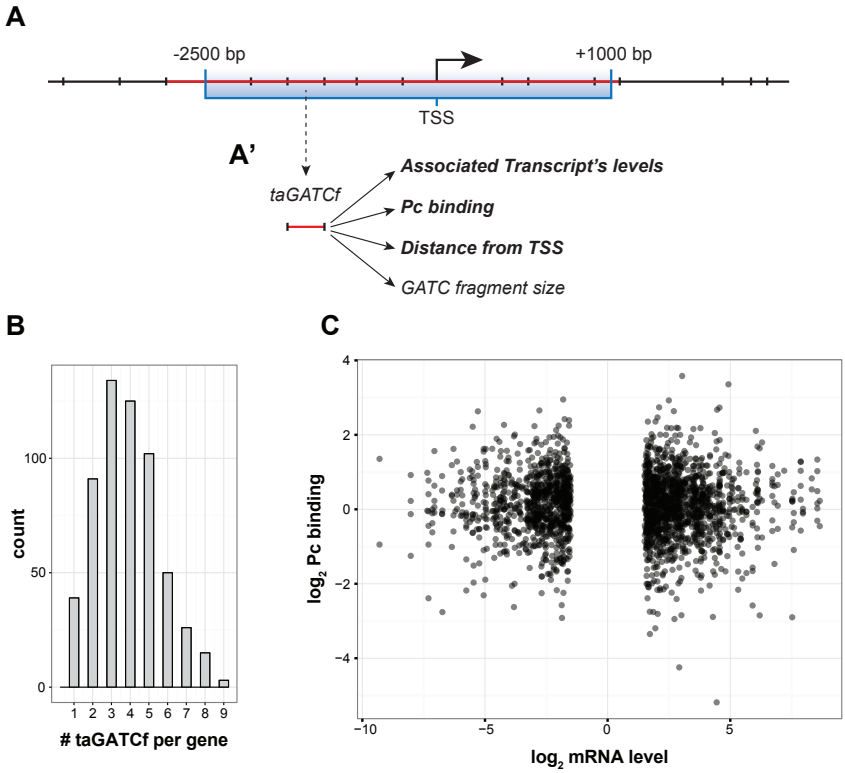

Figure 36. Study of the transcriptional-associated GATC fragments linked to differentially expressed genes.

(A) Scheme explaining transcriptional-associated GATC fragment (*taGATCf)* selection relative to the TSS of differentially expressed genes between WT and *scrib*[1] (-2500 bp to 1500 bp, blue area). (A') *taGATCf* can be associated by 5 different independent variables: *associated-transcript's levels* (***RNA level)***, *Pc binding* **(Pc binding)**, *distance from the TSS* **(dist)** and *fragment size* **(size)**. (B) Counts of *taGATCf* per gene. (C) Scatter plot showing absence of correlation between differentially expressed genes and Pc binding on *taGATCf.*

3.18 Analysis of Pc binding around TSS of differentially expressed genes revealed complex chromatin dynamics in tumour.

In addition to being described by the change in Pc binding and transcriptional level, taGA^{m}TCf could also be described by the distance from the TSS of the differentially expressed gene (taGA^{m}TCf$_{dist}$). In this analysis, I used the TS change based on HMM predictions to define the nature of Pc binding change between the two biological conditions for each taGA^{m}TCf, instead of absolute Pc binding differences (*cf.* 0) (Fig. 37). Finally, I took the taGA^{m}TCf fragment size into consideration (taGA^{m}TCf$_{size}$) (*cf. 3.20*). This analysis

yielded a linear regression model (M1) which also rejected the hypothesis of a binomial dependency between Pc binding and transcriptional levels.

$$\text{M1.} \qquad \text{taGA}^{\text{m}}\text{TCf}_{\textit{RNA level}} \sim \text{taGA}^{\text{m}}\text{TCf}_{\textit{Pc binding}}$$

Interestingly, when the variable distance from the TSS was taken in consideration as well as the taGA$^{\text{m}}$TC fragment size, a **multidimensional** regression model (M2) showed significant dependency when compared to M1 (M1 ~ M2).

$$\text{M2.} \qquad \text{taGA}^{\text{m}}\text{TCf}_{\textit{RNA level}} \sim \text{taGA}^{\text{m}}\text{TCf}_{\textit{Pc binding}} + \text{taGA}^{\text{m}}\text{TCf}_{\textit{dist}} + \text{taGA}^{\text{m}}\text{TCf}_{\textit{size}}$$

$$\text{M1}\sim\text{M2} \qquad \textit{p-val} = 0.018$$

This switch in significance between M1 to M2 demonstrates that the two variables taGA$^{\text{m}}$TCf$_{\textit{dist}}$ and taGA$^{\text{m}}$TCf$_{\textit{size}}$ can be used to describe the effect that changes of Pc binding has on gene expression.

Given the difficulties I encountered trying to describe a unique and general trend, I divided the differentially expressed genes into two groups with respect to their Pc binding behavior: *canonical* and *non-canonical gene. Canonical genes* were those genes that showed down or upregulation and an increase or decreased of Pc binding, respectively, all along the *locus*. *Non-canonical genes* were those genes that did not show any clear relationship between Pc binding and their transcriptional state.

This analysis showed that the gene *vestigial (vg)* was listed as a *canonical genes.* This was in agreement with previous reports that showed *vg* to be a PRC1 target gene as well as repressed during tumour formation in wing imaginal discsc [127, 128]. Importantly, novel potential Pc target genes were also classified as *canonical genes*, for example *Est21C, dIlp-8* and *chinmo.* These three genes showed transcriptional upregulation and loss in Pc binding in tumour samples when compared to wild type controls (Fig. 37).

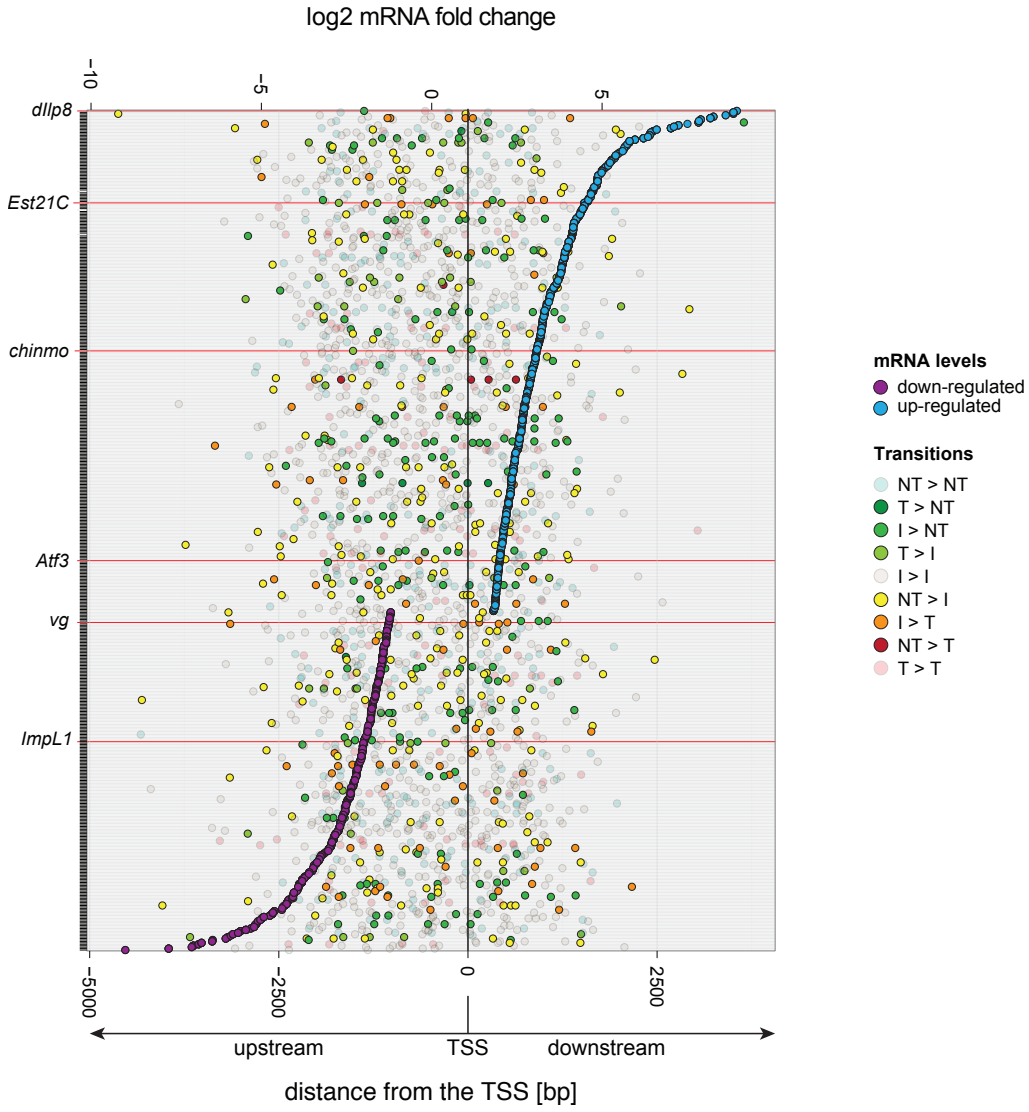

Figure 37. Dynamics of Pc binding affect specific genes expression during tumor formation.

Transcriptional levels of up regulated genes (blue dots) and down regulated genes (purple dots) in tumor (each grey line represent a single gene *locus*) are compared to the T-S of Pc binding around the TSS of each gene (-2500:1500 bp around the TSS). T-Ss (colored dots from red to green) that showed a difference from wild type to tumor were highlighted.

Among the *non-canonical genes,* the *loci* encoding the *Activating transcription factor 3 (Atf3)* and *Neurochondrin* were representative of the complexity of that group (Fig. 37, Fig. 38). *Atf3* showed gain of Pc binding despite of increasing expression levels during tumour formation (Fig. 38). In contrast, the *Neurochondrin* regulatory region displayed reduced Pc binding at the TSS while strong Pc binding could be found at around -1000 bp from the proximal promoter. However, Neurochondrin transcription increased in *scrib* tumors despite this strong Pc binding. This observation indicates a specific reorganisation of Pc binding around the TSS of certain genes which does not follow the classical cause-effect between Pc binding and transcriptional repression (Fig. 38).

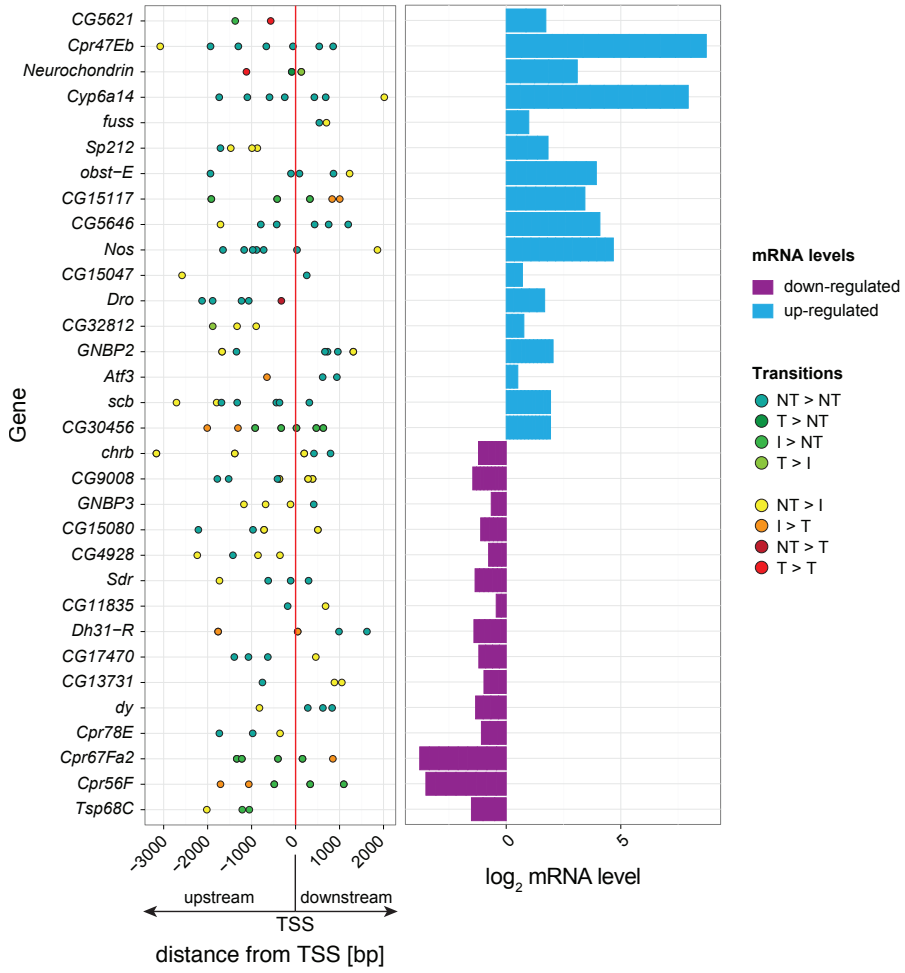

Figure 38. Pc binding is rearranged around the TSS of genes differentially expressed in tumor.

T-Ss of Polycomb binding (colored dots from red to green) are depicted across regulatory regions of gene differentially expressed in *scrib*[1] tumor. Bar graph represents mRNA expression levels (purple and blue indicate down and up regulation respectively).

3.19 Changes in Pc binding correlate with enrichment of specific Transcriptional Factors Binding Sites (TFBS).

Once clusters of gene differentially expressed between wild type and tumorous discs were defined, I analysed the regulatory regions of up- and downregulated genes around the TSS (*cfr. 3.17)* for enrichments of regulatory elements by using the i-*cis*Target algorithm [129, 130]. The selection of genes was additionally restricted by observed changes in Pc binding as defined by TS. Essentially, two groups of genes with canonical behaviour were

defined by: 1- upregulated genes with loss of Pc binding and 2- downregulated genes with gain of Pc binding (Table 1).

In the first group, the position weighted matrix (PWM) for the transcriptional repressor factor Lola showed to be enriched in genes high expressed in *scrib*^{1} tumour. The PWM for the transcriptional activator Jra also showed enrichment at these loci, albeit with a lower score than Lola. This result indicated a potential competition for Pc regulation between these two factors at these selected regions. In addition, the analysis reported enrichment for the acetyl-transferase Nejire (Nej/CBP) and the insulator factor CCCTC-binding Factor (CTCF).

Table 1. Enrichment of regulatory elements analysis on selected regions. Scores for enriched regulatory elements are reported as Normalized Enriched Score (NES, threshold NES > 3.00) [129, 130].

Regulatory Element	mRNA up - Pc Loss (NES)	mRNA down - Pc Gain (NES)
Nejire	5.52	n.s.
Lola	4.04	n.s.
Jra	3.27	n.s.
ZW5	n.s.	3.67
CTCF	3.52	3.22

In the second group, neither Lola nor Jra resulted to be enriched. In contrast, the two insulator factors Zeste-White 5 (ZW5) and CTCF showed high scores at these *loci*, together with common activators of gene transcription such as the TATA Binding Protein (TBP). Interestingly, Nej didn't show enrichment on these sequences but the JmjC domain-containing histone demethylase 1 (JHDM1). This indicates that different chromatin-associated proteins may guide Pc binding behavior.

The same approach was used to perform a genome-wide analysis of enriched regulatory elements on Pc binding domains as defined by their TS. As expected, H3K27me3 was strongly enriched in Pc target domain in both wild type and *scrib*^{1} tumour (T>T), such as at the *BX-C* cluster (Fig. 33C). In addition to this histone mark, the putative regulatory regions were enriched for Posterior sexcomb (Psc), Enhancer of Zeste (E(z)) and Polyhomeotic (Pho) binding, all components of the Polycomb Repressive Complexes, as identified by ChIP experiments in previously published studies. On the other hand, genomic regions that gained *de novo* Pc targeting in the tumour (NT>T) were mainly enriched by the presence of the insulator protein CTCF. TS domains transitoning from target to non-target (T>NT) state were especially enriched for binding by Posterior sexcomb (Psc), which is one of the components of the PRC1. Interestingly, the same TS class also showed enrichment for

the transcriptional repressor Lola. Neither Jra nor Nej motifs seemed to be enriched in such domains, pointing towards a more specific interaction with Pc in mediating gene regulation. Curiously, Nej was found to be highly enriched in static non-target Pc domain (NT>NT). Combined, these results indicated the potential existence of specific cross-talk between Pc and certain signalling pathways at specific *loci* during tumour formation.

3.20 Influence of GATC fragment size on Dam-ID data analysis results.

During my analysis, comparison of methylation levels at one *locus* between wild type and tumor samples related to the same GA^{m}TC fragments. Therefore, the variable *GATC fragment size* can be ignored. In contrast, any analysis that compares different *loci* within the same sample should also consider the influence of GATC fragment size on any results.

To test such hypothesis, I wanted to check whether there was any dependency between the length and the sequencing read counts for each GA^{m}TC fragment. More visible in the wild type sample, referencing Pc binding strength against GATC fragment size resulted in a skewed distribution from zero. Notably, the deviations from zero were different between two samples (Fig. 39A-B). In wild type wing imaginal discs, Polycomb exhibited decreased binding with increasing of GA^{m}TC fragment size (Fig. 39A). In contrast, *scrib*^{1} tumors did not have such drastic asymmetrical distribution with increasing GA^{m}TC fragments size (Fig. 39B).

In addition, comparison of DamID-seq profile obtained in different tissues show different distributions of dependency of Pc binding on GATC fragment size (Fig. 39A, D). Moreover, density plots correlating Pc binding with GATC fragment size described rather distinct distributions depending on the factor that was studied. For example, data obtained for WDS binding had a different behaviour to the one of Pc (Fig. 39C-D). Notably, both WDS and Pc profiles were generated in the same tissue and under same conditions. To understand whether this effect could be explained by any intrinsic technical variabilities, I compared the two independent technical replicates I run per sample. The distribution was consistent in both biological replicates. This analysis was confirmed by extended analysis of unpublished Dam profiles generated in both van Steensel and Pindyurin laboratories (data not shown).

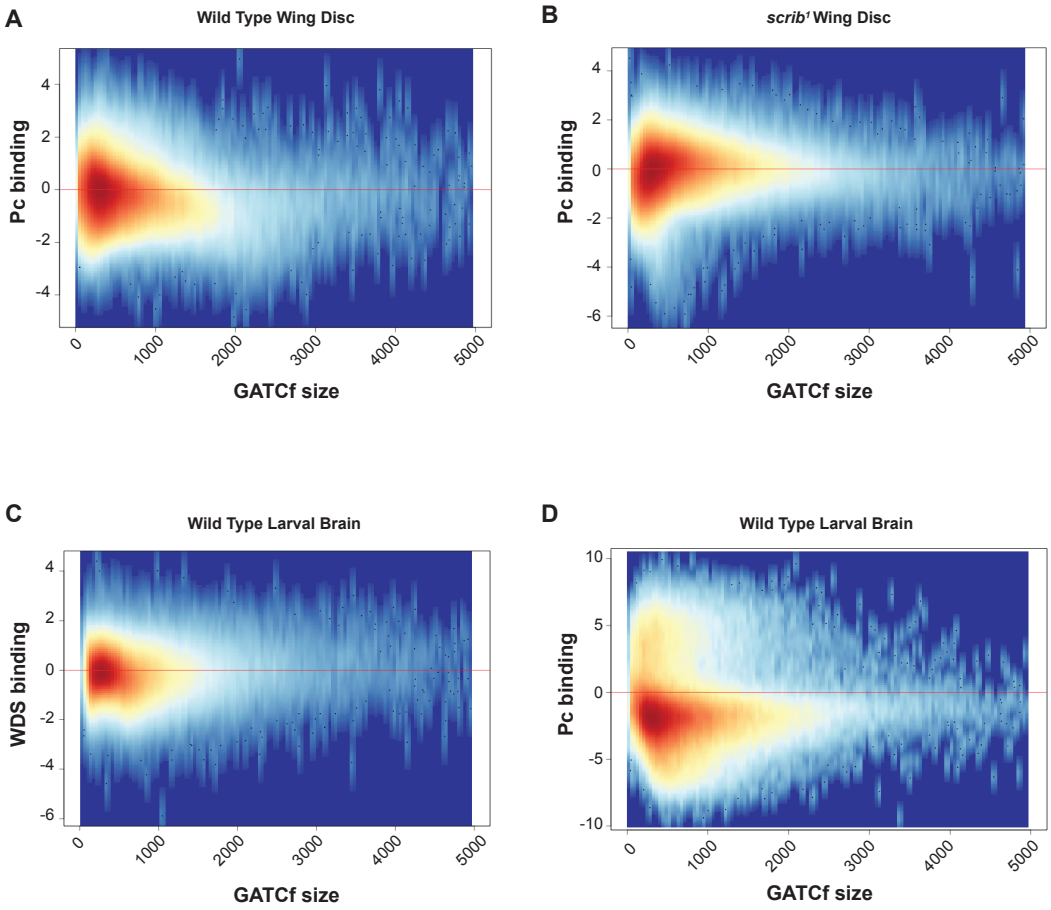

Figure 39. Pc binding is not indepented on GATC fragment size.

(A-B) Density heat-map of Pc binding as function of the GATC fragments size (GATCf size) in (A) wild type wing imaginal discs from 3rd instar larvae and (B) *scrib*^{1} wing imaginal discs. (C-D) Density heat-map of WDS binding as function of the GATC fragments size (GATCf size) in (C) brain of 3rd instar larvae. (D) Density heat-map of Pc binding as function of the GACT fragment size (GATCf size) in 3rd instar larvae brain.

My observations suggested that different GATC fragment sizes could be enriched for binding of specific chromatin factors. To describe the chromatin context to which each GATC fragment belonged to, I used the previously published 5-chromatin states [104] (Fig. 40A-B).

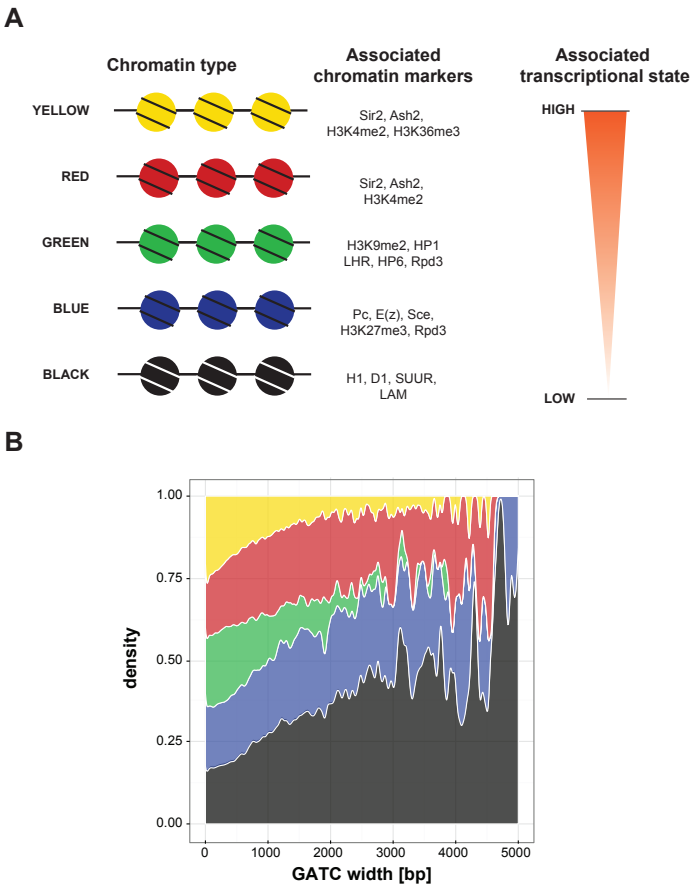

Figure 40. Large GATC fragments tend to be localized in highly repressed chromatin regions.

(A) Schematic representation of the 5 different chromatin states and their features [104]. (B) Cumulative density plot of GATC fragment sizes described by their individual chromatin state.

In wild type wing imaginal discs, GATC fragments didn't distribute homogenously across the 5 different chromatin states. Larger GATC fragments tended to be localised in highly repressed chromatin (BLACK chromatin). Notably, for large GATC fragments, GREEN chromatin, as well as YELLOW chromatin, was almost completely absent (Fig. 40B). Combined, these data indicate an important effect of $GATCf_{size}$ on the analysis of DamID-seq profiles while studying chromatin dynamics within the same sample. Comparison of DamID profiles of different *loci* can be strongly affected by the distribution of GATC fragment across them.

4 Material and Methods

4.1 Materials

4.1.1 Technical devices

Table 2 List of technical devices

Machine	Manufacturer
Mastercylcer NexusX2	Eppendorf
CFX Real-Time System	BioRad
Incubator 18 °C	CLF PlantClimatics GmbH
Incubator 25 °C MIR-154-PE	Panasonic
Centrifuge Fresco21	Thermo Scientific
Centrifuge Pico17	Thermo Scientific

4.1.2 Buffer, chemicals and consumables

Table 3 List of buffers, chemicals, consumables and their manufacturers

Buffer/ chemicals/ consumables	Manufacturer
1.5 ml and 0.5 ml tubes	Starstedt
15 ml and 50 ml tubes	Starstedt
Coverslips	Gerhard Menzel GmbH, Brauschweig
Dissection dish	Science Services GmbH, München
DAPI	Sigma-Aldrich Chemie GmbH, München
dNTPs	NEB
Ethanol 98%	Roth
Ethidium bromide	Roth
Immersion oil 518F	Carl Zeiss, Jena
Iso-propanol	Roth

Normal goat serum	BIOZOL Diagnostica Vertrieb GmbH, München
Methanol	Roth
Microscope slides	Carl Roth GmbH + Co. KG, Karlsruhe
Paraformaldehyde	Science Services GmbH, München
PBS	Sigma-Aldrich Chemie GmbH, München
PCR tubes	
Phalloidin Alexa488 and Alexa647	Life Technologies GmbH, Darmstadt
Phalloidin-TRITC	Sigma-Aldrich Chemie GmbH, München
Power SYBR Green Master Mix	Life Technologies GmbH, Darmstadt
Quibit assay tubes	Invitrogen
RNAlater	Quiagen GmbH, Hilden
Shields&Sang M3 medium	Sigma-Aldrich Chemie GmbH, München
SlowFade® Antifade Kit (Cat # S2828)	Life Technologies GmbH, Darmstadt
SlowFade® Gold Antifade reagent (Cat #S36936)	Life Technologies GmbH, Darmstadt
Triton-X 100	Sigma-Aldrich Chemie GmbH, München

4.1.3 Enzymes and kits

4.1.4 Antibodies

4.1.4.1 Primary antibodies

Table 4 Primary antibodies specificity

Antigen	Derived from	Provided by	Cat #	Dilution
H3S10p	mouse	Abcam	14955	1:2000
cCasp-3	rabbit	Cell Signalling	9661S	1:500
Dcp1	rabbit	Cell Signalling	9578	1:500
GFP	rabbit	Immunokontakt	210-PS-1GFP	1:2000
Nubbin	mouse	S. Cohen	---	1:100
βGal	rabbit	Capell		1:500
Zfh1	rat	R.Lehmann	---	1:500
Zfh2	rat	C. Doe	---	1:300

4.1.4.2 Secondary antibodies

Table 5 Secondary antibodies specificity

Antigen	Derived from	Label	Provided by	Dilution
Rabbit	Goat	Alex 488		
Mouse	Goat	and 647	Life Technologies	1:500
Guinea Pig	Goat	Alexa 647	GmbH, Darmstadt	
Rat	Goat	Alexa 647		

4.1.5 Kits

Kit	Manufacturer
TruSeq DNA PCR-Free Kit	Illumina
RNeasy Mini Kit	Qiagen
MinElute PCR Purification Kit	Qiagen

4.1.6 Oligonucleotides

4.1.6.1 qPCR primers

Table 6 Primers used for qPCR analysis.

GENE	STRAND	SEQ. 5'-3'	PRODUCT
upd1	Fwr	TCGATATGCGCTTTGTGAAG	Target
upd1	Rev	TGCTGCTGCTGTAGCAACTT	Target
upd2	Fwr	TACAAGTTCCTGCCGAACATGAC	Target
upd2	Rev	ACAAGTGGCGATTCTATAAGGGAAAC	Target
upd3	Fwr	CCCCTGAAGCACCTACAGAA	Target
upd3	Rev	AGGATCCTTTGGCGTTTCTT	Target
dome	Fwr	ATCGCAAAGAATACAAAATAAATTACAAAC	Target
dome	Rev	TCTGGAATCTGGAAACTAGAAACCAC	Target
hop	Fwr	TATCCGGATTTGGTATGGATGAATG	Target
hop	Rev	TTTTTAAAACAACACAAGCCAGACC	Target
STAT92E	Fwr	CATGCAATGTGCTCTTCACA	Target
STAT92E	Rev	AGATCTGGACGTGCTTTGCT	Target
hid	Fwr	ACAACTTCTTCCGGCAGCAG	Target
hid	Rev	GAAGGGAGGGGAATGGTGTG	Target
rpr	Fwr	CGACTCTGTTGCGGGAGG	Target
rpr	Rev	GGCTTGCGATATTTGCCGGA	Target
grim	Fwr	GTCGGAGTTTGGATGCTGGG	Target
girm	Rev	AGTCACGTCGTCCTCATCGT	Target
zfh1	Fwr	ACGAGCAGAGCAACATGAGC	Target
zfh1	Rev	CGGCGACATTTTGTTAGCAC	Target
zfh2	Fwr	TGCACACACAACAGATGCGT	Target

zfh2	Rev	GCACAGCTGACAAAGGAGCA	Target
kay	Fwr	CGAATAGCAAGAATCAGCTGGAGTA	Target
kay	Rev	CTGTCGTTGCTGTTGTGGTTGT	Target
GAPDH2	Fwr	GTGAAGCTGATCTCTTGGTACGAC	HK gene
GAPDH2	Rev	CCGCGCCCTAATCTTTAACTTTTAC	HK gene
CP1	Fwr	TGGTCATGGAGGAATGGCATACG	HK gene
CP1	Rev	ACGCTCCTCGGTTTCATCCTGATAG	HK gene
Act5C	Fwr	GGCGCAGAGCAAGCGTGGTA	HK gene
Act5C	Rev	GGGTGCCACACGCAGCTCAT	HK gene
αTub84B	Fwr	TGGGCCCGTCTGGACCACAA	HK gene
αTub84B	Rev	TCGCCGTCACCGGAGTCCAT	HK gene
RpL32	Fwr	AAGCGGCGACGCACTCTGTT	HK gene
RpL32	Rev	GCCCAGCATACAGGCCCAAG	HK gene
RpL13A	Fwr	AGCTGAACCTCTCGGGACAC	HK gene
RpL13A	Rev	TGCCTCGGACTGCCTTGTAG	HK gene

4.1.7 Microscopes

Table 7 Microscopes and microscopy equipment are listed.

Microscope	Equipment	Manufacturer
Confocal laser scanning microscope Leica TCS Sp5	Lasers: Diodenlaser 405 nm, 25 mV Argon Laser 458, 476, 488 and 514 nm DPSS Laser 561 nm, 10 mV HeNe Laser 633 nm, 10 mV Objectives: HCX PL APO Lambda Blue 20x 0.7 imm HCX PL APO Lambda Blue 63x 1.4 oil Software: Leica Application Suite Emission filters: detection spectrally adjusted	Leica, Heidelberg

Stereoscopic Zoom Microscope SMZ745	SMZ745 zooming body, C-PS plain focusing stand	Nikon
	Eyepieces: C-W10XB, 10x/22	
	Lightsource:	
	KL 1500 LCD with flexible light guides	Schott AG, Mainz
	Halogen lamp 15V/150W, Type 6423FO	Philips, Eindhoven
Fluorescence Stere	Optics:	
	Neolumar S 0.8x FWD 80mm, PI 10x/23 eyepieces	
Stereomicroscope StereoLumar v12	Filters: 38 HeGFP BP470/40, BP525/50	Carl Zeiss, Jena
	43 Cy3 BP545/25, BP605/70	
	Lightsource: HXP 120 C	

4.1.8 Software

Table 8 Software applications and their sources.

Application	Name	Source
	FIJI/Image J1.48 b	Wayne Rasband, NIH, USA; http://imagej.nih.gov/ij
	Adobe Photoshop CS5	Adobe Systems, Inc., San José
	Adobe Illustrator CS5	Adobe Systems, Inc., San José
	Helicon Focus Pro	Helicon Focus http://www.heliconfocus.de/helicon-focus-pro/?gclid=CPyNv57DusoCFU-3GwodGgkGZQ

Statistics and data processing	R(v3.0.1)	The R Foundation https://www.r-project.org/
	RStudio	RStudio, Boston (MA) https://www.rstudio.com/
	Perl	https://www.perl.org/
	Office 2007	Microsoft, Redmond
Conservation analysis	mVISTA	Universitiy of California, http://genome.lbl.gov/vista/index.shtml
Over-Rapressented transcription binding sites	Clover	Zhiping Lab http://zlab.bu.edu/clover/
Prediction of regulatory features	i-cisTarget	KU Leuven, Belgium https://gbiomed.kuleuven.be/apps/lcb/i-cisTarget/

4.1.9 Fly stocks

Table 9 List of all the fly stocks and their sources. Bloomington: BDSC Indiana University, IN. VDRC: VBCF-Vienna, Austria.

Genotypes	**Source**
w^{118}	
rn-Gal4,UAS-egr,tub-GAL80^{TS}/TM6b, tub-GAL80^{TS}	I Hariharan, R Smith-Bolton
UAS-FLP,Ubi-p63E.FRT>STOP>FRT-Stinger15F2	Bloomington
TRE-RFP	D Bohmann
TRE-GFP	D Bohmann
UAS-Bsk^{DN}	Bloomington
UAS-puc	Bloomington
10XSTATdGFP/Cyo	E Bach
dome^{G0441}/FM7, ubi-GFP	Bloomington
hop^{34}/FM7, ubi-GFP	N Perrimon
FRT82-Stat92E^{85C9}/TM6c	E Bach
UAS-dome$^{\Delta CYT}$/Cyo, ubi-GFP	E Bach
UAS-Socs36E	E Bach
zfh2[EAB]	F. J. Díaz-Benjumea, E. Sánchez-Herrero
UAS-upd1/Cyo, ubi-GFP	M Zeidler
w; UAS-upd2/Cyo	M Zeidler
dilp8-GFP	Bloomington

w; FRT 82B	Bloomington
yw, ey-FLP; act>y^{+}>GAL4, UAS-GFP/Cyo;FRT82B, tub-GAL80/TM6b	G Halder
yw, ey-FLP; UAS-Ras^{V12}/Cyo,FRT82B, scrib^{2}/TM6b	G Halder
ex[e1]-lacZ/SM6	G Halder
UAS-Ras^{V12}/Cyo; FRT82B, scrib^{2}, Stat92E^{85C9}/Tm6b	G Halder
UAS-p35	Bloomington
UAS-domeRNAi /Cyo, ubi-GFP	VDRC-KK106071
UAS-hopRNAi	BL-HMS00761
UAS-hopRNAi	BL-JF01268
UAS-Stat92ERNAi	BL-HMS00035
upd-lacZ/FM7a	Bloomington
STAT92E-GFP.FLAG/CyO;Dr/TM6c	Bloomington
MS1096-Gal4/FM7i;Sp/CyO;Dr/TM6c	Bloomington
UAS-zfh1.P	Bloomington
UAS-zfh1RNAi/TM3, Sb	BL-JF02509
UAS-zfh2RNAi/TM6b	VDRC-GD13305
Df(3L)H99/TM3, Sb	Bloomington
UAS-Dcr2/FM7i;en-Gal4,UAS-GFP	Bloomington

4.2 Fly husbandry and general experimental procedures

For detailed fly genotypes please refer to Table 9. Flies and experimental crosses were raised at room temperature, or at 18°C where necessary, on standard media. General procedures are described below:

- Cell ablation experiment:
  - Egg collection at 25 °C for 6 h on grape plate (Table 3). Egg collections where kept at 18 °C.
  - Larvae were picked after 2 days from the egg collection and kept at 18 °C.
  - Temperature shift at 30 °C was started 5, 6, 7 or 8 days after egg collection.
  - Temperature shift was stopped after 40 h and flies where kept at 18 °C in case they weren't dissected at R0.

- FLP/FRT experiments:

- 24 h egg collection at 25 °C in regular vials.
- Flies were kept at 25 °C.
- Heat-shock was induced 5 days after egg collection.
- Dissection was performed 48 h after heat-shock induction.

- DamID-seq experiment:
  - 1 day egg collection at 21 °C in regular vials.
  - Flies were kept at 21 °C.
  - Heat-shock at 37 °C was induced for 1 h after 5 or 6 days (wt and *scrib*^{1}) after egg collection.
  - Dissection was performed 2 days after heat-shock induction.

4.3 Cell Biological method

4.3.1 Flow cytometry

Flow cytometry analysis of wing imaginal disc cells was performed as described [131]. Briefly, 20-30 dissected wing imaginal discs were dissociated in PBS with 9XTrypsin-EDTA (Sigma) supplemented with 1.5 µg/ml Hoechst 33342 for 2-3 h at room temperature. Cell profiles were obtained using a FACS Aria II instrument (BD Biosciences) and analysed using FlowJo 8.8.7 (Tree Star) software.

4.3.2 Immunohistochemistry

Larvae were dissected in PBS and cuticles were fixed in 4% PFA for 15 min at room temperature. Washing steps were performed in 0.1% Triton X-100/PBS (PBT) and blocking was carried out using 5% NGS/PBT. Primary antibodies (Table 4) were incubated overnight at 4°C. Secondary antibodies (Table 5) were incubated for 2 h at room temperature. DAPI and phalloidin-TRITC (Table 3) were included as counter stains. Imaginal discs were fine dissected and mounted using Molecular Probes Antifade reagents. Imaging was performed using a Leica TCS-SP5 microscope and conditions were adjusted to obtain a linear signal range for image quantifications. Reference and experimental samples were processed at the same time and subsequently imaged using the exact same confocal settings. Images were handled and analysed using FIJI (ImageJ v1.47) software tools.

4.3.2.1 BrdU labelling

Larvae were dissected in Shields and Sang M3 medium and incubated for 30 min with 100µg/µl BrdU (Sigma) at room temperature. Cuticles were fixed in 4% PFA for 15 minutes and subsequently washed with 0.5% Triton X-100/PBS in all washing steps. Fixed tissues were incubated for 45 min in 2N HCl and washed with 0.1M H_3BO_3 for 2 min twice. Antibody incubations, sample mounting and analysis was carried out as described above.

4.3.3 Image quantification

4.3.3.1 General Information

Images were taken using 20X or 63X objectives (without additional optical zoom). Stacks were imaged at 1024x1024 pixel resolution and a z-step size of 1µm. Control and experimental samples were prepared under the same conditions on the same day, as well as imaged using the same conditions on the same day.

4.3.3.2 GFP volume quantification (G-trace lineage labelling)

Masks of the GFP signal were generated applying the 'Threshold' (settings: 'Triangle', stack histogram, dark background) and 'Remove Outliers' (settings: black and white pixels removal with radii= 1-10 at a constant threshold of 50) function to entire image stacks in FIJI. The resulting masks were analysed using the '3D Object Counter' function (settings: threshold= 128, min=10 max=Inf, Exclude Object On Edges=FALSE). Measured volumes for each disc were summed up and used to describe total GFP volume per disc.

4.3.3.3 pH3 and BrdU counts

Masks of pH3 (or BrdU) events per disc were generated by applying the 'Threshold' (settings: 'Li', stack histogram, dark background) and 'Remove Outliers' (settings: black and white pixels removal with radii= 1-5 at a constant threshold of 50) function to entire image stacks in FIJI. The resulting masks were analysed using the '3D Object Counter' function (settings: threshold= 128, min=10 max=Inf, Exclude Object On Edges=FALSE). The total number of counted particles was considered to represent mitotic or DNA replication events per disc.

4.3.3.4 pH3-positive mitotic events in G-trace lineage labelled cells)

To count the number of cells marked by pH3 within the GFP-positive, G-trace volume, the pH3 mask was 'Subtracted' (FIJI function) from the GFP mask. The resulting mask was analysed using the '3D Object Counter' function (settings: threshold= 128,

min=10 max=Inf, Exclude Object On Edges=FALSE). The new total counts of particles were considered to be mitotic events in GFP-positive cells.

4.3.3.5 TRE-reporter quantifications

Image stacks were manually curated to eliminate TRE-reporter activity signals arising from the peripodial membrane. The peripodium shows extensive TRE-reporter activity, which was not subject of this study. Maximum projections of the final image stacks were obtained in FIJI and

masks of the area with active reporter were generated using the 'Threshold' (settings: 'IsoData', stack histogram, dark background) and 'Remove Outliers' (settings: black and white pixels removal with radii=1-10 at a constant threshold of 50) function. The areas of resulting masks were quantified using the ROI analyzer in FIJI.

4.4 Molecular biological methods

4.4.1.1 Quantitative real-time PCR

RNA was extracted from ca. 80 wild type or cell ablated wing imaginal disc using Qiagen RNAlater preservation and RNeasy extraction kit protocols. cDNA libraries were prepared using standard protocols including DNase (Ambion TurboDNase) treatment and utilizing Superscript III First strand synthesis kits (Invitrogen). Quantitative real-time PCR was performed using Fast SYBR Green Master Mix (Applied Biosystems) on a CFX-96 Real-Time System machine (BioRad). Data was analysed using the $\Delta\Delta C_t$ method and expression levels were normalized to at least two different housekeeping genes (*RpL32*, *RpL13A*, α*Tub84B*, *Act5C*). Fold inductions are shown as average of at least three biological replicate. Primer sequences are listed in Table 6.

4.4.1.2 MNase reaction

Wing imaginal discs were dissected from 20 larvae and washed in 1 ml of 1% PBS. Once centrifuged at 1500 rpm for 10 min at 4 °C, dissected tissues were incubated in 600 µl cell lysis buffer (1% PBS, 0.3% Triton, Protease inhibitors) no longer than 10 min at 4 °C. Dissolved tissues were centrifuged at 3000 rpm for 10 min at 4 °C in order to obtain pellets of nuclei. Pellets were additionally wash in 1 ml of 1% PBS and then centrifuged at 3000 rpm for 10 min at 4 °C.

MNase reaction was run on nuclei pellets resupsended in 50 µl of EX100 buffer, 2mM CaCl2, Protease Inhibitor. MNase reactions were run for 1,5 min at 26 °C with

different enzyme concentrations: 0.2 U, 0.4 U and 0.8 U. The enzymatic reaction was blocked by adding 10 µl of EDTA 10 mM on ice.

4.4.1.3 DamID and library preparation

DamID-seq protocol was run on wing imaginal discs dissected from *Drosophila* 3rd instar larvae. Cell lyses buffer was modified from the published protocol as follow: Tris-HCl pH 8.0 [10 mM], EDTA pH 8.0 [10mM], NaCl 100mM, SDS 0.5%. gDNA was extracted and precipitated with a classical phenol-chloroform/ethanol precipitation. mePCR was performed as previously described [101, 106]. mePCR products were purified using Qiagen MinElute PCR purification Kit according to manufactures protocol (elution was done in 50 µl of the provided EB). Samples with a DNA concentration lower then 50 ng/µl were discarded and not used for library preparation. Illumina TruSeq PCR-free library preparation kit was used to obtain DamID-seq library according manufactures protocol. Next Generation Sequencing was run on Illumina GenomeAnalyzer IIx cBot machine.

4.5 Adult wings size analysis

Adult flies were collected right after eclosion and stored in 2-propanol (Sigma). For wing size scoring, five wing size phenotypes were defined (Fig. 5A). Wings from the same fly were scored independent of each other. A wing size index (Ws) was calculated as the weighted average of the five different wing phenotypes (w) weighted with the frequencies at which they occurred (f) within the entire population ($Ws = \Sigma w_i \times f_i / \Sigma f_i$). Wing size samples were compared in a paired manner to their control wings from the same experimental replicate by applying the Wilcoxon signed rank test. The alpha value was set to $\alpha=0.05$. $n \geq 3$ for all experiments.

4.6 Bioinformatics

4.6.1.1 Transcription factor binding site prediction

Bioinformatic analysis for potential transcription factor binding sites was performed using the program Clover (Cis-eLement OVERrepresentation) [115] in combination with position-weighted-matrices (PWM) obtained from the JASPAR collection [132]. The p-value threshold of all predictions was set to $p<0.05$. *Drosophila* chromosome 2R was used as background sequence in all calculations. For each gene, genomic sequences (dm6 genome

version) of 2.5 kb upstream from the transcriptional start site (TSS) and the entire coding sequence were selected for analysis. For short genes with a sequence shorter than 2 kb (e.g. *rpr* and *grim*) a 2.5 kb sequence downstream of the 3'UTR was add to the analysis. Data was visualized using USCS genome browser tools. mVISTA conservation analysis [118, 119] was run on *kay* and *hid* genomic region by comparing *D.melanogaster* to: *D.simulans*, *D. sechellia*, *D. erecta*, *D. yakuba*, *D. ananassae*, *D. pseudobscura*, *D. persimilis*, *D. willistoni*, *D. virilis*, *D. grimshawi*. Genomic sequences were obtained from FlyBase. ATAC-seq profiles were previously published (Davie et al., 2015) (GEO access number: GSE59078) and used as predictors of open chromatin regions.

4.6.1.2 RNA-seq data.

RNA-seq data were obtained from [72] and re-analysed using DESeq for gene expression levels [133]. Normalized values for gene expression are reported as RPKM value for each gene.

4.6.1.3 Analysis of enriched regulatory elements on selected sequences.

Selected sequences were submitted to analysis for enrichment in regulatory elements on *i-cis*Target [129, 130]. Sequences were screen for PWMs, TFBs, histone modifications, DHS and FAIRE-seq data. Default parameters were selected (Database version 3.0).

5 Discussion

5.1 JAK/STAT acts as pro-survival signaling during tissue stress response.

JNK activation in response to tissue stress promotes elimination of damaged cells by apoptosis [36, 37, 42, 48, 49] and drives compensatory proliferation necessary to replace lost tissues [33, 43, 50-52]. Large part of my doctoral studies have provided an answer to the central question of how these Janus-faced responses can be balanced downstream of JNK activation. JAK/STAT signalling downstream of JNK does not promote compensatory proliferation, but instead supports cell survival and thereby contributes to tissue growth (Fig. 7N).

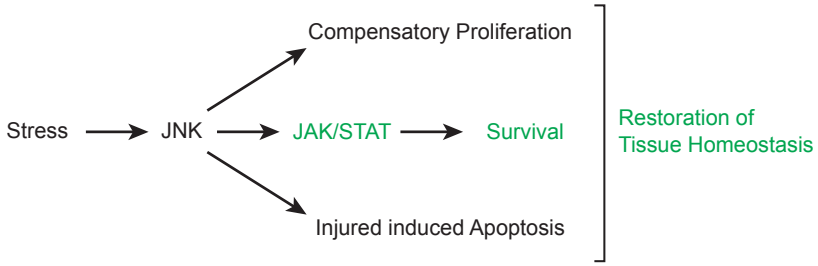

Figure 41. JAK/STAT promotes cell survival.

Cells activating JNK in response to stress induce compensatory proliferation as well as injured-induced apoptosis. JAK/STAT suppresses apoptosis, thereby limiting the extent of tissue damage and promoting compensatory responses, such as induction of development delays.

My functional data supports this conclusion. I demonstrate that JAK/STAT signalling in Eiger-stimulated discs declined at the time when high levels of compensatory proliferation occurred (R24). While correlative, this observation suggests that JAK/STAT signalling and proliferation may not be directly rather indirectly linked. However,

JAK/STAT promoting survival of stressed cells can also indirectly support regenerative growth by allowing JNK to induce dILP8-dependent developmental delays or to initiate Hippo/Yorkie-driven proliferation. This new interpretation of the role of JAK/STAT can be reconciled with previous studies, as loss of these responses in JAK/STAT mutant tissue causes a reduction in tissue size; a read-out that has been used in many studies and interpreted as a reduction in growth [40, 66, 69, 70], but which we I presented to be a consequence of excessive cell death.

My work highlighted the pro-survival function of JAK/STAT in the context of tissue stress induced by cell ablation, physical injury or tumours. A few studies have previously implicated JAK/STAT in promoting cell survival [81, 82]. For example, the apoptosis inhibitor *dIAP* has been suggested to be a positively regulated target of STAT92E to protect JAK/STAT-signalling cells from apoptosis [81, 82]. My analysis indicated the JAK/STAT effector Zfh2 as a potential repressor of *kay* and *hid* gene activity; a molecular pathway expected to restrain excessive JNK-activity, as well as JNK-dependent induction of apoptosis (Fig. S8A). Combined, my work and previous studies [81, 82, 84, 87] suggest that JAK/STAT and Zfh-proteins can promote cell survival by targeting multiple molecular pathways impinging on anti- and pro-apoptotic genes.

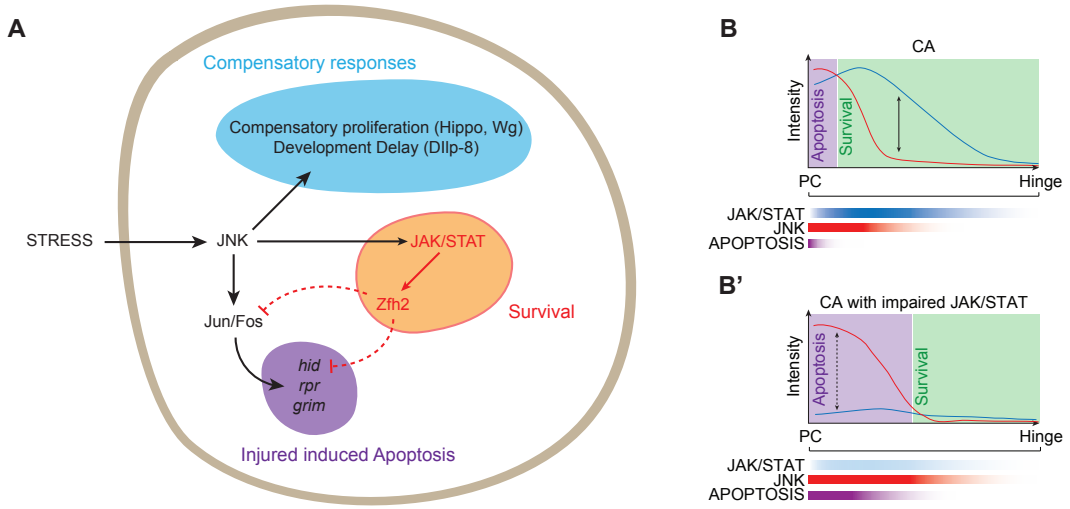

Figure 42. Model for repression of injured-induced apoptosis through the activation of Zfh2.

(A) Cells that activate JNK signalling in response to tissue stress induce compensatory responses as well as injured-induced apoptosis. JAK/STAT activates Zfh-2 to repress *hid* and *fos (kay),* thereby limiting strong JNK-activation and Hid-induced apoptosis. Suppression of apoptosis limits the extent of tissue damage and promotes compensatory responses by cells surviving JNK activation. This facilitates activation of compensatory proliferation and induction of development delays. (B) Non-autonomous activation of JNK and of JAK/STAT creates two differently sloped signalling gradients from the site of damage (cell ablation (CA) in the pouch centre (PC)). A low JNK/JAKSTAT ratio induces apoptosis, whereas a high low JNK/JAKSTAT ratio promotes survival. (B') If the JAK/STAT signalling gradient is disturbed (f.e. by heterozygosity for JAK/STAT components) all cells with JNK signalling have a low JNK/JAKSTAT ratio, making them more likely to die. Higher levels of apoptosis near the site of damage (PC) induce stronger non-autonomous activation of JNK, which in turn induces apoptosis at sites more

distant to the initial damage. This feed-forward loop, unrestrained by loss of JAK/STAT activity, drives spatial expansion of JNK signalling and apoptosis, thereby increasing the extent of tissue damage and limiting the ability of the tissue to induce regenerative responses.

My experiments do not address if JAK/STAT promotes cell survival only under conditions of cellular stress or also during normal development. Cells carrying mutations in JAK/STAT pathway components have been observed to be eliminated from wing discs by apoptosis [80]. While this developmental phenotype has been linked to a non-autonomous process called cell competition, I suggest that more studies are needed to dissect the functional contribution of stress-signals in this context; especially in the light of recent studies, which implicate chronic JNK-signalling in loser cell states [78]. In contrast, overexpression of Upd has been previously reported to drive cell proliferation and tissue growth [67, 68, 70]. However, overexpression of Upd can also induce apoptosis (data not shown) and, thus very likely causes JNK activation. Additional studies are needed to clearly distinguish between JAK/STAT-functions that are dependent or independent of cooperativity with JNK during development or tissue stress.

While the role of mammalian IL-6/STAT3 in tissue regeneration needs to be further investigated, many evidences point to JNK and JAK/STAT pathways as crucial mediators of compensatory responses and tumorigenesis in mammalian tissues [49]. A recent report suggests that JAK/STAT activation during mouse liver regeneration potentially confers a cell-protective function, similarly facilitating initiation of compensatory responses, rather then directly promoting cell proliferation [134]. Therefore, the dominant pro-survival function of JAK/STAT in response to tissue stress, which I find to be essential for successful restoration of tissue homeostasis, may be highly relevant to human contexts of cellular stress in physiological or pathological conditions.

5.2 The JAK/STAT and JNK signaling cross talk.

My data supports a model by which the decision between JAK/STAT-dependent survival and JNK-induced apoptosis may depend on the relative cellular ratio between JAK/STAT and JNK signalling, which is determined by the position of cells within the respective signalling gradients (Fig. S8B, B'). My data collected for this analysis, reveals a a spatial segregation of the JNK and JAK/STAT signalling domains. Based on this I suggest a

three states model to describe the activation and the cross talk between the two signalling during tissue stress response (Fig. 43).

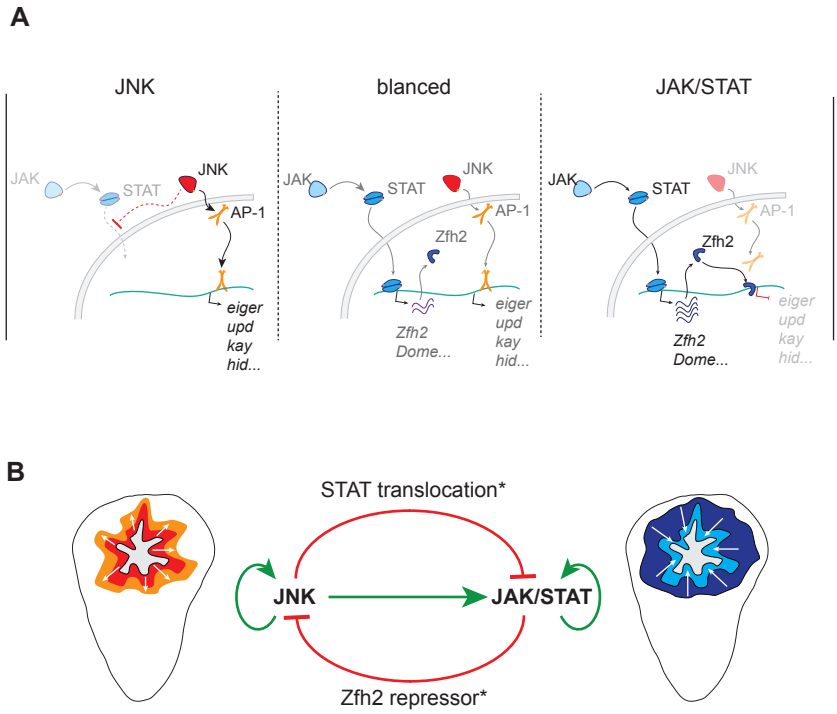

Figure 43. The three states model of JNK-JAK/STAT cross-talk during tissue stress response.

(A) Three state model explaining how signaling cross-talk spatial stratification potential differences between JAK/STAT and JNK activation/repression during tissue stress response. (B) Model of the cross-talk between JAK/STAT and JNK signaling leading to spatial segregation of signaling domains. Green arrows indicate positive feedback loops causing pathway activation previously described in the literature. JNK, for examples, drives expression of Eiger, thereby cell-autonomously amplifying and stabilizing, as well as non-autonomously propagating JNK signaling. JNK drives *upd* transcription, thereby causing cell non-autonomous activation of JAK/STAT. JAK/STAT drives expression of the Dome receptor thereby cell-autonomously amplifying and stabilizing JAK/STAT signaling. The red repression arrows marked by stars indicate the contribution from the current work: Zfh2 activation by JAK/STAT and prevention of STAT nuclear translocation by JNK represses the other signaling pathway cell-autonomously leading to spatial segregation of the two signaling domains. Our work demonstrates that elimination of the JAK/STAT signaling induces aberrant spread of the JNK signaling from the pouch centre (red to orange in the cartoon) increasing cell death rates. Reduction in the JNK levels should result in the spreading of the JAK/STAT signaling towards the pouch centre (dark blue to light blue in the cartoon) possibly affecting apoptosis patterns that necessary for a proper stress response.

In the first state, JAK/STAT signalling seems to be totally absent in cells that show high JNK activation levels. This conclusion arises from experiments in which cell ablation is driven alongside *p35* over expression. The resulting undead cells, exhibiting high levels of JNK activity, do not show any activation of the JAK/STAT pathway. I demonstrated that in this specific group of cells, STAT92E does not translocate into the nucleus indicating that JNK may interfere with JAK/STAT signal transduction (Fig. 15E, Fig. 43).

The second state is characterised by a balance of both JNK and JAK/STAT signalling activities. In these cells, JNK is non-autonomously induced and its levels are not as high as in the first state. Coexistence with JAK/STAT signaling allows cells to activate compensatory responses mediated by JNK activity without driving additional cell death. As discussed above, JNK activation is buffered and kept in check by the activation of the JAK/STAT pathway.

In the third state, representing cells farthest away from the stress source, JAK/STAT activation reaches its peak while the JNK pathway is totally silenced. In these region the activation of the JAK/STAT completely prevents activation and spreading of JNK signalling (Fig. 43). Notably, although the JAK/STAT signalling is very high, compensatory responses that are directly linked to the JNK pathway cannot be autonomously activated in these cells. Therefore, *dILP-8* activation, as well as activation of Hpo/Yki signalling is not readily detectable far from the wound site [3, 50](Fig).

5.3 Polycomb protein regulates specific genes during tumor growth.

During tissue stress responses, the ability to dynamically change the chromatin landscape of cells mediating compensatory responses is a crucially important. Mutation in genes encoding chromatin factors often decrease the compensatory responses leading to severe phenotypes (Fig. 30). The PRC1 complex is known to be a key factor in regulating and maintaining gene silencing throughout development and adulthood [72, 92, 97, 135]. My studies specifically focused on the PRC1 component Pc and its dynamic binding to DNA during tumour formation in *scrib*^{1} mutant tissues. Combining already published RNA-seq data with DamID-seq profiles of Pc in wild type and *scrib* mutant tissue allowed me to identify a series of differentially expressed gene that show a relevant change in Pc binding in their regulatory regions.

Specifically, *dIlp-8* was shown to be up regulated during wounding and neoplasiae formation [99, 121, 122]. So far, dynamic regulation of this gene has not been associated with Pc activity. My DamID data analysis revealed a loss of Pc binding close to the transcriptional start site (TSS) in tumours. The loss of Pc binding in tumours could explain the high transcriptional levels of *dIlp-8.* Similarly, other genes implicated in tumor formation, such as *chinmo* and *Ets21c* follow the same logic. Chinmo is a transcriptional repressor that is known to be activated by JAK/STAT signalling [66, 83]. Chinmo has been shown to be important for the maintenance of stemness during *Drosophila* gonad development in as well

as being a promoter of tumor malignancy [83]. Thus, it is tempting to speculate that the activation of *chinmo* may promote tumour formation by giving to tumour cells a stem-like nature. The activation of Ets21c has similarly been shown to be important for tumour progression in *Drosophila* [136]. Just like *dIlp-8* this transcription factor is a downstream target of JNK. These observations indicate that *dilp8* and *Ets21c* represent optimal *loci* to study a possible interactions between JNK and Polycomb activity during gene regulation.

My data also uncovered a series of genes where the link between Pc binding and transcriptional levels was harder to establish. This is the case for *atf3* or *Neurochondrin.* At these *loci*, changes in the transcriptional levels seem to be dependent on the relative position of Pc with respect the TSS of these genes. For other genes, the level Pc bound around the TSS seems to be maintained stable although the transcriptional levels are significantly changed during tumour formation (e.g. *Cpr56F*) (Fig.38). The changes in Pc are in its redistribution around the TSS rather than the total level of binding, which remains, on average, unchanged. These observations emphasize how important a full description of DNA-protein interaction along a single *locus* is in order to fully describe chromatin dynamics during physiological processes and stress responses.

5.4 Polycomb activity may interact with specific signaling pathways

My bioinformatic analysis for enrichment of regulatory elements on differentially bounded Pc regions suggested a strong link between Pc and the transcriptional repressor Lola, the transcriptional activator Jra, the acetyl-transferase Nejre and insulator factors CTCF and ZW5. Lola has been previously reported to interact with Polycomb proteins [137]. In addition, mutations in *lola* can lead to tumor formation [138]. My data indicates that in *scrib* tumors, enrichment of Lola motifs was preferentially found in regions where Pc binding was lost rather then gained. PRC1 and Lola may thus act together on *loci* that are specifically activated during tumour formation. My data strongly supports the hypothesis that synergistic interactions between Pc and Lola may prevent tumour formation in wild type tissues.

Similarly, Jra was enriched in regions where Pc binding was lost. Jra is a positive regulator of gene transcription activated by JNK signalling [46, 139]. Although previous work suggested a potential interaction between JNK signalling and Pc function, to date, this cross-talk has never been demonstrated directly [140, 141]. My data thus strongly suggests a

link between PRC1 function and JNK signalling. Because of their opposite functions, those regions that showed a decrease in Pc binding and enrichment in Lola and Jra, could be direct targets of the AP-1 during tumour formation otherwise silenced by the repressive module Lola-Pc.

Nejire (Nej/CBP) is an acetyl-transferase that has been found to associate with the methyl-transferase ASH1 and N-Trx. This specific complex is known to be important for gene transcription, especially during elongation. Like Jra and Lola, the enrichment for Nej binding is high in regions that tend to loose Pc binding. Considering the opposite nature of the two factors, the data describes a system were Pc and Nej tend to exclude each other from common targets. Interestingly, in genes that are down regulated in tumour Nej is not enriched.

An additional factor that is specific to only one TS change condition is the insulator factor Zeste-White 5 (ZW5). Insulators are known to be mainly involved in reorganising chromatin architecture and in controlling gene expression. Due to its enrichment in down regulated gene with higher Pc binding in tumour, ZW5 could function together with Pc in promoting gene silencing. Considering the specificity of ZW5 enrichment in repressed *loci* with high Pc in tumors, the repressive module ZW5-Pc could be responsible of the transcriptional state of tumor-suppressor genes during stress responses.

Such TS state specificity could not be identified for the insulator factor CTCF. CTCF is known to act on chromatin architecture as well as on control of gene transcription. CTCF displays context-specific effects, which has lead to divergent conclusions about its general function [142, 143]. Therefore, from the analysis I run, it is hard to discuss a clear activity of CTCF in relation to Pc presence and gene transcription. However, it is not surprising to find CTCF enriched in all genes that have been analysed for enrichment of regulatory elements. The activity of CTCF is linked to chromatin boundaries formation. This is an important feature in chromatin organisation in defining different chromatin types within the same nucleus.

In the future, a more extended analysis of PRC1 as well as PRC2 components should be performed in the same biological context. Collecting such data would provide a more complete picture of the dynamic changes involving the Polycomb Repressive Complexes and signalling pathways that are associated with them during tumour formation.

5.5 DamID-seq technique can be used to study chromatin accessibility.

DamID-seq is a method that facilitates the study of protein-DNA interaction using an inducible, genetics-based system. In my analysis, I asked whether it would be possible to describe differences in Pc binding by comparing binding profiles between different genomic regions from the same sample. More specifically, I wondered whether differences in Pc binding at promoters could be linked to a specific transcriptional change. To perform this computational analysis, I needed to consider a new important variable in the data analysis: namely the GATC fragment size, or the length of a sequence between two GATC sites. In my thesis, I integrated GATC fragment size with the definition of GATC site density: essentially, two DNA sequences that have the same length can be described by their GATC content independently. Intuitively, any sequence with higher GATC density also has a higher number of GATC fragments. Therefore, a higher frequency of GATC sites translates into an enrichment of shorter GATC fragments.

In my work, I demonstrated how strong of an effect the variable GATC fragment size can have on the outcome of DamID analysis. As GATCs do not distribute homogeneously across the genome, the presence of GATC sites does not correlate linearly with DNA sequence length. Certain regions have a lower GC content, making GATC sites less likely to occur than in sequences with high GC content. In addition, regions with high and low GC content tend to cluster in specific chromatic compartments with specific chromatin features (Fig. 40B). Thus, while studying the differential binding of a chromatin factor across one specific *locus,* one needs to take into account how GATC density changes across the *locus*. In fact, analysis of the amount of reads as a function of the GATC fragment size showed an important dependency (Fig. 39). Interestingly, this dependency strongly correlates with the nature of the chromatin factor that was mapped as well as the tissue in which the experiments was performed (Fig. 39). Thus, the dependency of profiling results on GATC fragment size distribution in the genome seems to be specific to the biological sample rather than a bias induced by the technique.

Importantly, another interesting observation indicated that in wild type wing imaginal discs Pc binding decreases in GATC fragments which are longer then 1,5 kb. On the other hand, the same GATC fragments show an increased Pc binding in tumours if compared to wild type (Fig. 39 A-B). In tumor, in the TS domain describing gain of Pc binding were larger then the ones were Pc was lost.

Chromatin domains targeted by Polycomb during tumor formation are larger (Fig. 35). This evidence suggests that the removal of Pc is a more restrained process while gain of Pc occurs on broader DNA domains.

6 Conclusions

The work undertaken during my doctoral studies have provided novel insights important for our understanding of tissue stress responses and tumor formation.

My work redefined the role of the JAK/STAT signalling during stress responses. Previously being described as direct controller of compensatory proliferation, I provide evidences that clearly assign a pro-survival function to JAK/STAT signalling which directly buffers excessive activation of JNK signalling, a major mediator of stress-induced apoptosis. By doing so, JAK/STAT allows cells to generate proper compensatory responses, such as tissue sealing and regenerative proliferation, that are necessary to restore tissue homeostasis. I identified the transcriptional repressor Zfh2 as mediator of the survival function of JAK/STAT. I also extended my conclusion also to chronic situation of stress induction, such as tumor formation.

In addition, the present work characterised the importance of chromatin change during responses to chronic stress. Analysis of the dynamic variations of Polycomb binding during tumor formation showed a particular reorganisation of chromatin interactions during such event. This specificity is additionally confirmed by the presence of defined regulatory elements across genomic regions that are differentially bound by Polycomb, thus suggesting that modulation of chromatin dynamics is mediated by specific cellular signalling pathways.

References

1. Fulda, S., et al., *Cellular stress responses: cell survival and cell death.* Int J Cell Biol, 2010. **2010**: p. 214074.
2. Levayer, R. and E. Moreno, *Mechanisms of cell competition: themes and variations.* J Cell Biol, 2013. **200**(6): p. 689-98.
3. Sun, G. and K.D. Irvine, *Control of growth during regeneration.* Curr Top Dev Biol, 2014. **108**: p. 95-120.
4. Vriz, S., S. Reiter, and B. Galliot, *Cell death: a program to regenerate.* Curr Top Dev Biol, 2014. **108**: p. 121-51.
5. Varga, M., et al., *Autophagy is required for zebrafish caudal fin regeneration.* Cell Death Differ, 2014. **21**(4): p. 547-56.
6. Bryant, P.J., *Regeneration and duplication in imaginal discs.* Ciba Found Symp, 1975. **0**(29): p. 71-93.
7. Haynie, J.L. and P.J. Bryant, *Intercalary regeneration in imaginal wing disk of Drosophila melanogaster.* Nature, 1976. **259**(5545): p. 659-62.
8. Katsuyama, T., et al., *During Drosophila disc regeneration, JAK/STAT coordinates cell proliferation with Dilp8-mediated developmental delay.* Proc Natl Acad Sci U S A, 2015. **112**(18): p. E2327-36.
9. Grusche, F.A., et al., *The Salvador/Warts/Hippo pathway controls regenerative tissue growth in Drosophila melanogaster.* Dev Biol, 2011. **350**(2): p. 255-66.
10. Herrera, S.C., R. Martin, and G. Morata, *Tissue homeostasis in the wing disc of Drosophila melanogaster: immediate response to massive damage during development.* PLoS Genet, 2013. **9**(4): p. e1003446.
11. Smith-Bolton, R.K., et al., *Regenerative growth in Drosophila imaginal discs is regulated by Wingless and Myc.* Dev Cell, 2009. **16**(6): p. 797-809.
12. Kashio, S., F. Obata, and M. Miura, *Interplay of cell proliferation and cell death in Drosophila tissue regeneration.* Dev Growth Differ, 2014. **56**(5): p. 368-75.

13. Razzell, W., W. Wood, and P. Martin, *Swatting flies: modelling wound healing and inflammation in Drosophila.* Dis Model Mech, 2011. **4**(5): p. 569-74.
14. Sustar, A., et al., *Drosophila twin spot clones reveal cell division dynamics in regenerating imaginal discs.* Dev Biol, 2011. **356**(2): p. 576-87.
15. Bosch, M., J. Baguna, and F. Serras, *Origin and proliferation of blastema cells during regeneration of Drosophila wing imaginal discs.* Int J Dev Biol, 2008. **52**(8): p. 1043-50.
16. Herrera, S.C. and G. Morata, *Transgressions of compartment boundaries and cell reprogramming during regeneration in Drosophila.* Elife, 2014. **3**: p. e01831.
17. Repiso, A., C. Bergantinos, and F. Serras, *Cell fate respecification and cell division orientation drive intercalary regeneration in Drosophila wing discs.* Development, 2013. **140**(17): p. 3541-51.
18. Schuster, K.J. and R.K. Smith-Bolton, *Taranis Protects Regenerating Tissue from Fate Changes Induced by the Wound Response in Drosophila.* Dev Cell, 2015. **34**(1): p. 119-28.
19. Ohlstein, B. and A. Spradling, *The adult Drosophila posterior midgut is maintained by pluripotent stem cells.* Nature, 2006. **439**(7075): p. 470-4.
20. Jiang, H., et al., *Cytokine/Jak/Stat signaling mediates regeneration and homeostasis in the Drosophila midgut.* Cell, 2009. **137**(7): p. 1343-55.
21. Osman, D., et al., *Autocrine and paracrine unpaired signaling regulate intestinal stem cell maintenance and division.* J Cell Sci, 2012. **125**(Pt 24): p. 5944-9.
22. Staley, B.K. and K.D. Irvine, *Warts and Yorkie mediate intestinal regeneration by influencing stem cell proliferation.* Curr Biol, 2010. **20**(17): p. 1580-7.
23. Teng, X. and Y. Toyama, *Apoptotic force: active mechanical function of cell death during morphogenesis.* Dev Growth Differ, 2011. **53**(2): p. 269-76.
24. Sarkissian, T., et al., *Cell death regulates muscle fiber number.* Dev Biol, 2016.
25. Martin, F.A., A. Perez-Garijo, and G. Morata, *Apoptosis in Drosophila: compensatory proliferation and undead cells.* Int J Dev Biol, 2009. **53**(8-10): p. 1341-7.
26. Manjon, C., E. Sanchez-Herrero, and M. Suzanne, *Sharp boundaries of Dpp signalling trigger local cell death required for Drosophila leg morphogenesis.* Nat Cell Biol, 2007. **9**(1): p. 57-63.
27. Igaki, T., *Correcting developmental errors by apoptosis: lessons from Drosophila JNK signaling.* Apoptosis, 2009. **14**(8): p. 1021-8.
28. Lohmann, I., et al., *The Drosophila Hox gene deformed sculpts head morphology via direct regulation of the apoptosis activator reaper.* Cell, 2002. **110**(4): p. 457-66.
29. Monier, B., et al., *Apico-basal forces exerted by apoptotic cells drive epithelium folding.* Nature, 2015.
30. Gilbert SF, S.M., *Developmental Biology*, ed. t. edition. 2000.
31. Suzanne, M., et al., *Coupling of apoptosis and L/R patterning controls stepwise organ looping.* Curr Biol, 2010. **20**(19): p. 1773-8.

32. Perez-Garijo, A., Y. Fuchs, and H. Steller, *Apoptotic cells can induce non-autonomous apoptosis through the TNF pathway.* Elife, 2013. **2**: p. e01004.
33. Ryoo, H.D., T. Gorenc, and H. Steller, *Apoptotic cells can induce compensatory cell proliferation through the JNK and the Wingless signaling pathways.* Dev Cell, 2004. **7**(4): p. 491-501.
34. Fan, Y. and A. Bergmann, *Distinct mechanisms of apoptosis-induced compensatory proliferation in proliferating and differentiating tissues in the Drosophila eye.* Dev Cell, 2008. **14**(3): p. 399-410.
35. Fan, Y. and A. Bergmann, *Apoptosis-induced compensatory proliferation. The Cell is dead. Long live the Cell!* Trends Cell Biol, 2008. **18**(10): p. 467-73.
36. Luo, X., et al., *Foxo and Fos regulate the decision between cell death and survival in response to UV irradiation.* Embo J, 2007. **26**(2): p. 380-90.
37. Moreno, E., M. Yan, and K. Basler, *Evolution of TNF signaling mechanisms: JNK-dependent apoptosis triggered by Eiger, the Drosophila homolog of the TNF superfamily.* Curr Biol, 2002. **12**(14): p. 1263-8.
38. Brumby, A.M. and H.E. Richardson, *scribble mutants cooperate with oncogenic Ras or Notch to cause neoplastic overgrowth in Drosophila.* Embo J, 2003. **22**(21): p. 5769-79.
39. Uhlirova, M., H. Jasper, and D. Bohmann, *Non-cell-autonomous induction of tissue overgrowth by JNK/Ras cooperation in a Drosophila tumor model.* Proc Natl Acad Sci U S A, 2005. **102**(37): p. 13123-8.
40. Wu, M., J.C. Pastor-Pareja, and T. Xu, *Interaction between Ras(V12) and scribbled clones induces tumour growth and invasion.* Nature, 2010. **463**(7280): p. 545-8.
41. Zhu, M., et al., *Activation of JNK signaling links lgl mutations to disruption of the cell polarity and epithelial organization in Drosophila imaginal discs.* Cell Res, 2010. **20**(2): p. 242-5.
42. Shlevkov, E. and G. Morata, *A dp53/JNK-dependant feedback amplification loop is essential for the apoptotic response to stress in Drosophila.* Cell Death Differ, 2012. **19**(3): p. 451-60.
43. Bosch, M., et al., *JNK signaling pathway required for wound healing in regenerating Drosophila wing imaginal discs.* Dev Biol, 2005. **280**(1): p. 73-86.
44. Ramet, M., et al., *JNK signaling pathway is required for efficient wound healing in Drosophila.* Developmental biology, 2002. **241**(1): p. 145-56.
45. Lee, N., et al., *Suppression of Polycomb group proteins by JNK signalling induces transdetermination in Drosophila imaginal discs.* Nature, 2005. **438**(7065): p. 234-7.
46. Eferl, R. and E.F. Wagner, *AP-1: a double-edged sword in tumorigenesis.* Nat Rev Cancer, 2003. **3**(11): p. 859-68.
47. Rios-Barrera, L.D. and J.R. Riesgo-Escovar, *Regulating cell morphogenesis: the Drosophila Jun N-terminal kinase pathway.* Genesis, 2013. **51**(3): p. 147-62.

48. Bogoyevitch, M.A., et al., *c-Jun N-terminal kinase (JNK) signaling: recent advances and challenges.* Biochim Biophys Acta, 2010. **1804**(3): p. 463-75.
49. Chen, F., *JNK-induced apoptosis, compensatory growth, and cancer stem cells.* Cancer Res, 2012. **72**(2): p. 379-86.
50. Sun, G. and K.D. Irvine, *Regulation of Hippo signaling by Jun kinase signaling during compensatory cell proliferation and regeneration, and in neoplastic tumors.* Dev Biol, 2011. **350**(1): p. 139-51.
51. Bergantinos, C., M. Corominas, and F. Serras, *Cell death-induced regeneration in wing imaginal discs requires JNK signalling.* Development, 2010. **137**(7): p. 1169-79.
52. Mattila, J., et al., *Role of Jun N-terminal Kinase (JNK) signaling in the wound healing and regeneration of a Drosophila melanogaster wing imaginal disc.* Int J Dev Biol, 2005. **49**(4): p. 391-9.
53. Wells, B.S., E. Yoshida, and L.A. Johnston, *Compensatory proliferation in Drosophila imaginal discs requires Dronc-dependent p53 activity.* Curr Biol, 2006. **16**(16): p. 1606-15.
54. Kondo, S., et al., *DRONC coordinates cell death and compensatory proliferation.* Mol Cell Biol, 2006. **26**(19): p. 7258-68.
55. Huh, J.R., M. Guo, and B.A. Hay, *Compensatory proliferation induced by cell death in the Drosophila wing disc requires activity of the apical cell death caspase Dronc in a nonapoptotic role.* Curr Biol, 2004. **14**(14): p. 1262-6.
56. Morata, G., E. Shlevkov, and A. Perez-Garijo, *Mitogenic signaling from apoptotic cells in Drosophila.* Dev Growth Differ, 2011. **53**(2): p. 168-76.
57. Pastor-Pareja, J.C. and T. Xu, *Dissecting social cell biology and tumors using Drosophila genetics.* Annu Rev Genet, 2013. **47**: p. 51-74.
58. Pahlavan, P.S., et al., *Prometheus' challenge: molecular, cellular and systemic aspects of liver regeneration.* J Surg Res, 2006. **134**(2): p. 238-51.
59. Perez-Garijo, A., F.A. Martin, and G. Morata, *Caspase inhibition during apoptosis causes abnormal signalling and developmental aberrations in Drosophila.* Development, 2004. **131**(22): p. 5591-8.
60. Perez-Garijo, A., E. Shlevkov, and G. Morata, *The role of Dpp and Wg in compensatory proliferation and in the formation of hyperplastic overgrowths caused by apoptotic cells in the Drosophila wing disc.* Development, 2009. **136**(7): p. 1169-77.
61. Myllymaki, H. and M. Ramet, *JAK/STAT pathway in Drosophila immunity.* Scand J Immunol, 2014. **79**(6): p. 377-85.
62. Gregory, L., P.J. Came, and S. Brown, *Stem cell regulation by JAK/STAT signaling in Drosophila.* Semin Cell Dev Biol, 2008. **19**(4): p. 407-13.
63. Ayala-Camargo, A., et al., *The JAK/STAT pathway regulates proximo-distal patterning in Drosophila.* Dev Dyn, 2007. **236**(10): p. 2721-30.

64. Ayala-Camargo, A., et al., *JAK/STAT signaling is required for hinge growth and patterning in the Drosophila wing disc.* Dev Biol, 2013. **382**(2): p. 413-26.
65. Arbouzova, N.I. and M.P. Zeidler, *JAK/STAT signalling in Drosophila: insights into conserved regulatory and cellular functions.* Development, 2006. **133**(14): p. 2605-16.
66. Amoyel, M., A.M. Anderson, and E.A. Bach, *JAK/STAT pathway dysregulation in tumors: a Drosophila perspective.* Semin Cell Dev Biol, 2014. **28**: p. 96-103.
67. Bach, E.A., et al., *A sensitized genetic screen to identify novel regulators and components of the Drosophila janus kinase/signal transducer and activator of transcription pathway.* Genetics, 2003. **165**(3): p. 1149-66.
68. Tsai, Y.C. and Y.H. Sun, *Long-range effect of upd, a ligand for Jak/STAT pathway, on cell cycle in Drosophila eye development.* Genesis, 2004. **39**(2): p. 141-53.
69. Mukherjee, T., J.C. Hombria, and M.P. Zeidler, *Opposing roles for Drosophila JAK/STAT signalling during cellular proliferation.* Oncogene, 2005. **24**(15): p. 2503-11.
70. Classen, A.K., et al., *A tumor suppressor activity of Drosophila Polycomb genes mediated by JAK-STAT signaling.* Nat Genet, 2009. **41**(10): p. 1150-5.
71. Davie, K., et al., *Discovery of Transcription Factors and Regulatory Regions Driving In Vivo Tumor Development by ATAC-seq and FAIRE-seq Open Chromatin Profiling.* PLoS Genet, 2015. **11**(2): p. e1004994.
72. Bunker, B.D., et al., *The transcriptional response to tumorigenic polarity loss in Drosophila.* Elife, 2015. **4**.
73. Vaccari, T. and D. Bilder, *The Drosophila tumor suppressor vps25 prevents nonautonomous overproliferation by regulating notch trafficking.* Dev Cell, 2005. **9**(5): p. 687-98.
74. Herz, H.M., et al., *vps25 mosaics display non-autonomous cell survival and overgrowth, and autonomous apoptosis.* Development, 2006. **133**(10): p. 1871-80.
75. Moberg, K.H., et al., *Mutations in erupted, the Drosophila ortholog of mammalian tumor susceptibility gene 101, elicit non-cell-autonomous overgrowth.* Dev Cell, 2005. **9**(5): p. 699-710.
76. Pastor-Pareja, J.C., M. Wu, and T. Xu, *An innate immune response of blood cells to tumors and tissue damage in Drosophila.* Dis Model Mech, 2008. **1**(2-3): p. 144-54; discussion 153.
77. Lin, G., N. Xu, and R. Xi, *Paracrine Unpaired Signaling through the JAK/STAT Pathway Controls Self-renewal and Lineage Differentiation of Drosophila Intestinal Stem Cells.* J Mol Cell Biol, 2009.
78. Kolahgar, G., et al., *Cell Competition Modifies Adult Stem Cell and Tissue Population Dynamics in a JAK-STAT-Dependent Manner.* Dev Cell, 2015.
79. Schroeder, M.C., et al., *A non-cell-autonomous tumor suppressor role for Stat in eliminating oncogenic scribble cells.* Oncogene, 2013. **32**(38): p. 4471-9.

80. Rodrigues, A.B., et al., *Activated STAT regulates growth and induces competitive interactions independently of Myc, Yorkie, Wingless and ribosome biogenesis.* Development, 2012. **139**(21): p. 4051-61.
81. Betz, A., et al., *STAT92E is a positive regulator of Drosophila inhibitor of apoptosis 1 (DIAP/1) and protects against radiation-induced apoptosis.* Proc Natl Acad Sci U S A, 2008. **105**(37): p. 13805-10.
82. Hasan, S., P. Hetie, and E.L. Matunis, *Niche signaling promotes stem cell survival in the Drosophila testis via the JAK-STAT target DIAP1.* Dev Biol, 2015. **404**(1): p. 27-39.
83. Flaherty, M.S., et al., *chinmo is a functional effector of the JAK/STAT pathway that regulates eye development, tumor formation, and stem cell self-renewal in Drosophila.* Dev Cell, 2010. **18**(4): p. 556-68.
84. Ohayon, D., et al., *Zfh1 promotes survival of a peripheral glia subtype by antagonizing a Jun N-terminal kinase-dependent apoptotic pathway.* EMBO J, 2009. **28**(20): p. 3228-43.
85. Leatherman, J.L. and S. Dinardo, *Zfh-1 controls somatic stem cell self-renewal in the Drosophila testis and nonautonomously influences germline stem cell self-renewal.* Cell Stem Cell, 2008. **3**(1): p. 44-54.
86. Perea, D., et al., *Multiple roles of the gene zinc finger homeodomain-2 in the development of the Drosophila wing.* Mech Dev, 2013. **130**(9-10): p. 467-81.
87. Guarner, A., et al., *The zinc finger homeodomain-2 gene of Drosophila controls Notch targets and regulates apoptosis in the tarsal segments.* Dev Biol, 2014. **385**(2): p. 350-65.
88. Maurange, C., N. Lee, and R. Paro, *Signaling meets chromatin during tissue regeneration in Drosophila.* Curr Opin Genet Dev, 2006. **16**(5): p. 485-9.
89. Katsuyama, T. and R. Paro, *Epigenetic reprogramming during tissue regeneration.* FEBS Lett, 2011. **585**(11): p. 1617-24.
90. Shaw, T. and P. Martin, *Epigenetic reprogramming during wound healing: loss of polycomb-mediated silencing may enable upregulation of repair genes.* EMBO Rep, 2009. **10**(8): p. 881-6.
91. Schuettengruber, B., et al., *Genome regulation by polycomb and trithorax proteins.* Cell, 2007. **128**(4): p. 735-45.
92. Zhang, Y., et al., *Mechanism of Polycomb group gene silencing.* Cold Spring Harb Symp Quant Biol, 2004. **69**: p. 309-17.
93. Wang, H., et al., *Role of histone H2A ubiquitination in Polycomb silencing.* Nature, 2004. **431**(7010): p. 873-8.
94. Roure, V. and F. Bantignies, *Polycomb group-mediated gene silencing mechanisms: stability versus flexibility.* Epigenomics, 2009. **1**(2): p. 301-18.

95. de Napoles, M., et al., *Polycomb group proteins Ring1A/B link ubiquitylation of histone H2A to heritable gene silencing and X inactivation.* Dev Cell, 2004. **7**(5): p. 663-76.
96. Martinez, A.M. and G. Cavalli, *Uncovering a tumor-suppressor function for Drosophila polycomb group genes.* Cell Cycle, 2010. **9**(2): p. 215-6.
97. Benitz, S., et al., *Polycomb repressor complex 1 promotes gene silencing through H2AK119 mono-ubiquitination in acinar-to-ductal metaplasia and pancreatic cancer cells.* Oncotarget, 2016. **7**(10): p. 11424-33.
98. Axelson, H., *Eyeing tumorigenesis: Notch signaling and epigenetic silencing of Rb in Drosophila.* Bioessays, 2006. **28**(7): p. 692-5.
99. Skinner, A., S.J. Khan, and R.K. Smith-Bolton, *Trithorax regulates systemic signaling during Drosophila imaginal disc regeneration.* Development, 2015. **142**(20): p. 3500-11.
100. Lobner-Olesen, A., O. Skovgaard, and M.G. Marinus, *Dam methylation: coordinating cellular processes.* Curr Opin Microbiol, 2005. **8**(2): p. 154-60.
101. Vogel, M.J., D. Peric-Hupkes, and B. van Steensel, *Detection of in vivo protein-DNA interactions using DamID in mammalian cells.* Nat Protoc, 2007. **2**(6): p. 1467-78.
102. Southall, T.D., et al., *Cell-type-specific profiling of gene expression and chromatin binding without cell isolation: assaying RNA Pol II occupancy in neural stem cells.* Dev Cell, 2013. **26**(1): p. 101-12.
103. Grigolon, G., *Establishing a cell-type specific approach for Polycomb-DamID to investigate chromatin plasticity in tissue regeneration*, in *Dept. Biology*. 2015, Universitá degli studi di Padova.
104. Filion, G.J., et al., *Systematic protein location mapping reveals five principal chromatin types in Drosophila cells.* Cell, 2010. **143**(2): p. 212-24.
105. Moorman, C., et al., *Hotspots of transcription factor colocalization in the genome of Drosophila melanogaster.* Proc Natl Acad Sci U S A, 2006. **103**(32): p. 12027-32.
106. Tolhuis, B., et al., *Genome-wide profiling of PRC1 and PRC2 Polycomb chromatin binding in Drosophila melanogaster.* Nat Genet, 2006. **38**(6): p. 694-9.
107. van Bemmel, J.G., et al., *The insulator protein SU(HW) fine-tunes nuclear lamina interactions of the Drosophila genome.* PLoS One, 2010. **5**(11): p. e15013.
108. Negre, N., et al., *Chromosomal distribution of PcG proteins during Drosophila development.* PLoS Biol, 2006. **4**(6): p. e170.
109. Yin, H., et al., *A high-resolution whole-genome map of key chromatin modifications in the adult Drosophila melanogaster.* PLoS Genet, 2011. **7**(12): p. e1002380.
110. Terriente Felix, J., M. Magarinos, and F.J. Diaz-Benjumea, *Nab controls the activity of the zinc-finger transcription factors Squeeze and Rotund in Drosophila development.* Development, 2007. **134**(10): p. 1845-52.
111. Evans, C.J., et al., *G-TRACE: rapid Gal4-based cell lineage analysis in Drosophila.* Nat Methods, 2009. **6**(8): p. 603-5.

112. Igaki, T. and M. Miura, *The Drosophila TNF ortholog Eiger: emerging physiological roles and evolution of the TNF system.* Semin Immunol, 2014. **26**(3): p. 267-74.
113. Chatterjee, N. and D. Bohmann, *A versatile PhiC31 based reporter system for measuring AP-1 and Nrf2 signaling in Drosophila and in tissue culture.* PLoS One, 2012. **7**(4): p. e34063.
114. Bach, E.A., et al., *GFP reporters detect the activation of the Drosophila JAK/STAT pathway in vivo.* Gene Expr Patterns, 2007. **7**(3): p. 323-31.
115. Frith, M.C., et al., *Detection of functional DNA motifs via statistical over-representation.* Nucleic Acids Res, 2004. **32**(4): p. 1372-81.
116. Postigo, A.A., et al., *zfh-1, the Drosophila homologue of ZEB, is a transcriptional repressor that regulates somatic myogenesis.* Mol Cell Biol, 1999. **19**(10): p. 7255-63.
117. Postigo, A.A. and D.C. Dean, *Independent repressor domains in ZEB regulate muscle and T-cell differentiation.* Mol Cell Biol, 1999. **19**(12): p. 7961-71.
118. Frazer, K.A., et al., *VISTA: computational tools for comparative genomics.* Nucleic Acids Res, 2004. **32**(Web Server issue): p. W273-9.
119. Bray, N., I. Dubchak, and L. Pachter, *AVID: A global alignment program.* Genome Res, 2003. **13**(1): p. 97-102.
120. Buenrostro, J.D., et al., *Transposition of native chromatin for fast and sensitive epigenomic profiling of open chromatin, DNA-binding proteins and nucleosome position.* Nat Methods, 2013. **10**(12): p. 1213-8.
121. Colombani, J., D.S. Andersen, and P. Leopold, *Secreted peptide Dilp8 coordinates Drosophila tissue growth with developmental timing.* Science, 2012. **336**(6081): p. 582-5.
122. Garelli, A., et al., *Imaginal discs secrete insulin-like peptide 8 to mediate plasticity of growth and maturation.* Science, 2012. **336**(6081): p. 579-82.
123. Leong, G.R., et al., *Scribble mutants promote aPKC and JNK-dependent epithelial neoplasia independently of Crumbs.* BMC Biol, 2009. **7**: p. 62.
124. Faralli, H., et al., *UTX demethylase activity is required for satellite cell-mediated muscle regeneration.* J Clin Invest, 2016. **126**(4): p. 1555-65.
125. van Bemmel, J.G., et al., *A network model of the molecular organization of chromatin in Drosophila.* Mol Cell, 2013. **49**(4): p. 759-71.
126. Nagata, S., et al., *Degradation of chromosomal DNA during apoptosis.* Cell Death Differ, 2003. **10**(1): p. 108-16.
127. Khan, S.J., et al., *Epithelial neoplasia in Drosophila entails switch to primitive cell states.* Proc Natl Acad Sci U S A, 2013. **110**(24): p. E2163-72.
128. Okulski, H., et al., *Quantitative analysis of polycomb response elements (PREs) at identical genomic locations distinguishes contributions of PRE sequence and genomic environment.* Epigenetics Chromatin, 2011. **4**: p. 4.

129. Imrichova, H., et al., *i-cisTarget 2015 update: generalized cis-regulatory enrichment analysis in human, mouse and fly.* Nucleic Acids Res, 2015. **43**(W1): p. W57-64.
130. Herrmann, C., et al., *i-cisTarget: an integrative genomics method for the prediction of regulatory features and cis-regulatory modules.* Nucleic Acids Res, 2012. **40**(15): p. e114.
131. de la Cruz, A.F. and B.A. Edgar, *Flow cytometric analysis of Drosophila cells.* Methods Mol Biol, 2008. **420**: p. 373-89.
132. Mathelier, A., et al., *JASPAR 2014: an extensively expanded and updated open-access database of transcription factor binding profiles.* Nucleic Acids Res, 2014. **42**(Database issue): p. D142-7.
133. Anders, S. and W. Huber, *Differential expression analysis for sequence count data.* Genome Biol, 2010. **11**(10): p. R106.
134. Wuestefeld, T., et al., *Interleukin-6/glycoprotein 130-dependent pathways are protective during liver regeneration.* J Biol Chem, 2003. **278**(13): p. 11281-8.
135. Abed, J.A. and R.S. Jones, *H3K36me3 key to Polycomb-mediated gene silencing in lineage specification.* Nat Struct Mol Biol, 2012. **19**(12): p. 1214-5.
136. Kulshammer, E., et al., *Interplay among Drosophila transcription factors Ets21c, Fos and Ftz-F1 drives JNK-mediated tumor malignancy.* Dis Model Mech, 2015. **8**(10): p. 1279-93.
137. Ferres-Marco, D., et al., *Epigenetic silencers and Notch collaborate to promote malignant tumours by Rb silencing.* Nature, 2006. **439**(7075): p. 430-6.
138. Southall, T.D., et al., *Dedifferentiation of neurons precedes tumor formation in Lola mutants.* Dev Cell, 2014. **28**(6): p. 685-96.
139. Kockel, L., J.G. Homsy, and D. Bohmann, *Drosophila AP-1: lessons from an invertebrate.* Oncogene, 2001. **20**(19): p. 2347-64.
140. Tiwari, V.K., et al., *A chromatin-modifying function of JNK during stem cell differentiation.* Nat Genet, 2012. **44**(1): p. 94-100.
141. Blanco, E., et al., *Gene expression following induction of regeneration in Drosophila wing imaginal discs. Expression profile of regenerating wing discs.* BMC Dev Biol, 2010. **10**: p. 94.
142. Mourad, R. and O. Cuvier, *Computational Identification of Genomic Features That Influence 3D Chromatin Domain Formation.* PLoS Comput Biol, 2016. **12**(5): p. e1004908.
143. Magbanua, J.P., et al., *A variably occupied CTCF binding site in the ultrabithorax gene in the Drosophila bithorax complex.* Mol Cell Biol, 2015. **35**(1): p. 318-30.

Appendix

6.1 Appendix I – Experimental procedure for cell ablation induction in wing imaginal discs

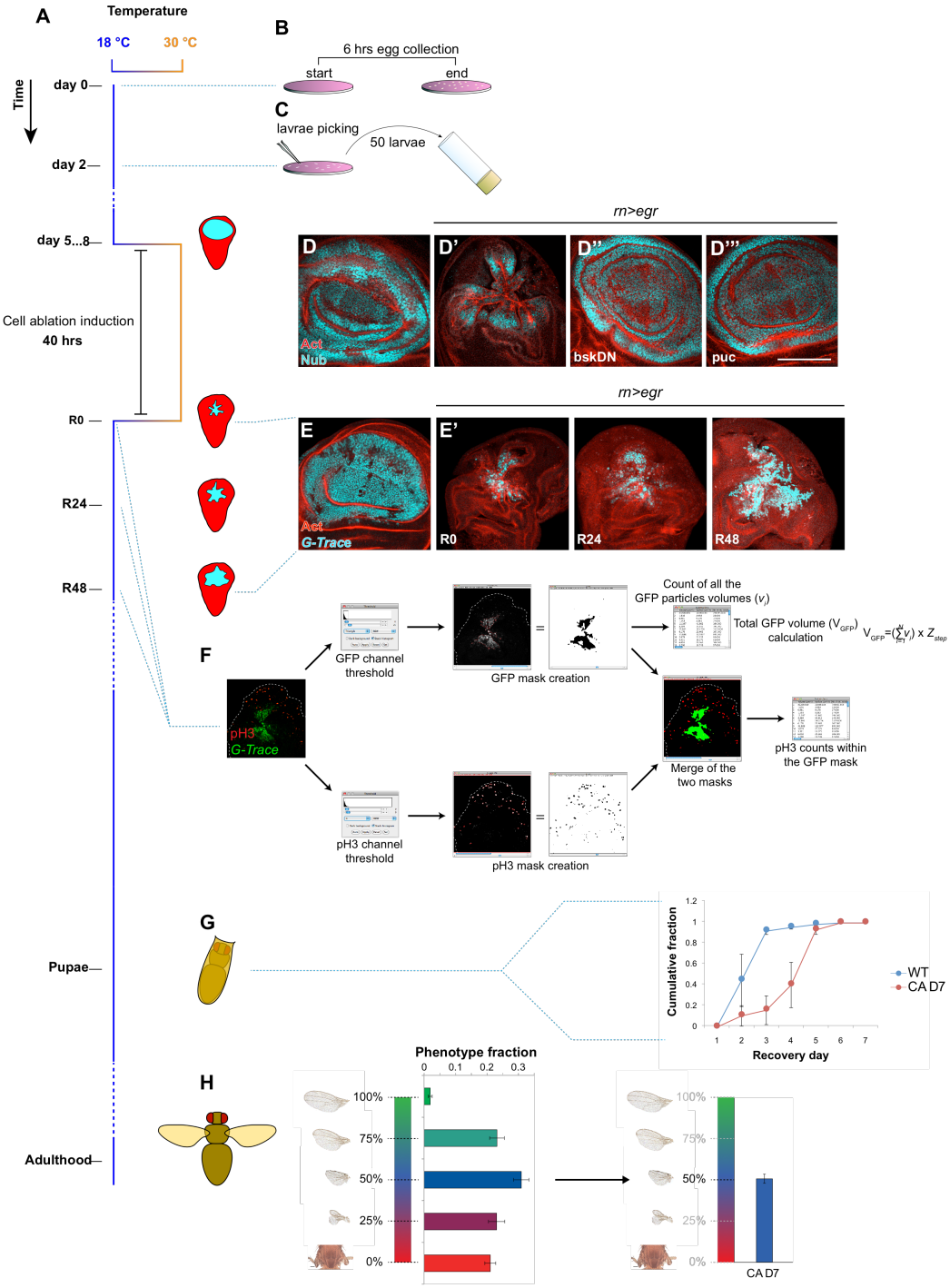

Appendix I - Figure 1. Experimental procedure.

(A) Time line of development and induction of cell ablation by eiger-expression as a function of rearing temperature. Flies were raised at 18°C (blue) and transferred to 30°C (orange) for 40 hours to induce eiger-expression and cell ablation (CA) in wing imaginal discs. CA was induced at different stages of development: 5 days (D5) after egg deposition (AED) or at day 6 (D6), day (D7) or day (D8). Unless otherwise noted, experiments were performed at D7. (B) 6 hour egg collections were performed on grape juice plates (D0). (C) 2 days after egg deposition (D2) 50 first instar larvae were collected in a vial. (D) Wing pouch region in third instar wild type disc, wing disc after Eiger-mediated cell ablation at D7 (D'), wing disc after induction of *eiger*-expression with *rotund(rn)GAL4*-mediated co-expression a dominant-negative JNK (*bskDN*) (D'') or of the JNK-inhibitor Puckered (*puc*) (D''') stained for Actin (red) and for Nubbin (cyan) to visualize a lineage similar to *rnGAL4*-derived cells. Note that inhibition of JNK prevents Eiger-induced cell ablation. (E) Wing pouch of a wild type disc, where cells of the *rnGAL4*-

lineage were permanently labeled by GFP-expression using the GFP-lineage labeling system (*G-trace*). (E') *rnGAL4*, *G-trace* labeled cells which survived eiger-expression at recovery time point 0 hrs (R0), 24 hours (R24) and 48 hours (R48). Active proliferation of cells surviving eiger-expression contributes to compensatory proliferation. (F) Schematic representation of automated workflows in Fiji to quantify volumes and particle counts in Eiger-stimulated discs. (G) Cumulative fraction of larvae undergoing larval-pupal transitions, which carry wild type wing discs (WT) or wing discs that experienced eiger-expression for 40 h at D7 (CA). Compensatory responses to tissue stress induced by Eiger-mediated cell ablation induce a 2-day developmental delay at the larval to pupae transition. (H) Quantification of average adult wing sizes developing from disc after Eiger-mediated cell ablation at D7. By scoring five different wing size phenotypes, quantifications were summarized as weighted averages of all different phenotypes (see Method).

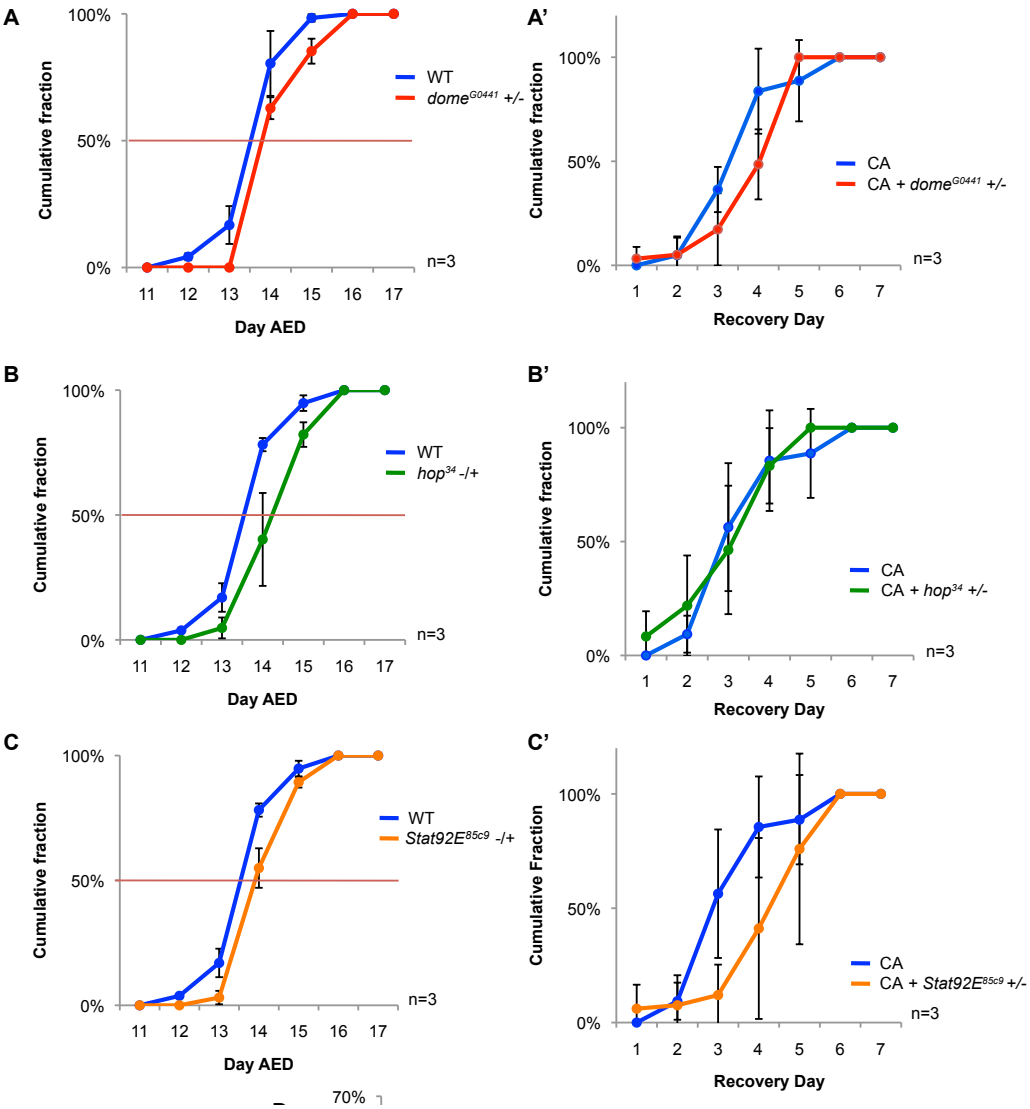

Appendix I - Figure 2. Analysis of normal development delay in the JAK/STAT heterozygous mutants allows correct experimental synchronization for the CA-protocol.

(A, B, C) Quantification of larva-to-pupa transition between wild type flies and heterozygous mutant for JAK/STAT components *domeG*^{0441}, *hop*^{34} and *Stat92E*^{85c9} indicate a 6 h difference in larva-to-pupa transition. (B) *hop*^{34} mutants had 12 h development delay when compared to the wild type. (A'-C') Quantification of development delay upon cell ablation in wild type and heterozygous mutants, after adjustment for the developmental stage (6 h or 12 h), didn't result in any significant difference.

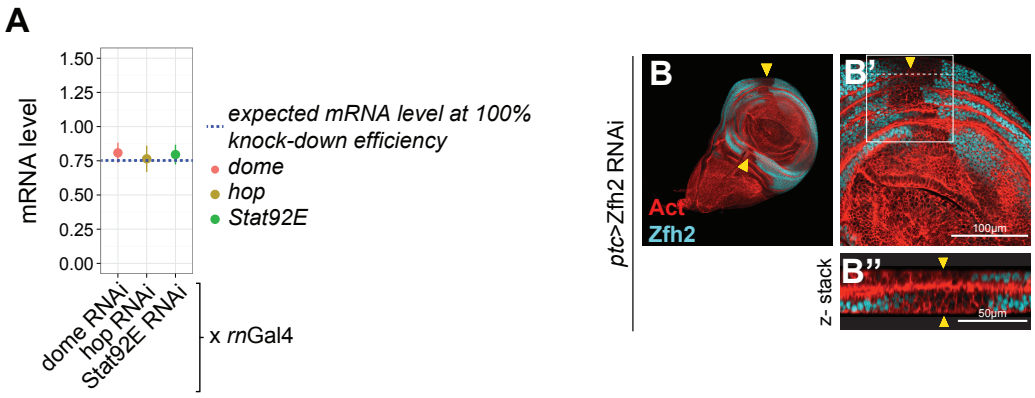

Appendix I - Figure 3. Control of RNAi lines efficiencies.

(A) Knock-down efficiency of UAS-RNAi transgenes targeting *dome, hop* and *Stat92E* was quantified by qRT-PCR. Wing imaginal discs expressing the constructs continuously under the control of *rnGAL4* were compared to wild type wing discs. Only about 25% of the total discs used for this analysis drives expression by *rnGAL4* (see Fig. 3B). Therefore, the maximum expected reduction of transcript levels at 100% RNAi efficiency is only 25% (blue dashed line). Each graph shows mean ± S.E.M for n=2 biological replicates. (B) Wing disc expressing a RNAi construct targeting *zfh2* under the control of *ptcGAL4*. The disc was stained for Zfh2, confirming that Zfh2 signals disappeared in the *ptc* domain (yellow arrowheads, B, B'). Transverse section confirms loss of Zfh2 in the *ptc* domain (B'').

6.2 Appendix II – Wing size analysis

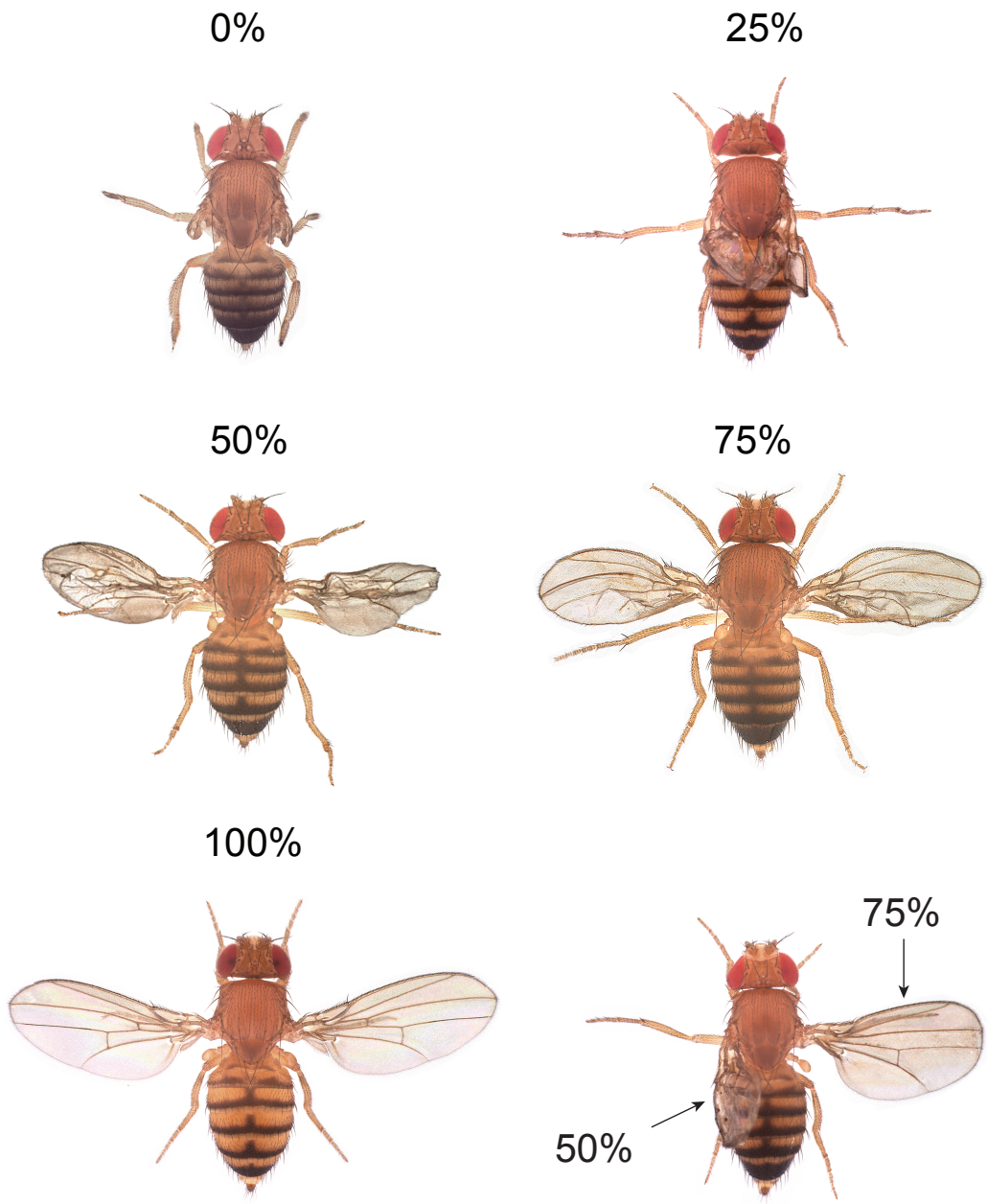

Appendix II - Figure 1. List of binned wing phenotypes after induction of cell ablation.

Five adult wing size phenotypes were classified to score tissue damage after *eiger*-expression at D7.

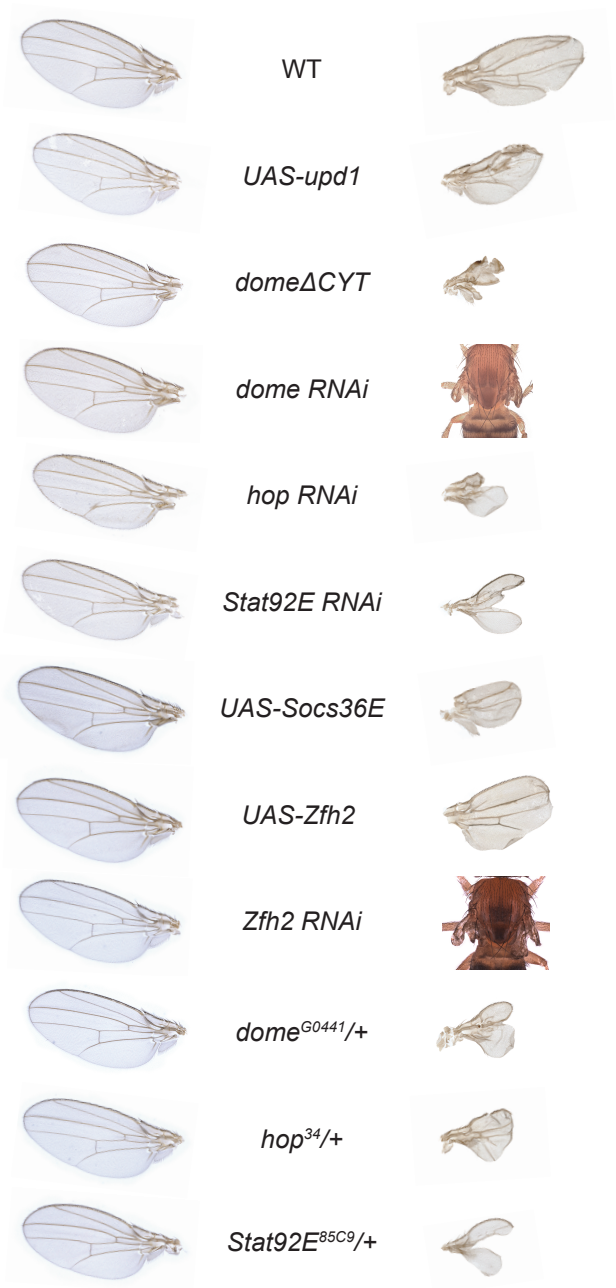

Appendix II - Figure 2. Transient downregulation of the JAK/STAT pathway during normal development doesn't cause severe reduction of wing size compared to flies co-expressing *egr*. Listed pictures represent the most frequent phenotype scored in each line.

6.3 Appendix III – DamID-seq analysis

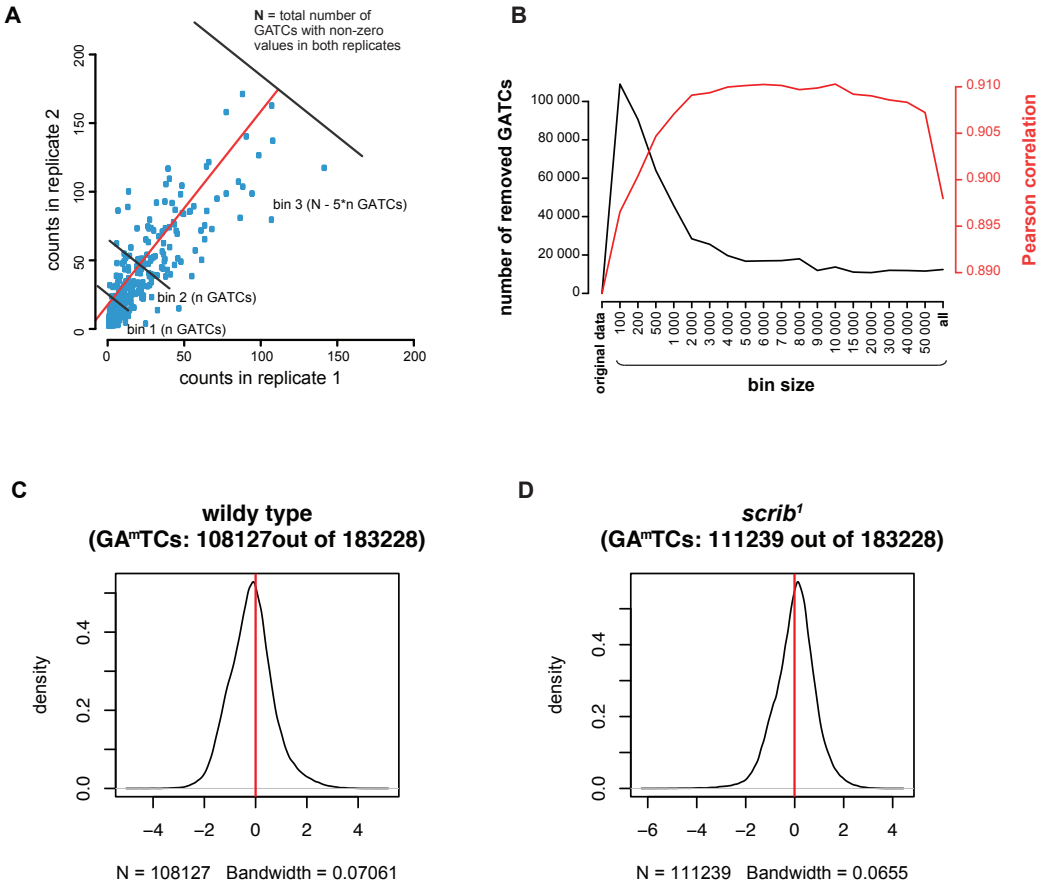

Appendix III - Figure 1. Preliminary analysis on DamID-seq data. (A) Scatter plot of GATCs counts in two replicates. GATCs with counts exceeding 2σ from the fitting line (red line) were discarded. (B) Bin size was selected in order to obatin the highest Person's correlation value by remouving the lowest amount of GATCs. (C) Denisty plot of GA^{m}TCs in relation to the Pc binding intensity in widly type and in (D) *scrib*^{1} samples.

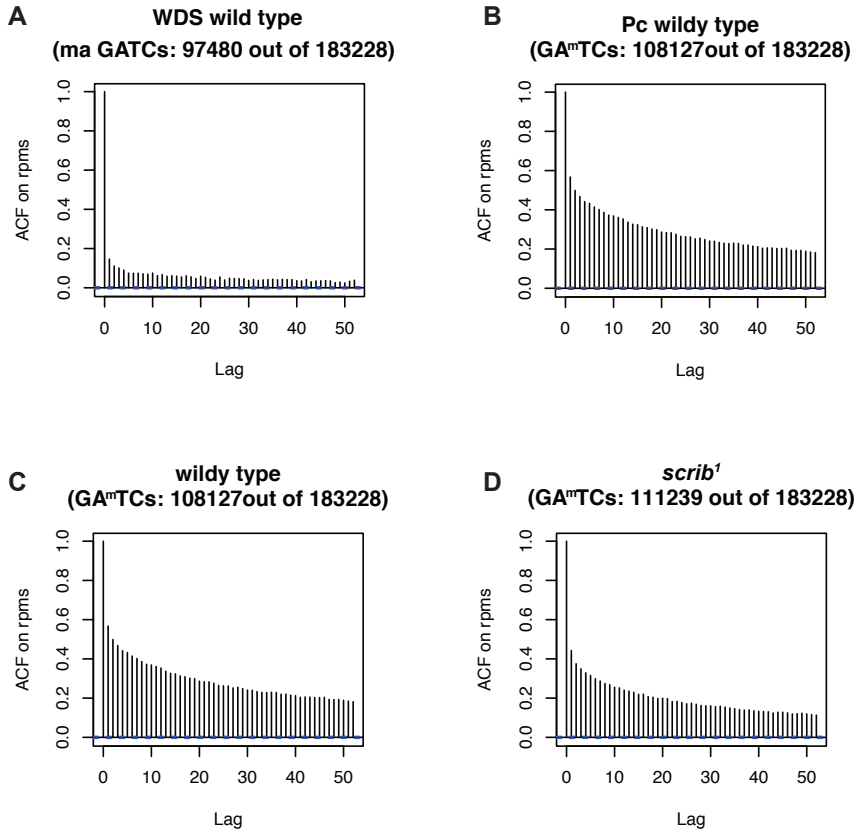

Appendix III - Figure 2. ACF profiles. Auto-correlation Function plots are shown for WDS (A) and Pc (B) from wild type brain tissues. (C) ACF profile of Pc in wild type wing imaginal discs and (D) in *scrib*^{1} tumor (WDS profile are from Dr. Alexey Pindyurin).

6.4 Appendix IV – Raw data.

Appendix IV - Table 1 G-Trace volume measurements

Stage	Genotype	Total Vol [µm^3]	G-Trace [µm^3]	Ratio Vol
R0	*CA*	2120410.602	30073.749	0.014182984
R0	*CA*	1196791.2	52431.193	0.043809808
R0	*CA*	2579688.736	56515.712	0.021907958
R0	*CA*	1584237.525	38937.702	0.024578197
R0	*CA*	1763087.067	56232.496	0.031894339
R0	*CA*	2173066.772	42549.167	0.019580239
R0	*CA*	2288324.576	67429.751	0.029466865
R0	*CA*	2801975.456	46144.001	0.016468382
R0	*CA*	1874104.988	21124.199	0.01127162
R0	*CA*	3162470.948	117850.693	0.037265384
R0	*CA*	2954055.739	105798.24	0.035814571
R0	*CA*	2796963.464	72916.171	0.026069762
R0	*CA*	1624202.391	59499.734	0.036633202
R0	*CA*	1441601.586	77258.863	0.053592382
R0	*CA*	2067309.468	67482.739	0.032642785
R0	*CA*	1864223.024	111205.536	0.059652485
R0	*domeDCYT*	1623102.693	11959.822	0.007368
R0	*domeDCYT*	2374501.85	3057.888	0.001288
R0	*domeDCYT*	1949378.409	4865.437	0.002496
R0	*domeDCYT*	2090062.24	6653.653	0.003183
R0	*domeDCYT*	2220402.451	5654.094	0.002546
R0	*domeDCYT*	2465429.934	12310.515	0.004993
R0	*domeDCYT*	1987228.512	4877.5	0.002454
R0	*domeDCYT*	2750714.4	8110.683	0.002949
R0	*domeKK*	2699861.152	40748.602	0.015093
R0	*domeKK*	1981089.222	22130.564	0.011171
R0	*domeKK*	2374957.208	29911.27	0.012594
R0	*domeKK*	2095235.78	28774.98	0.013734
R0	*domeKK*	2207547.657	14940.43	0.006768

R0	*domeKK*	2557308.27	14304.089	0.005593
R0	*domeKK*	1486658.08	18700.513	0.012579
R0	*domeKK*	1181246.535	5185.541	0.00439
R0	*SOCS*	1754774.575	2482.62	0.001414778
R0	*SOCS*	2774052.596	4057.74	0.001462747
R0	*SOCS*	2371504.38	15779.7	0.006653879
R0	*SOCS*	1406912.775	3496.2	0.002485013
R0	*SOCS*	2157671.048	7811.64	0.003620404
R0	*SOCS*	1652121.834	7969.28	0.004823662
R24	*CA*	2269836.85	55141.05	0.024293
R24	*CA*	1796950.463	43869.341	0.024413
R24	*CA*	2534230.152	47674.039	0.018812
R24	*CA*	1596330.479	41329.816	0.025891
R24	*CA*	1461182.208	53110.191	0.036347
R24	*CA*	1944568.604	76798.789	0.039494
R24	*CA*	2123629.5	82418.31	0.03881
R24	*CA*	3088235.997	60498.822	0.01959
R24	*CA*	2692226.88	68629.064	0.025492
R24	*CA*	3348420.348	83556.28	0.024954
R24	*CA*	3560683.05	89217.988	0.025056425
R24	*CA*	1912542.759	54812.461	0.02865947
R24	*domeDCYT*	2514684.795	7750.402	0.003082
R24	*domeDCYT*	3729014.272	12175.627	0.003265
R24	*domeDCYT*	2839776.862	17545.462	0.006178
R24	*domeDCYT*	2762667.6	19509.311	0.007062
R24	*domeDCYT*	2226244.446	29663.72	0.013325
R24	*domeDCYT*	2680676.351	11883.289	0.004433
R24	*domeDCYT*	1107196.024	7623.886	0.006886
R24	*domeDCYT*	2136729.46	24677.48	0.011549
R24	*domeDCYT*	2958185.625	14934.141	0.005048
R24	*domeDCYT*	1984341.6	11200.891	0.005645
R24	*domeDCYT*	2603419.884	19877.837	0.007635
R24	*domeDCYT*	2349835.326	32053.065	0.013641
R24	*domeKK*	1973100.96	40097.825	0.020322
R24	*domeKK*	2849602.69	24221.39	0.0085
R24	*domeKK*	1962627.876	42635.447	0.021724

R24	*domeKK*	2413852.663	55578.088	0.023025
R24	*domeKK*	2760066.96	105809.319	0.038336
R24	*domeKK*	2363825.989	81807.311	0.034608
R24	*domeKK*	3483782.304	145928.33	0.041888
R24	*domeKK*	1431817.582	50744.627	0.035441
R24	*domeKK*	2176481.82	100774.829	0.046302
R24	*SOCS*	3470520.816	40434.27	0.011650779
R24	*SOCS*	2714632.544	45204.88	0.016652302
R24	*SOCS*	2422155.415	53218.98	0.021971746
R24	*SOCS*	2421915.408	43201.96	0.017837929
R24	*SOCS*	1589246.673	29566.81	0.018604293
R24	*SOCS*	2915113.887	54226.16	0.018601729
R48	*CA*	4518745.856	113995.834	0.025227
R48	*CA*	3115742.454	116334.966	0.037338
R48	*CA*	3928788.768	147411.848	0.037521
R48	*CA*	3704911.947	116946.719	0.031565
R48	*CA*	2422727.069	75661.631	0.03123
R48	*CA*	2909147.594	298460.109	0.102594
R48	*CA*	2799618.973	139308.217	0.04976
R48	*CA*	3190499.815	164118.436	0.05144
R48	*CA*	2054830.44	156322.204	0.076075
R48	*CA*	3523342.2	204674.779	0.058091
R48	*CA*	2043478.668	135839.426	0.066475
R48	*CA*	1759712.12	153571.666	0.087271
R48	*CA*	1860644.16	56239.934	0.030226
R48	*domeDCYT*	2688909.22	42921.386	0.015962
R48	*domeDCYT*	2434356.646	11525.611	0.004735
R48	*domeDCYT*	1767800.06	19461.525	0.011009
R48	*domeDCYT*	2101035.389	34392.594	0.016369
R48	*domeDCYT*	1583632.072	37530.83	0.023699
R48	*domeDCYT*	2336546.927	59941.322	0.025654
R48	*domeKK*	2140150.222	209320.203	0.097806
R48	*domeKK*	4454963.388	306682.33	0.068841
R48	*domeKK*	3809725.3	179522.111	0.047122
R48	*domeKK*	3809725.3	240475.629	0.063122
R48	*domeKK*	4498930.41	316524.206	0.070355

R48	*domeKK*	4684388.352	199131.848	0.04251
R48	*domeKK*	3462830.385	273771.141	0.07906
R48	*domeKK*	4840507.425	264833.474	0.054712
R48	*domeKK*	3441601.262	199721.615	0.058032
R48	*domeKK*	2945695.72	236015.83	0.080122
R48	*domeKK*	3160232.44	88798.372	0.028099
R48	*domeKK*	2646379.92	163268.195	0.061695
R48	*SOCS*	3129003.36	75170.46	0.024023772
R48	*SOCS*	2385084.34	88567.74	0.037134008
R48	*SOCS*	2553127.416	121452.98	0.047570277
R48	*SOCS*	1854162.342	93237.05	0.050285269
R48	*SOCS*	2744425.04	109176.28	0.039781113
R48	*SOCS*	1651287.84	71446.5	0.043267139

Appendix IV - Table 2 pH3 counts in G-Trace

Genotype	Stage	# Disc	# G-Trace	G-Trace [µm^3]	Ratio pH3 #G-Trace/#Disc	Ratio #G-trace/G-Trace counts/[µm^3]
CA	R0	265	19	30073.749	0.071698113	0.00063178
CA	R0	209	51	52431.193	0.244019139	0.000972703
CA	R0	217	51	56515.712	0.235023041	0.000902404
CA	R0	161	46	38937.702	0.285714286	0.001181374
CA	R0	219	56	56232.496	0.255707763	0.000995865
CA	R0	347	70	42549.167	0.201729107	0.001645156
domeDCYT	R0	329	34	11959.822	0.103343465	0.002842852
domeDCYT	R0	359	11	3057.888	0.030640669	0.003597254
domeDCYT	R0	363	21	4865.437	0.05785124	0.004316159
domeDCYT	R0	291	20	6653.653	0.068728522	0.003005868
domeKK	R0	187	16	40748.602	0.085561497	0.000392652
domeKK	R0	189	6	22130.564	0.031746032	0.000271118
domeKK	R0	359	38	29911.27	0.105849582	0.001270424
domeKK	R0	384	15	28774.98	0.0390625	0.000521286
CA	R0	135	9	67429.751	0.066666667	0.000133472
CA	R0	178	16	46144.001	0.08988764	0.000346741
CA	R0	204	10	21124.199	0.049019608	0.000473391

CA	R0	195	15	117850.693	0.076923077	0.00012728
CA	R0	249	22	105798.24	0.088353414	0.000207943
CA	R0	256	10	72916.171	0.0390625	0.000137144
domeDCYT	R0	275	1	5654.094	0.003636364	0.000176863
domeDCYT	R0	168	7	12310.515	0.041666667	0.00056862
domeDCYT	R0	260	10	4877.5	0.038461538	0.002050231
domeDCYT	R0	191	7	8110.683	0.036649215	0.000863059
domeKK	R0	165	10	14940.43	0.060606061	0.000669325
domeKK	R0	154	3	14304.09	0.019480519	0.00020973
domeKK	R0	122	7	18700.51	0.057377049	0.000374321
domeKK	R0	169	3	5185.54	0.017751479	0.000578532
CA	R24	420	36	53110.19	0.085714286	0.000677836
CA	R24	794	188	76798.79	0.236775819	0.002447955
CA	R24	715	41	82418.31	0.057342657	0.000497462
CA	R24	895	43	60498.82	0.048044693	0.000710758
domeDCYT	R24	1074	58	29663.72	0.054003724	0.00195525
domeDCYT	R24	663	6	11883.29	0.009049774	0.000504911
domeDCYT	R24	728	4	7623.89	0.005494505	0.000524667
domeDCYT	R24	802	48	24677.48	0.059850374	0.001945093
domeDCYT	R24	1286	18	14934.141	0.01399689	0.001205292
domeDCYT	R24	1162	13	11200.891	0.011187608	0.001160622
domeDCYT	R24	1475	37	19877.837	0.025084746	0.00186137
domeDCYT	R24	588	73	32053.07	0.12414966	0.002277473
domeKK	R24	962	50	105809.32	0.051975052	0.000472548
domeKK	R24	470	48	81807.311	0.10212766	0.000586745
domeKK	R24	645	66	145928.33	0.102325581	0.000452277
domeKK	R24	213	9	50744.627	0.042253521	0.000177359
domeKK	R24	406	55	100774.829	0.13546798	0.000545771
CA	R24	1621	236	55141.05	0.145589143	0.004279933
CA	R24	1023	145	43869.341	0.14173998	0.00330527
CA	R24	1547	113	47674.039	0.073044602	0.002370263
CA	R24	915	99	41329.816	0.108196721	0.002395365
domeDCYT	R24	1964	19	7750.402	0.009674134	0.002451486
domeDCYT	R24	1601	13	12175.627	0.008119925	0.001067707
domeDCYT	R24	1525	79	17545.462	0.051803279	0.004502589
domeDCYT	R24	1647	27	19509.311	0.016393443	0.001383955

domeKK	R24	1776	113	40097.825	0.063626126	0.002818108
domeKK	R24	1181	124	24221.39	0.104995766	0.005119442
domeKK	R24	568	55	55578.088	0.096830986	0.000989599
domeKK	R24	1889	348	5645.955	0.184224457	0.061637048
CA	R48	550	98	113995.834	0.178181818	0.000859681
CA	R48	727	145	116334.966	0.199449794	0.001246401
CA	R48	2208	319	147411.848	0.144474638	0.002164005
CA	R48	900	152	116946.719	0.168888889	0.001299737
domeDCYT	R48	1119	103	42921.386	0.09204647	0.002399736
domeDCYT	R48	1015	63	11525.611	0.062068966	0.005466088
domeDCYT	R48	1121	113	19461.525	0.100802855	0.005806328
domeDCYT	R48	1049	216	34392.594	0.205910391	0.006280422
domeKK	R48	949	370	209320.2	0.389884089	0.001767627
domeKK	R48	477	76	306682.33	0.15932914	0.000247813
domeKK	R48	812	228	179522.11	0.280788177	0.001270039
domeKK	R48	780	256	240475.63	0.328205128	0.001064557
domeKK	R48	888	239	316524.21	0.269144144	0.000755077
domeKK	R48	533	66	199131.85	0.123827392	0.000331439
domeKK	R48	666	104	273771.14	0.156156156	0.000379879
domeKK	R48	1012	240	264833.47	0.23715415	0.00090623
domeKK	R48	332	72	199721.62	0.21686747	0.000360502
domeKK	R48	1047	286	236015.83	0.273161414	0.001211783
domeKK	R48	238	23	88798.37	0.096638655	0.000259014
domeKK	R48	602	186	163268.2	0.3089701	0.00113923
domeDCYT	R48	164	51	37530.83	0.31097561	0.001358883
domeDCYT	R48	369	47	31670.51	0.127371274	0.00148403
domeDCYT	R48	417	134	59941.32	0.321342926	0.00223552
CA	R48	994	240	75661.63	0.241448692	0.003172017
CA	R48	437	69	298460.11	0.157894737	0.000231187
CA	R48	683	341	139308.22	0.499267936	0.00244781
CA	R48	1459	513	164118.44	0.351610692	0.003125791
CA	R0	201	11	59499.73	0.054726368	0.000184875
CA	R0	216	20	77258.86	0.092592593	0.00025887
CA	R0	213	21	67482.74	0.098591549	0.000311191
CA	R0	111	20	111205.54	0.18018018	0.000179847
SOCS	R0	299	55	2482.62	0.183946488	0.02215405

SOCS	R0	220	51	4057.74	0.231818182	0.012568585
SOCS	R0	318	123	15779.7	0.386792453	0.007794823
SOCS	R0	173	27	3496.2	0.156069364	0.007722679
SOCS	R0	405	83	7811.64	0.204938272	0.010625168
SOCS	R0	238	48	7969.28	0.201680672	0.006023131
CA	R24	506	60	68629.06	0.118577075	0.000874265
CA	R24	547	126	83556.28	0.230347349	0.001507966
CA	R24	700	146	89217.99	0.208571429	0.001636441
CA	R24	524	48	54812.46	0.091603053	0.000875713
SOCS	R24	855	190	40434.27	0.222222222	0.004698984
SOCS	R24	943	182	45204.88	0.19300106	0.004026114
SOCS	R24	1014	281	53218.98	0.277120316	0.005280071
SOCS	R24	1249	443	43201.96	0.354683747	0.010254166
SOCS	R24	431	99	29566.81	0.229698376	0.003348349
SOCS	R24	1003	298	54226.16	0.297108674	0.005495503
SOCS	R48	1237	122	75170.46	0.098625707	0.001622978
SOCS	R48	523	76	88567.74	0.145315488	0.0008581
SOCS	R48	563	168	121452.98	0.298401421	0.001383251
SOCS	R48	478	98	93237.05	0.205020921	0.001051084
SOCS	R48	642	113	131702.34	0.176012461	0.000857995
SOCS	R48	448	69	71446.5	0.154017857	0.000965758
CA	R48	447	164	156322.2	0.36689038	0.001049115
CA	R48	1710	353	204674.78	0.206432749	0.001724687
CA	R48	1266	245	135839.43	0.193522907	0.0018036
CA	R48	978	314	153571.67	0.321063395	0.002044648
CA	R48	712	103	56239.93	0.144662921	0.001831439

Appendix IV - Table 3. qPCR data on JAK/STAT component.

Recovery	Sample	Target Gene	2^{-ddCt}	House-keeping gene
R0	D5	*dome*	1.093684246	*RpL32*
R0	D5	*dome*	0.766610811	*RpL13*
R0	D5	*dome*	0.873281499	*Act5C*
R0	D5	*dome*	1.847730203	*bTub*
R0	D5	*hop*	1.017504605	*RpL32*
R0	D5	*hop*	0.71321319	*RpL13*
R0	D5	*hop*	0.551523511	*Act5C*

R0	D5	*hop*	1.16693947	*bTub*
R0	D5	*STAT92E*	1.952444651	*RpL32*
R0	D5	*STAT92E*	1.368553293	*RpL13*
R0	D5	*STAT92E*	1.865940569	*Act5C*
R0	D5	*STAT92E*	3.948045105	*bTub*
R0	D5	*upd1*	7.161048268	*RpL32*
R0	D5	*upd1*	5.019489892	*RpL13*
R0	D5	*upd1*	1.504668375	*Act5C*
R0	D5	*upd1*	3.183648351	*bTub*
R0	D5	*upd2*	40.52303451	*RpL32*
R0	D5	*upd2*	28.40435569	*RpL13*
R0	D5	*upd2*	21.61083492	*Act5C*
R0	D5	*upd2*	45.72522429	*bTub*
R0	D5	*upd3*	26.38364791	*RpL32*
R0	D5	*upd3*	18.49344524	*RpL13*
R0	D5	*upd3*	10.75101941	*Act5C*
R0	D5	*upd3*	22.74751418	*bTub*
R0	D7	*dome*	1.421048737	*RpL32*
R0	D7	*dome*	2.697871951	*RpL13*
R0	D7	*dome*	2.477492703	*Act5C*
R0	D7	*dome*	2.310840333	*bTub*
R0	D7	*dome*	3.51282874	*RpL32*
R0	D7	*dome*	2.436056873	*RpL13*
R0	D7	*dome*	3.11425064	*RpL32*
R0	D7	*dome*	6.144744309	*RpL13*
R0	D7	*hop*	1.005859975	*RpL32*
R0	D7	*hop*	1.909632895	*RpL13*
R0	D7	*hop*	1.367460299	*Act5C*
R0	D7	*hop*	1.275475972	*bTub*
R0	D7	*hop*	5.973334174	*RpL32*
R0	D7	*hop*	4.142354452	*RpL13*
R0	D7	*hop*	0.599366979	*RpL32*
R0	D7	*hop*	1.182614137	*RpL13*
R0	D7	*STAT92E*	1.474762162	*RpL32*
R0	D7	*STAT92E*	2.799847301	*RpL13*
R0	D7	*STAT92E*	1.787150233	*Act5C*
R0	D7	*STAT92E*	1.666934815	*bTub*
R0	D7	*STAT92E*	2.008614945	*RpL32*

R0	D7	*STAT92E*	1.472621035	*RpL13*
R0	D7	*STAT92E*	0.69003476	*RpL32*
R0	D7	*STAT92E*	1.361511212	*RpL13*
R0	D7	*upd1*	9.206534214	*RpL32*
R0	D7	*upd1*	17.47867598	*RpL13*
R0	D7	*upd1*	9.99983886	*Act5C*
R0	D7	*upd1*	9.327184268	*bTub*
R0	D7	*upd1*	1.607326303	*RpL32*
R0	D7	*upd1*	3.171423979	*RpL13*
R0	D7	*upd2*	51.0786919	*RpL32*
R0	D7	*upd2*	96.97328922	*RpL13*
R0	D7	*upd2*	42.79694175	*Act5C*
R0	D7	*upd2*	39.91813943	*bTub*
R0	D7	*upd2*	190.3204285	*RpL32*
R0	D7	*upd2*	345.329382	*RpL13*
R0	D7	*upd3*	36.29133329	*RpL32*
R0	D7	*upd3*	68.89937523	*RpL13*
R0	D7	*upd3*	33.01737639	*Act5C*
R0	D7	*upd3*	30.79641162	*bTub*
R0	D7	*upd3*	24.00781821	*RpL32*
R0	D7	*upd3*	47.36995232	*RpL13*
R0	D8	*dome*	1.216440399	*RpL32*
R0	D8	*dome*	0.822070691	*RpL13*
R0	D8	*hop*	0.822070691	*RpL32*
R0	D8	*hop*	0.555555556	*RpL13*
R0	D8	*STAT92E*	1	*RpL32*
R0	D8	*STAT92E*	0.675800222	*RpL13*
R0	D8	*upd1*	3.941266893	*RpL32*
R0	D8	*upd1*	2.66350904	*RpL13*
R0	D8	*upd2*	7.094280408	*RpL32*
R0	D8	*upd2*	4.794316272	*RpL13*
R0	D8	*upd3*	11.57805046	*RpL32*
R0	D8	*upd3*	7.824449067	*RpL13*

Appendix IV - Table 4. qPCR data on pro-apoptotic genes.

Recovery	Sample	Target gene	2^{-ddCt}	House-keeping gene

R0	D7	*grim*	2.1606224	*RpL32*
R0	D7	*grim*	1.367387812	*RpL32*
R0	D7	*grim*	1.055877134	*RpL32*
R0	D7	*hid*	2.698897186	*RpL32*
R0	D7	*hid*	2.342651517	*RpL32*
R0	D7	*hid*	2.308627733	*RpL32*
R0	D7	*kay*	0.728609095	*RpL32*
R0	D7	*kay*	0.690721715	*RpL32*
R0	D7	*kay*	0.678960896	*RpL32*
R0	D7	*kay*	0.643655202	*RpL32*
R0	D7	*rpr*	0.238705339	*RpL32*
R0	D7	*rpr*	1.6289503	*RpL32*
R0	D7	*rpr*	3.281900243	*RpL32*

Appendix IV - Table 5. qPCR data on pro-apoptotic gene (CA vs CA+*STAT92E*^{85c9})

Recovery	**Sample**	**Target gene**	**2^{-ddCt}**	**House-keeping gene**
R0	D7	*hid*	22.92617821	*RpL13*
R0	D7	*hid*	11.47319314	*RpL32*
R0	D7	*kay*	47.86978419	*RpL13*
R0	D7	*kay*	28.80968336	*RpL32*

Appendix IV - Table 6. qPCR data on Zfh1 and Zfh2.

Recovery	**Sample**	**Target gene**	**2^{-ddCt}**	**House-keeping gene**
R0	D7	*zfh1*	0.445456312	*RpL32*
R0	D7	*zfh1*	0.203385157	*RpL32*
R0	D7	*zfh1*	2.743323372	*RpL32*
R0	D7	*zfh2*	1.336670255	*RpL32*
R0	D7	*zfh2*	1.058399931	*RpL32*
R0	D7	*zfh2*	2.636967206	*RpL32*

Appendix IV - Table 7. Pc binding dynamics around TSS of differentially expressed genes.

GENE SYMB	**T-S**	**TRANSCRIPT (LOG_2)**
AcCoAS	NT>NT	4.692942276
al	T>T	-3.253586023

alpha-Est9	NT>NT	4.07157879
Amy-p	NT>I	5.36911473
ana	NT>NT	-3.581306209
Ance	NT>I	-1.719657497
Atf3	NT>NT	1.684687343
Atf3	I>T	1.684687343
ATP8B	NT>NT	3.00928869
b	NT>NT	1.867362847
b	I>NT	1.867362847
BBS8	NT>NT	1.79189159
beat-IIb	T>T	-2.229414545
bmm	NT>NT	2.740274321
CAHbeta	NT>I	1.751338725
CarT	NT>NT	-2.509381589
Cct2	NT>NT	1.56340976
Cct2	I>NT	1.56340976
CG10089	NT>NT	3.584565739
CG10089	I>NT	3.584565739
CG10137	I>NT	5.322938695
CG10208	NT>NT	1.640640013
CG10232	NT>I	3.607975429
CG10311	NT>I	-1.757797405
CG10337	I>NT	2.726022916
CG10359	I>NT	-1.790491767
CG10365	NT>I	3.822517855
CG10383	NT>NT	3.069902654
CG10407	NT>I	2.005534362
CG10527	T>T	2.923756165
CG10559	NT>NT	4.368740593
CG10657	NT>NT	-1.807914259
CG10738	NT>I	2.097730955
CG10916	T>T	1.810520167
CG11155	T>T	1.899741994
CG11437	I>T	-2.448580286
CG11529	NT>I	4.024161945
CG11835	NT>NT	-2.181207694

CG11835	NT>I	-2.181207694
CG12065	T>NT	2.02892846
CG12112	T>T	1.802507274
CG12239	I>NT	-4.987942857
CG12481	NT>I	-6.351292029
CG12655	NT>I	3.71594209
CG12688	T>T	-3.177144707
CG1273	NT>NT	-4.502123636
CG12868	NT>I	1.643481115
CG12880	NT>I	1.701994916
CG12883	NT>NT	1.812779286
CG13003	NT>I	1.696817786
CG13023	T>I	-6.140092806
CG13044	NT>I	-2.169457635
CG13046	I>NT	-1.552689807
CG13053	NT>I	-4.35172797
CG13082	NT>NT	-1.639623973
CG13108	NT>NT	2.101198262
CG13108	I>NT	2.101198262
CG13124	NT>NT	3.008336441
CG13124	I>NT	3.008336441
CG13258	NT>I	-4.225646179
CG13313	I>NT	-3.472966617
CG13678	NT>I	-2.901701809
CG13692	NT>NT	3.561267325
CG13699	NT>NT	-3.341746048
CG13731	NT>NT	-3.234803392
CG13731	NT>I	-3.234803392
CG13857	NT>I	4.678731371
CG13982	T>I	5.057636183
CG14183	NT>I	-1.543354315
CG14257	NT>I	-4.411291531
CG14304	I>NT	-1.723362888
CG14372	NT>NT	-2.509789476
CG14372	I>NT	-2.509789476
CG14395	T>T	-3.252760575

CG14567	T>I	3.436228715
CG14608	I>T	3.605028763
CG14608	T>T	3.605028763
CG14695	NT>I	2.982223031
CG14780	I>NT	3.805787187
CG14880	NT>I	4.047813066
CG14982	NT>I	-2.982385712
CG15047	NT>NT	3.538392538
CG15047	NT>I	3.538392538
CG15080	NT>NT	-1.854446231
CG15080	NT>I	-1.854446231
CG15117	I>NT	4.291622073
CG15117	I>T	4.291622073
CG15186	T>I	5.489346733
CG15279	NT>I	2.898998643
CG15484	NT>NT	1.655860876
CG15611	NT>I	2.279803102
CG1572	NT>I	3.272293291
CG15739	I>NT	2.041357143
CG15765	NT>I	-4.622018122
CG15766	NT>I	2.269761122
CG15784	T>T	3.005647065
CG1673	I>T	2.03479059
CG16984	NT>NT	-1.626400885
CG17108	I>NT	5.910316671
CG17121	I>NT	2.084681775
CG17124	I>NT	4.444986226
CG17323	I>NT	-2.288622684
CG17470	NT>NT	-2.985827233
CG17470	NT>I	-2.985827233
CG17549	I>NT	2.26025727
CG17843	T>T	2.210121564
CG18278	NT>NT	3.053996081
CG18507	NT>I	2.110983498
CG18577	NT>NT	-6.205501733
CG18641	NT>I	3.039468564

CG2064	I>T	2.415389467
CG2065	I>T	2.026069674
CG2157	NT>I	4.979901978
CG2611	NT>NT	1.668531477
CG2663	NT>NT	-5.333863513
CG30016	NT>NT	-1.707218608
CG30456	I>NT	1.610525408
CG30456	I>T	1.610525408
CG3104	NT>I	2.937015331
CG31098	I>NT	2.906089682
CG31140	NT>I	-1.998972216
CG31176	NT>NT	-2.937552254
CG31176	I>NT	-2.937552254
CG31262	T>T	-4.108048906
CG31324	NT>I	1.579054989
CG31370	I>NT	3.221123548
CG31373	NT>NT	1.607100323
CG31436	I>NT	2.324946311
CG31475	NT>NT	-1.800409954
CG31475	I>NT	-1.800409954
CG31559	NT>NT	-4.698418984
CG31869	NT>I	2.631453127
CG32037	I>NT	2.274426711
CG32082	I>NT	1.682130874
CG32150	NT>NT	-3.898333777
CG32165	NT>NT	-1.594818382
CG32214	I>NT	-5.463883647
CG32373	NT>I	-2.542228404
CG32392	I>T	-4.224909945
CG32447	I>T	-2.187252934
CG32812	T>I	2.565143238
CG32812	NT>I	2.565143238
CG33062	NT>I	-1.646595629
CG3355	I>NT	-2.249081274
CG34193	NT>NT	-2.197165366
CG34247	NT>I	-7.062033804

CG3823	NT>I	-3.422018196
CG42322	NT>NT	-2.713087062
CG42322	I>NT	-2.713087062
CG42326	I>T	7.872221059
CG4238	NT>I	-2.042060882
CG42390	NT>I	3.761436565
CG42492	NT>NT	7.535553392
CG42666	NT>NT	2.1792028
CG42675	NT>NT	2.635571116
CG42807	NT>NT	2.45491144
CG43293	NT>NT	2.696498183
CG43293	I>NT	2.696498183
CG43324	I>T	7.199654244
CG4408	NT>I	-3.670048442
CG4570	NT>I	1.799272739
CG4607	T>T	-4.549863236
CG4678	NT>NT	-2.089586753
CG4928	NT>NT	-1.918292288
CG4928	NT>I	-1.918292288
CG5065	NT>I	-2.338668135
CG5144	T>I	-3.130129118
CG5278	NT>I	3.782631772
CG5282	NT>NT	-5.989926051
CG5621	I>NT	8.647676068
CG5621	T>T	8.647676068
CG5646	NT>NT	3.716503878
CG5646	NT>I	3.716503878
CG5687	NT>NT	-1.787351207
CG5835	T>T	1.657533104
CG5888	T>T	1.715430196
CG5921	T>I	-3.819400155
CG6231	NT>NT	-1.906786152
CG6280	NT>NT	-5.616775065
CG6330	NT>I	4.462959621
CG6602	NT>NT	-2.033768276
CG6749	I>NT	2.25085838

CG7059	NT>I	3.600698023
CG7201	NT>NT	-3.698575914
CG7294	I>NT	2.956724511
CG7296	I>NT	2.375471388
CG7512	I>T	-2.781291955
CG7675	I>NT	-1.871835386
CG7720	NT>I	-1.821827295
CG7900	T>T	-7.146772951
CG8086	NT>NT	3.362252708
CG8170	NT>NT	-2.480724643
CG8172	I>T	-4.266038122
CG8192	NT>NT	-2.522175368
CG8192	I>NT	-2.522175368
CG8303	NT>I	2.019300387
CG8369	NT>I	2.861116235
CG8547	I>T	1.559172473
CG8745	NT>I	6.295540397
CG8800	NT>NT	2.495063555
CG8854	NT>NT	2.544137725
CG8854	I>NT	2.544137725
CG9008	NT>NT	-1.619684349
CG9008	NT>I	-1.619684349
CG9259	I>NT	5.415542226
CG9411	NT>NT	2.889783163
CG9416	I>T	-3.304788003
CG9813	T>T	2.364335962
CG9961	NT>NT	-2.702265684
Chd64	NT>NT	1.894535752
cher	NT>NT	2.024310096
chinmo	T>I	2.766870342
chrb	NT>NT	-1.510239261
chrb	NT>I	-1.510239261
Cpr47Eb	NT>NT	6.714848319
Cpr47Eb	NT>I	6.714848319
Cpr49Ac	NT>I	1.842272786
Cpr51A	NT>NT	-3.569692943

Cpr56F	I>NT	-4.380380811
Cpr56F	I>T	-4.380380811
Cpr67Fa1	NT>NT	-4.117519223
Cpr67Fa1	I>NT	-4.117519223
Cpr67Fa2	I>NT	-4.192007185
Cpr67Fa2	I>T	-4.192007185
Cpr78E	NT>NT	-3.603491225
Cpr78E	NT>I	-3.603491225
CR32111	T>T	-1.748232365
CR33294	NT>NT	2.689583006
CR42861	I>NT	1.659997287
CR43087	T>I	4.435589691
CR43144	NT>I	1.980575792
CR43431	T>T	-3.00487128
Cyp4e1	I>NT	-2.104714316
Cyp6a13	NT>NT	2.933040046
Cyp6a14	NT>NT	6.108935886
Cyp6a14	NT>I	6.108935886
Cyt-c-p	NT>I	1.640943431
DAAM	I>NT	1.944697415
dac	I>T	-2.517609276
dac	T>T	-2.517609276
danr	I>NT	-2.690214709
dar1	T>T	2.049082143
daw	T>I	3.375048455
Ddr	NT>NT	-1.727783228
Dgp-1	T>T	3.827095256
Dh31-R	NT>NT	-2.347822118
Dh31-R	I>T	-2.347822118
Dif	NT>I	2.417832952
disco	NT>NT	-2.559722757
disco-r	T>T	-2.685138036
Doc2	T>T	-1.829558367
dpr18	T>T	2.54740161
drd	NT>I	1.95048334
Drep2	I>T	2.594554001

Drep2	NT>T	2.594554001
Drip	NT>NT	2.888266057
drm	T>T	1.789204808
Dro	NT>NT	3.355112806
Dro	NT>T	3.355112806
Dscam4	NT>I	8.548927156
dsx	NT>I	-1.753893062
Dtg	T>T	-2.344467699
dy	NT>NT	-3.336104076
dy	NT>I	-3.336104076
E(spl)m7-HLH	NT>I	-1.918768174
Efhc1.2	I>T	-2.610830612
Eip78C	I>T	-2.51383585
Ets21C	T>I	4.174429595
exp	NT>I	1.733752663
FASN2	NT>NT	3.92965222
FASN2	I>NT	3.92965222
fbp	I>NT	-2.074478048
fu12	I>NT	-4.377658883
fuss	NT>NT	4.924685117
fuss	NT>I	4.924685117
Gbs-70E	NT>I	-3.957714558
GEFmeso	NT>I	1.843303994
GILT3	NT>I	2.595559567
GNBP2	NT>NT	1.704211616
GNBP2	NT>I	1.704211616
GNBP3	NT>NT	-1.631163879
GNBP3	NT>I	-1.631163879
Gs2	NT>NT	-2.197931894
Gyc-89Da	NT>NT	2.832746635
hui	I>T	1.627052201
Idgf2	T>T	4.158182044
Idgf3	T>T	3.817109022
Ilp6	NT>I	1.59702804
Ilp8	NT>NT	8.549061667
ImpL1	I>NT	-2.29165003

Inos	T>T	1.562851851
inv	I>T	-1.571321682
Ir40a	NT>NT	1.866018182
Irc	I>NT	2.919899773
Itgbn	NT>I	2.53005358
kirre	NT>I	-2.019270891
Klp68D	NT>NT	1.941680958
Klp68D	I>NT	1.941680958
klu	T>T	-2.329579441
kn	I>T	-4.704554444
Ktl	NT>NT	5.093497748
l(2)03659	NT>NT	2.137431825
l(2)34Fc	NT>NT	-2.813294313
lab	NT>NT	2.654236684
Lip1	I>NT	-4.200080923
Mal-A5	NT>NT	1.655971651
Men	T>T	2.942984313
MFS3	I>NT	1.718675859
mirr	T>T	-2.03442611
Mnn1	NT>NT	-1.934875924
moody	NT>NT	3.711333548
Mst36Fa	NT>I	-1.95797104
Mst36Fb	NT>I	-2.371658285
mtg	NT>NT	2.281883553
mthl8	I>NT	-6.73594585
MtnA	I>T	4.173701602
na	NT>I	5.204147665
nAChRbeta3	T>I	3.146365152
Ndg	I>T	3.46176132
Nep1	T>I	-2.67451556
NetA	T>I	-2.311673487
Neurochondrin	T>NT	6.1997672
Neurochondrin	T>I	6.1997672
Neurochondrin	T>T	6.1997672
Nhe2	NT>I	1.775314273
NijC	T>T	2.316729678

ninaC	T>I	-1.925156236
Nos	NT>NT	3.594726099
Nos	NT>I	3.594726099
Nplp4	NT>I	-3.079069988
nub	T>T	-3.222726231
Obp56a	NT>I	-4.107467986
obst-E	NT>NT	4.369077527
obst-E	NT>I	4.369077527
odd	T>T	1.773134902
Optix	NT>NT	-2.884950731
Oseg4	I>NT	-1.633214214
p38a	NT>NT	1.877525167
p38a	I>NT	1.877525167
path	NT>I	2.743180447
pdm2	T>T	-2.59301989
pdm3	I>T	-3.763892452
Pepck	I>NT	1.626311524
Peritrophin-A	I>NT	2.137270729
PGRP-SA	NT>I	4.709548648
PK2-R2	NT>I	2.495105788
ppk13	I>NT	2.356374583
pst	NT>NT	1.882332161
Ptr	NT>NT	-2.814809633
pxb	I>T	2.234896357
pxb	T>T	2.234896357
Pxd	NT>I	-4.526065824
Ras64B	NT>NT	1.55406515
Rcd2	T>I	3.06833886
Rcd6	NT>I	2.490251716
reb	NT>NT	1.623168305
rempA	T>I	1.635643271
Ret	I>NT	3.649189781
Sans	NT>NT	-1.849292623
sca	NT>I	-2.123024213
scb	NT>NT	1.611198388
scb	NT>I	1.611198388

Sclp	NT>NT	2.133796446
Sclp	I>NT	2.133796446
Scr	NT>I	2.699196215
Sdr	NT>NT	-1.941375148
Sdr	NT>I	-1.941375148
sens	T>T	-4.239282436
SK	T>I	-6.284205542
Sox102F	T>T	-1.698886152
Sp212	NT>NT	4.561859554
Sp212	NT>I	4.561859554
Spn47C	I>NT	7.525196136
Spn55B	T>T	2.724330201
stil	I>T	-2.460125049
subdued	NT>NT	1.600137872
sv	I>T	-2.180915722
svp	NT>NT	-1.753311926
svp	T>NT	-1.753311926
Tbh	NT>NT	2.844395287
Tektin-C	I>NT	2.06242595
Tep3	I>NT	1.724001655
Thor	I>T	4.569069368
Tig	NT>NT	3.941057843
Tig	I>NT	3.941057843
Tmhs	NT>I	-1.813262814
trh	T>T	-1.88000783
Tsp68C	I>NT	-5.054988609
Tsp68C	NT>I	-5.054988609
tty	I>NT	-1.860878139
tut	NT>I	3.479622598
TwdlE	I>NT	-2.086211456
tx	T>T	1.950716464
upd3	NT>NT	4.430058708
vg	I>T	-1.561779788
vir-1	I>NT	2.784710402
wbl	NT>NT	-2.313438298
wbl	I>NT	-2.313438298

wgn	I>T	-1.720884835
yellow-b	NT>NT	3.541257337
yellow-c	NT>NT	2.351705272
yellow-c	I>NT	2.351705272
yellow-e2	I>T	-1.643272067

7 Curriculum Vitae

Marco La Fortezza
Born 17/02/1986 in Livorno, Italy

EDUCATION

Ludwig-Maximilians-Universität München, Germany. 2011 - present

- **Ph.D.** in the lab of Dr. AK. Classen

Topic: *"Cellular signalling and chromatin dynamics during tissue stress response in D. melanogaster."*

- **Graduate programs:**
  - *Life Sciences Munich* (**LSM**) funded by LMU.
  - *Integrated Research Training Group* (**IRTG**) funded by *Sonderforschungbereit* (SFB) *1064* – Chromatin Dynamics.

Sapienza Universitá di Roma, Italy. 2006-2009

- **M.Sc., Genetics and Molecular Biology** with *summa cum laudae.*
- **B.Sc., Biology** with *summa cum laudae.*

PUBLICATIONS

La Fortezza M., Schenk M., Cosolo A., Kolybaba A., Grass I., Classen A.K.
JAK-STAT mediates cell survival in response to tissue stress.
Development, 2016 Aug.

Bielmeier C. and Alt S., Weichselberger V., **La Fortezza M.**, Harz H., Jülicher F., Salbreux G., and Classen A.K.
Interface contractility between differently fated cells drives cell elimination and cyst formation.

Curr Biol. 2016

Verdone L., **La Fortezza M.**, Ciccarone F., Caiafa P., Zampieri M., Caserta M.
Poly(ADP-Ribosy)lation affects histone acetylation and transcription.
PLoS One 2015 Dec.

Bastonini E., Verdone L., Morrone S., Santoni A., Settimo G., Marsili G., **La Fortezza M.**, Di Mauro E., Caserta M.
Transcriptional modulation of a human monocyte cell line exposed to PM(10) from an urban area.
Environ Res. 2011 Aug.